AD-752 210

SHOCK IMPINGEMENT CAUSED BY BOUNDARY LAYER SEPARATION AHEAD OF BLUNT FINS

Louis G. Kaufman, II, et al

Aerospace Research Laboratories
Wright-Patterson Air Force Base, Ohio

August 1972

ARL 72-0118
AUGUST 1972

Aerospace Research Laboratories

SHOCK IMPINGEMENT CAUSED BY BOUNDARY LAYER SEPARATION AHEAD OF BLUNT FINS

LOUIS G. KAUFMAN II, MAJOR, USAF RESERVE
GRUMMAN AEROSPACE CORPORATION

ROBERT H. KORKEGI
LEO C. MORTON, LT COLONEL, USAF
HYPERSONIC RESEARCH LABORATORY

PROJECT 7064

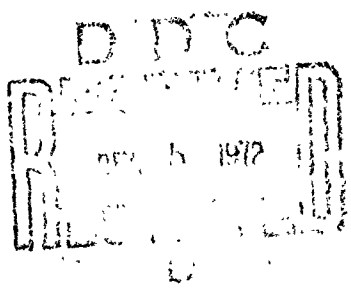

AIR FORCE SYSTEMS COMMAND
United States Air Force

NOTICES

When Government drawings, specifications, or other data are used for any purpose other than in connection with a definitely related Government procurement operation, the United States Government thereby incurs no responsibility nor any obligation whatsoever; and the fact that the Government may have formulated, furnished, or in any way supplied the said drawings, specifications, or other data, is not to be regarded by implication or otherwise as in any manner licensing the holder or any other person or corporation, or conveying any rights or permission to manufacture, use, or sell any patented invention that may in any way be related thereto.

Agencies of the Department of Defense, qualified contractors, and other Government agencies may obtain copies from:

Defense Documentation Center
Cameron Station
Alexandria, VA 22314

This document has been released (for sale to the public) to:

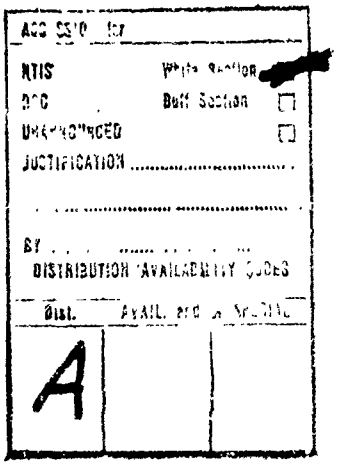

National Technical Information
Services
Clearinghouse
Springfield, VA 22151

Copies of ARL Technical Reports should not be returned to the Aerospace Research Laboratories unless return is required by security considerations, contractual obligations, or notices on a specific document.

AIR FORCE/56780/12 October 1972 — 300

UNCLASSIFIED

Security Classification

DOCUMENT CONTROL DATA - R & D

(Security classification of title, body of abstract and indexing annotation must be entered when the overall report is classified)

1 ORIGINATING ACTIVITY *(Corporate author)*
Aerospace Research Laboratories
Hypersonic Research Laboratory
Wright-Patterson AFB, Ohio 45433

2a. REPORT SECURITY CLASSIFICATION
Unclassified

2b. GROUP

3 REPORT TITLE
SHOCK IMPINGEMENT CAUSED BY BOUNDARY LAYER SEPARATION AHEAD OF BLUNT FINS

4 DESCRIPTIVE NOTES *(Type of report and inclusive dates)*
Scientific Interim

5 AUTHOR(S) *(First name, middle initial, last name)*
Louis G. Kaufman II, Major, USAF Reserve
Robert H. Korkegi
Leo G. Morton, Lt Col, USAF

6 REPORT DATE	7a. TOTAL NO OF PAGES	7b NO OF REFS
August 1972	88	64

8a. In-house Research	9a. ORIGINATOR'S REPORT NUMBER(S)
b. PROJECT NO 7064-02-06	ARL 72-0118
c DoD Element: 61102F	9b. OTHER REPORT NO(S) *(Any other numbers that may be assigned this report)*
d. DoD Subelement: 681307	Code "T"

10 DISTRIBUTION STATEMENT
Approved for public release; distribution unlimited.

Details of illustrations in this document may be better studied on microfiche

11 SUPPLEMENTARY NOTES	12 SPONSORING MILITARY ACTIVITY
TECH OTHER	Aerospace Research Laboratories (LH) Wright-Patterson AFB, Ohio 45433

13 ABSTRACT

High speed flow past a blunt fin on a surface results in a complex, three dimensional, inviscid-viscid interaction flow field. Characteristically, the fin bow shock causes the boundary layer to separate from the surface ahead of the fin, resulting in a separated flow region composed of horseshoe vortices near the surface and a lambda-type shock pattern in the plane of symmetry ahead of the fin. The shock wave emanating from the separated flow region impinges on the fin bow shock and causes intense heating and high pressures locally on the fin leading edge. The heating and pressure in this local area can be more than 10 times larger than the undisturbed stagnation line values; the amplification depends strongly on local flow conditions.

A research program was conducted to examine and to obtain a better understanding of these interaction flow fields; the most recent experiments included detailed pitot pressure flow field surveys for Mach three flows ahead of blunt fins on a flat plate surface with turbulent boundary layers. Turbulent boundary layer separation is shown to result in the type of shock impingement that causes the greatest amplification of heating rates and pressures. Very large pressures and heating rates were also found on the plate surface in the immediate vicinity of the fin root. The experiments also revealed that the separated flow was very unsteady.

DD FORM 1 NOV 65 1473

UNCLASSIFIED

Security Classification

Ia

UNCLASSIFIED

Security Classification

14 KEY WORDS	LINK A		LINK B		LINK C	
	ROLE	WT	ROLE	WT	ROLE	WT
Viscous-Inviscid Interactions						
Boundary Layer Separation						
Three-Dimensional Flows						
Shock Impingement						

U S Government Printing Office 1972 759-486 130

Security Classification

ARL 72-0118

SHOCK IMPINGEMENT CAUSED BY BOUNDARY LAYER SEPARATION AHEAD OF BLUNT FINS

LOUIS G. KAUFMAN II, MAJOR, USAF RESERVE
GRUMMAN AEROSPACE CORPORATION

ROBERT H. KORKEGI
LEO C. MORTON, LT COLONEL, USAF
HYPERSONIC RESEARCH LABORATORY

AUGUST 1972

PROJECT 7064

AEROSPACE RESEARCH LABORATORIES
AIR FORCE SYSTEMS COMMAND
UNITED STATES AIR FORCE
WRIGHT-PATTERSON AIR FORCE BASE, OHIO

FOREWORD

This report was prepared under Project 7064, entitled "High Velocity Fluid Mechanics." The subject work started in August 1969 and continued through March 1972.

The authors wish to express their gratitude to the staff of the AEDC von Karman Facility and particularly to Messrs. Jack D. Coats, Ernest J. Lucas, Joseph C. Donaldson, and Billy Price for their helpfulness in conducting the tests, and for their continued cooperation. The authors also wish to thank their colleagues, particularly Wilbur Hankey of the ARL Hypersonic Research Laboratory, and William Hill of the Grumman Research Department, for many helpful discussions and concultations.

Louis Kaufman, a Staff Scientist with the Grumman Research Department, is an Air Force Reservist assigned to the ARL Hypersonic Research Laboratory. Both organizations supported his contributions to this work.

Lt. Col. Leo Morton is currently at Headquarters, Ogden Air Materiel Area, Hill Air Force Base, Utah.

This report is also available as Grumman Research Department Report RE-428 from: Research Department, Plant 35, Grumman Aerospace Corporation, Bethpage, New York 11714.

ABSTRACT

High speed flow past a blunt fin on a surface results in a complex, three dimensional, inviscid-viscid interaction flow field. Characteristically, the fin bow shock causes the boundary layer to separate from the surface ahead of the fin, resulting in a separated flow region composed of horseshoe vortices near the surface and a lambda-type shock pattern in the plane of symmetry ahead of the fin. The shock wave emanating from the separated flow region impinges on the fin bow shock and causes intense heating and high pressures locally on the fin leading edge. The heating and pressure in this local area can be more than 10 times larger than the undisturbed stagnation line values; the amplification depends strongly on local flow conditions.

A research program was conducted to examine and to obtain a better understanding of these interaction flow fields; the most recent experiments included detailed pitot pressure flow field surveys for Mach three flows ahead of blunt fins on a flat plate surface with turbulent boundary layers. Turbulent boundary layer separation is shown to result in the type of shock impingement that causes the greatest amplification of heating rates and pressures. The experiments revealed that the separated flow was very unsteady; this intrinsic oscillatory condition is attributed to a pulsating, scavenging action of the horseshoe vortices. In addition to the peak pressures and heating rates at shock impingement on the fin leading edge, there are very large pressures (approaching free stream pitot pressure values) and heating rates on the plate surface in the immediate vicinity of the fin root. Results from this program and many other sources were analyzed and compared with theoretical results to provide a better description of interaction flow fields.

TABLE OF CONTENTS

LIST OF ILLUSTRATIONS

SYMBOLS

d	fin thickness (inches)
h	fin height (inches)
ℓ_{sep}	extent of separated flow ahead of fin (inches)
M	Mach number
p	pressure (psia); static pressure when referenced to p_1, total pressure when referenced to p_{o2}
p_{pk}	peak pressure for turbulent boundary layer separation (psia)
p_{pl}	plateau pressure for laminar boundary layer separation (psia)
p_o	wind tunnel stagnation pressure (psia)
p_{op}	local pitot pressure (psia)
p_{o2}	free stream pitot pressure (psia)
Rey_{inch}	Reynolds number based on free stream conditions and a unit length of one inch
Rey_{sep}	Reynolds number based on undisturbed flat plate flow conditions and length s_{sep}
s_{sep}	streamwise distance from plate leading edge to separation point (inches)
s_{trans}	streamwise distance from plate leading edge to undisturbed boundary layer transition location (inches)
x,y,z	coordinates with origin on plate surface at fin leading edge (cf. Fig. 3)
z_{tp}	vertical coordinate referenced to the "triple point" location (cf. Fig. 26)
δ	boundary layer thickness (inches)

Subscripts

1	average undisturbed flow conditions over flat plate surface
∞	tunnel free stream conditions

INTRODUCTION

Severe local heating occurs when a shock wave impinges on a downstream surface. The destruction of an X-15 ventral fin and the damage to portions of the Holloman Rocket Test Sled, described by Korkegi (Ref. 1), are examples of the possible severity of shock impingement effects. To obtain a better understanding of shock impingement, we conceived and conducted pertinent experimental programs, and analyzed our results along with those from many other investigations. This report provides a description of our most recent experimental program, which included shock impingement flow field surveys and revealed a severe unsteadiness of the interaction flow. A critical analysis of the interaction flow field is presented and compared with theoretical methods.

Many different types of shock impingement interactions have been observed and different flow models postulated. Some are dominated by inviscid effects, whereas viscosity is of prime importance in others. In some instances, such as a bow shock from the nose of a vehicle impinging on a wing leading edge, the strength and location of the impinging shock are known. More frequently, however, shock impingement results from an inviscid-viscous flow interaction and neither the strength nor the location of the impingement are known beforehand. A comprehensive review of viscous interactions, by Korkegi (Ref. 1), and an extensive survey of the literature (listing over 900 references), by Ryan (Ref. 2), summarize results for different types of interaction flows. Features of some of these interaction flows are described in the following section.

A frequently encountered type of shock impingement interaction, which results in particularly severe local heating, occurs when an

oblique shock wave impinges on the detached bow shock ahead of a blunt leading edge. The impinging shock can be generated by an extraneous surface, or can result from boundary layer separation ahead of a protuberance from a surface. In addition to local regions of extreme heating and large pressure loads on the blunt leading edge, the pressures and heating rates are increased on the adjacent surface in the separated flow region. Some of these effects were observed in earlier investigations of separated flows (Refs. 3-6). The seriousness and practical importance of shock impingement caused by boundary layer separation prompted our earlier investigation of supersonic flows past blunt fins mounted on a flat plate (Refs. 7 and 8). The experimental research described herein was designed to supplement the results of earlier experimental programs and to provide detailed surveys of the shock impingement interaction flow field. The experiments were conducted in the 12-inch supersonic tunnel at Arnold Engineering Development Center during July 1970 (Ref. 9).

FEATURES OF INTERACTIONS FLOWS

Separated Flow

Certain aspects of the separated flow in the plane of symmetry ahead of a blunt fin are somewhat similar to two dimensional separated flows ahead of steps or ramps (Refs. 7, 10, and 11). The pressure rise across the fin bow shock presents a strong adverse pressure gradient to the boundary layer flow on the adjoining flat plate surface, causing the boundary layer to separate from the surface and forming a region of reverse flow adjacent to the plate surface. The effects of the pressure rise are propagated upstream through the reverse flow region. The surface pressure increases in the neighborhood of the separation point to a peak value that corresponds to the compression of the stream flow as it separates from the surface and passes over the reverse flow region.

As sketched in Fig. 1, the reverse flow forms a "horseshoe" vortex in which the flow quickly curves downstream, away from the plane of symmetry. Immediately downstream of this vortex, there appears to be one or more additional horseshoe vortices (Refs. 7 and 12-19). The reverse flow in the vortices is constantly replenished by the separated stream flow, unlike "trapped" two dimensional reverse flows, and spirals downstream very rapidly. Thus, the vortices bring high energy air flow into proximity with the surface. Severe heating rates and large pressures have been observed in local regions on the surface adjacent to protuberances (Refs. 1, 7, and 20-25).

Oil film flow photographs, such as those in Fig. 2, indicate the surface streamlines on the flat plate surface and the extent

of separation. At separation there is an accumulation of oil, whereas the oil is swept away from reattachment regions. Apparent from inspection of these photographs, the direction of flow in the vortices is predominantly outboard and bears little resemblance to two dimensional separated flows except in the plane of symmetry. The predominance of the transverse flow masks the nature of the flow along the boundary between the two vortices, but there apparently is a third, small and counter rotating horseshoe vortex between the two larger vortices (Refs. 7 and 12-14). This additional vortex is clearly evident in Winkelmann's (Ref. 14) excellent oil film flow photographs. The extent of the separated flow depends primarily on the fin diameter and character of the boundary layer on the plate surface (Refs. 1, 7, 17-19, and 26-30).

The flow at the foot of the fin is highly three dimensional and quite complex. There are large pressure, as well as velocity, gradients in this region. The compressed separated flow ahead of the fin accelerates to supersonic speeds in escaping around the fin to lower pressure regions (Refs. 17-19). A strong vortex starts at the foot of the fin and spreads out as it follows the fin root downstream (Ref. 7).

Profile flow photographs,[†] like those in Fig. 3, show features of the interaction in the model centerplane: the compression wave from the plate leading edge, the separation of the boundary layer from the plate surface, the resulting shock wave, and the impingement of this shock on the fin bow shock. The intersection of the impinging shock and fin bow shock resembles a lambda type shock

[†] The vertical line in these photographs is a wire on the outside of the tunnel window. It serves as a photo reference guide, it intersects the plane of the plate surface 2.30 inches downstream of the plate leading edge.

interaction pattern that is unique to three dimensional flows. For two dimensional flows ahead of steps, the separated flow is "trapped" in the region ahead of the step and the stream flow reattaches at the top of the step (Ref. 11). In both the schlieren and shadowgraph photographs in Fig. 3, there is a light spot near the foot of the fin. This can be attributed to the locally accelerating flow mentioned in the previous paragraph.

Unsteadiness

Although the microsecond schlieren photographs shown in Fig. 4 were obtained during the same tunnel run, the extent of separation ahead of the fin is 10 percent greater in Fig. 4b than in Fig. 4a. The separation and interaction flow are unsteady. This unsteadiness is responsible for the lack of crispness in the 1-millisecond exposure flow photographs shown in Fig. 3 (Ref. 9). Zukoski (Ref. 11), Goldman et al. (Ref. 31), Holden (Ref. 32), and others[†] have observed oscillations of two dimensional turbulent separation locations having amplitudes less than half that of the undisturbed boundary layer thickness and a frequency of several thousand Hertz. In the present case, the oscillations of the separation location are much larger in amplitude than the undisturbed boundary layer thickness. This relatively large movement of the separation location, which we attribute to a pulsating and scavenging action of the flow comprising the multiple horseshoe vortices, results in comparatively large oscillations of the impinging shock wave.

[†]For example: Wilhelm Behrens, California Institute of Technology, January 1971, private communication.

Shock Impingement

Hains and Keyes (Ref. 33) and Edney et al. (Refs. 34-36) obtained excellent schlieren photographs that clearly show the structure of a shock impingement region, as shown in Fig. 5. The impinging shock was generated by a separate wedge (not by boundary layer separation), and the flow in the shock interaction region was steady. The oblique shock impinges on the bow shock and is reflected. A shear layer (inviscidly, a slip line) starts at this "triple" point and separates the subsonic flow behind the bow shock from a jet of supersonic flow. The flow in this supersonic jet passes through several oblique shocks before stagnating on the fin leading edge. Therefore, this flow is compressed nearly isentropically and leads to extremely large pressures, pressure gradients, and heat transfer rates locally on the fin leading edge.

Using inviscid, two dimensional flow relations, Edney et al. (Refs. 34-36) categorized six different types of shock impingements that depend on the inclination of the impinging shock and on the fin sweep. The type shown in Fig. 5 leads to the most severe heating and largest pressure gradients. Unfortunately, the location of the point "Q" in Fig. 5, as noted by Edney, is indeterminate in his analysis. Thus, the width of the supersonic jet (and therefore the peak value of the heating rate on the fin leading edge) cannot be calculated. The width of the jet must be obtained from flow photographs.

Bushnell (Ref. 37) and Newlander (Ref. 38) also used separate wedges to generate impinging shock waves, but in most investigations (e.g., Refs. 20, 21, and 39-46), the protuberance was mounted directly on the same wedge or body used to generate the impinging shock. In these cases, there were usually two shock impingements:

an outboard one caused by the wedge shock, and an inboard one resulting from boundary layer separation ahead of the protuberance.

Attention herein is focused on "self-induced" shock impingement caused by boundary layer separation ahead of a fin. The important parameters influencing this type of shock impingement are: fin sweep, height and diameter; stream Mach number; and the boundary layer character and thickness on the adjacent surface. The interaction for swept fins generally results in less severe impingement effects (Refs. 21, 36-38, and 47-50). Indeed, for sufficiently large sweepback, there is no separation ahead of the fin and thus no self-induced shock impingement effects. Some tendencies resulting from varying fin height with respect to the fin diameter or with respect to the boundary layer thickness have been described (e.g., Refs. 51-54) but only for limited ranges of flow conditions. For very short fins (in comparison with either the boundary layer thickness or fin diameter), or for low supersonic Mach numbers, the shock wave emanating from the separated flow region does not impinge on the fin but passes above it (Refs. 12, 13, 55, and 56).

EXPERIMENTAL PROGRAM

Model

The model design and tunnel flow conditions were carefully chosen to permit the examination of self-induced shock impingement interaction flows in the absence of extraneous influences. Cylindrical leading edge fins were mounted on a flat plate that had a machined sharp leading edge, a 12-inch chord, and that spanned the tunnel. For the tunnel flow pressures and Mach numbers, boundary layer displacement and end effects were negligible so that the pressure was constant over the flat plate surface.

The slab type fins had hemicylindrical leading edges and thicknesses of 3/8, 3/4, and 1.0-inch. These thicknesses were several times larger than the local boundary layer thickness on the plate for all test conditions. The fins were mounted on the plate centerline with their leading edges 5.85 inches downstream of the plate leading edge. The two thinner fins had heights of 3.0 inches, and the thickest fin was 2.5 inches high. All fin heights were sufficient to avoid any tip effects in the shock impingement region (Refs. 7, 51, and 53).

The basic plate and two thinner fins were available from our earlier program (Refs. 7 and 8). The 1-inch fin was designed with movable total pressure probes to survey the interaction flow field. This fin was made larger in order to increase the size of the shock impingement interaction flow region without causing tunnel blockage and without having end effects. Photographs of the 1-inch fin mounted on the flat plate are shown in Figs. 6 and 7.

As indicated in Fig. 8, pressure taps were located along the plate centerline and along one spanwise line on the plate surface.

Pressure taps were also located along the leading edges of the two thicker fins.

The 1-inch fin had two total pressure probes that could be individually, remotely driven to extend forward from the fin leading edge. One probe, designed to examine the over-all interaction flow region, had a travel of 2.0 inches, an O.D. of 0.065 inch, and an I.D. of 0.043 inch (cf. Fig. 6). The other probe, resembling a hypodermic needle with an O.D. of 0.025 inch and an I.D. of 0.014 inch, had a travel of 0.6 inch and was designed to examine the flow field in the immediate shock impingement vicinity. Spacers were fabricated for the 1-inch fin so that it, and the total pressure probes, could be shimmed up, in 1/32-inch intervals, up to 1/2-inch above the plate surface. Thus, total pressure probe traverses could be made at 1/32-inch intervals at distances above the plate surface varying from 1/4- to 3/4-inch for the larger probe and from 3/4- to 5/4-inches for the smaller probe. This permitted obtaining detailed flow field surveys (with intervals comparable in size to the probe diameter). The fins and spacers were sealed to the plate prior to each run to avoid any bleed of air between them.

Tunnel Flow Conditions

The experiments were performed in the von Karman Facility Tunnel "D" at AEDC during July 1970. This is an intermittent supersonic wind tunnel with a 12-inch-square test section. The tunnel has a flexible plate type nozzle, shown in Fig. 9, and can provide Mach 4.5 to 5.0 flows (Ref. 57) with stagnation pressures up to 60 psia.

Nominal values of the tunnel flow conditions chosen for this program are listed in Table I. The unit Reynolds numbers are based

TABLE I – TUNNEL FLOW CONDITIONS

M_∞	p_o (psia)	Rey_{inch}	Fin Thicknesses (inch)
2.5	46	800,000	0, 3/8, 3/4
3.0	60	800,000	0, 3/8, 3/4, 1
4.0	60	470,000	0, 3/8, 3/4

on free stream conditions and a length of 1 inch. Relatively high pressures were chosen primarily to ensure turbulent boundary layers on the plate surface in the vicinity of the fins. Further, the Mach 3 flow conditions match those chosen for our earlier tests (Ref. 7) and the higher pressures generally lead to greater accuracy and better flow photographs. The tunnel flow stagnation temperature was approximately 530°R for all test runs.

Static pressures were measured and schlieren flow photographs were taken for the flat plate alone and with the 3/8 and 3/4 fins for all tunnel flow conditions listed in Table I. For Mach 4, the 3/4-inch fin model was tested with and without a boundary layer trip on the plate surface (cf. Fig. 7). The 1-inch fin was tested and total pressure surveys obtained only for the Mach 3 conditions listed in Table I. Many profile flow photographs were taken during the probe traverses; in all, over 400 schlieren and shadowgraph flow photographs were obtained.

Oil film flow photographs were taken for the test conditions listed in Table I to determine the flow direction on the flat plate surface. Zyglo fluorescent oil was sprayed on the plate surface and then "rubbed-in" using fine grit emery cloth (to reduce the

oil film surface tension). The oil film flow was observed under ultraviolet light during the tunnel run, which was terminated once the flow pattern on the plate surface became well established, and the flow pattern was then photographed under ultraviolet light (cf. Fig. 2).

To assess Reynolds number effects, schlieren and shadowgraph flow photographs were obtained at many pressure levels below those listed in Table I. This was easily accomplished during one tunnel run by momentarily stabilizing the tunnel pressure, photographing the flow, and then increasing the pressure to the next level.

Undisturbed Flow Over Plate

The flat plate was tested with no fin attached. Schlieren flow photographs were taken for many sets of flow conditions and the undisturbed surface pressures were measured and recorded for the test conditions listed in Table I.

Flat plate boundary layer thicknesses were calculated and compared with the schlieren flow photographs. Boundary layer transition locations for undisturbed flow over the flat plate were estimated using results presented by Pate and Schueler (Ref. 58), who obtained transition data in the same wind tunnel. Using these transition locations, and an empirical boundary layer method (Ref. 59), undisturbed boundary layer thicknesses were calculated at many stations downstream of the plate leading edge. For example, for the flow conditions indicated in Fig. 10, the end of transition is approximately 4.5 inches downstream of the leading edge (from Ref. 58), and the calculated boundary layer thicknesses at stations 6 and 12 inches downstream of the leading edge are approximately 0.094 and 0.236 inches. These calculated values are indicated in

Fig. 10 and appear to agree well with the schlieren flow photograph. Transition locations for undisturbed flow over the plate (s_{trans}) and boundary layer thicknesses at a station 5.85 inches downstream of the plate leading edge [$\delta(5.85]$, obtained in this manner, are listed in Table II for various tunnel flow conditions.

TABLE II – APPROXIMATE UNDISTURBED BOUNDARY LAYER TRANSITION LOCATIONS AND THICKNESSES CALCULATED AT FIN LEADING EDGE STATION

M_∞	p_o (psia)	Rey_{inch}	s_{trans} (inch)	$\delta(5.85)$ (inch)
2.5	30	520,000	4.0	0.088
	46	800,000	3.1	0.095
3.0	30	400,000	4.5	0.092
	40	530,000	3.9	0.097
	50	670,000	3.5	0.099
	60	800,000	3.1	0.102
4.0	60	470,000	4.3	0.109

For $M_\infty = 3$, the average value of the undisturbed static pressures measured on the plate surface was within 1 percent of the free stream static pressure. However, for Mach 2.5 and 4.0, the average values of the undisturbed pressure on the plate surface (p_1) were slightly higher than p_∞. To ascertain the true pressure rise caused by the interaction flow, the measured pressures were nondimensionalized using the average value of the undisturbed flow pressures on the plate surface shown in Table III. For these small pressure rises, the local flow Mach numbers (M_1) differ by less than 1 percent from M_∞.

TABLE III – AVERAGE VALUES OF p_1/p_∞ FOR UNDISTURBED FLOWS OVER FLAT PLATE SURFACE

M_∞	2.5	3.0	4.0
$\frac{p_1}{p_\infty}$	1.03	1.00	1.05

Extent of Separation and Interaction Pressure Distribution on Plate Surface

The shape and standoff distance of the fin bow shock depend only on M_∞ and the fin diameter (d). Hence, the position of the inviscid pressure rise on the flat plate surface depends only on M_∞ and d. Therefore, if inviscid effects predominate, one would suspect that the pressure distributions on the flat plate surface might scale, for each Mach number, by using coordinates nondimensionalized with respect to the fin diameters (Ref. 7). Accordingly, the nondimensional streamwise and spanwise coordinates x/d and y/d are used to plot the pressure distributions, and to scale the oil film flow photographs.

Surface pressure distributions were obtained at $M_\infty = 3$ and $Rey_{inch} = 800{,}000$ each time a new spacer was placed under the 1-inch-thick fin. These data, obtained from 16 tunnel runs, are plotted in Fig. 11. Probably the most striking aspect of this illustration is the apparent large scatter in the data for essentially identical test conditions. The apparent scatter is caused by the unsteadiness of the separated flow ahead of the fin.

Dashed curves are faired through the sets of data corresponding to the most forward and most aft locations of separation ahead of the fin. A solid curve is drawn through the arithmetic mean average of the p/p_1 values measured at each tap location. Generally, the pressure starts to rise approximately two diameters ahead of the fin, reaches a peak value, and then falls off until just in front of the fin. Very high pressures occur on the surface in the immediate vicinity of the fin foot. For the pressure tap at $x = -0.17$ d, the pressures ranged from 7.5 to 8.4 p_1. Also indicated in Fig. 11, the shock standoff distance for $M_\infty = 3$ is 0.35 d (Refs. 60 and 61). The solid vertical line indicates the separation location determined by measuring the distance to the oil accumulation line on the plate surface immediately following the "oil film" tunnel run.

The schlieren photographs in Fig. 12 correspond to the most forward and the most aft separation locations indicated by the dashed vertical lines in Fig. 11. There is approximately a 17 percent difference in the lengths of separation between these two extreme locations. This change of length corresponds to 6 or 7 times the undisturbed boundary layer thickness at the separation point location on the flat plate. As noted on page 5, the amplitude of this movement of separation ahead of a fin is an order of magnitude larger than for separated two dimensional flows. Robertson (Refs. 12 and 13) notes that fluctuating pressure levels in separated flow regions ahead of fins are an "order of magnitude" larger than for two dimensional separated flow regions.

Centerline pressure distributions ahead of the 5/8- and 3/4-inch-diameter fins are plotted in Fig. 13 along with the average p/p_1 value for the 1-inch fin. The distribution for the 3/4-inch fin was obtained from two tunnel runs, one run being made with the

fin moved forward 1/8-inch (effectively halving the distance between pressure taps to obtain a denser pressure distribution). The data follow the same trends as those shown in Fig. 11 and described above. The Mach 2.5 data also indicate separation approximately two diameters ahead of the fin, but the pressure rise is somewhat less than for the Mach 3.0 data. The separation locations indicated in Fig. 13 were obtained by measuring the distance to the oil accumulation line after each oil film flow tunnel run.

The Mach 4 centerline pressure data, plotted in Fig. 14, exhibit characteristics typical of transitional separated flow (cf. Refs. 3 and 4). The pressure first rises to a laminar plateau value and then rises again to a turbulent peak value. To ensure turbulent separation, a boundary layer trip was used with the 3/4-inch fin configuration for one tunnel run. The trip was a serrated piece of fiberglass tape (0.007-inch thick) placed from 0.81 to 1.13 inches downstream of the plate leading edge (cf. Fig. 7). The trip changed the character of the boundary layer and delayed separation; the resulting pressure distribution resembles those for turbulent separation. The schlieren flow photograph in Fig. 15 was scaled to determine the separation location indicated by the dashed vertical line in Fig. 14.

The other separation locations indicated in Fig. 14 were obtained by measuring the location of the oil accumulation line on the plate surface after each oil film flow tunnel run. Relatively little tunnel running time was required before the oil film flow pattern became established and stabilized. The separation line was well defined in all cases except for $M_\infty = 4$ and $d = 3/4$-inch. For this case, the oil accumulation was blurred, particularly near

the plate centerline (cf. Fig. 16), and it was not possible to determine a specific separation location. Schlierer flow photographs (Fig. 17) taken during this oil film flow tunnel run show a particularly large (30 percent) shift in the length of separation.

The extent of separated flow ahead of the fin (ℓ_{sep}) is particularly sensitive to the character of the boundary layer in the vicinity of separation. The dependence of ℓ_{sep} on the character of the boundary layer is similar to that for two dimensional separated flows, which is indicated in the following sketch.

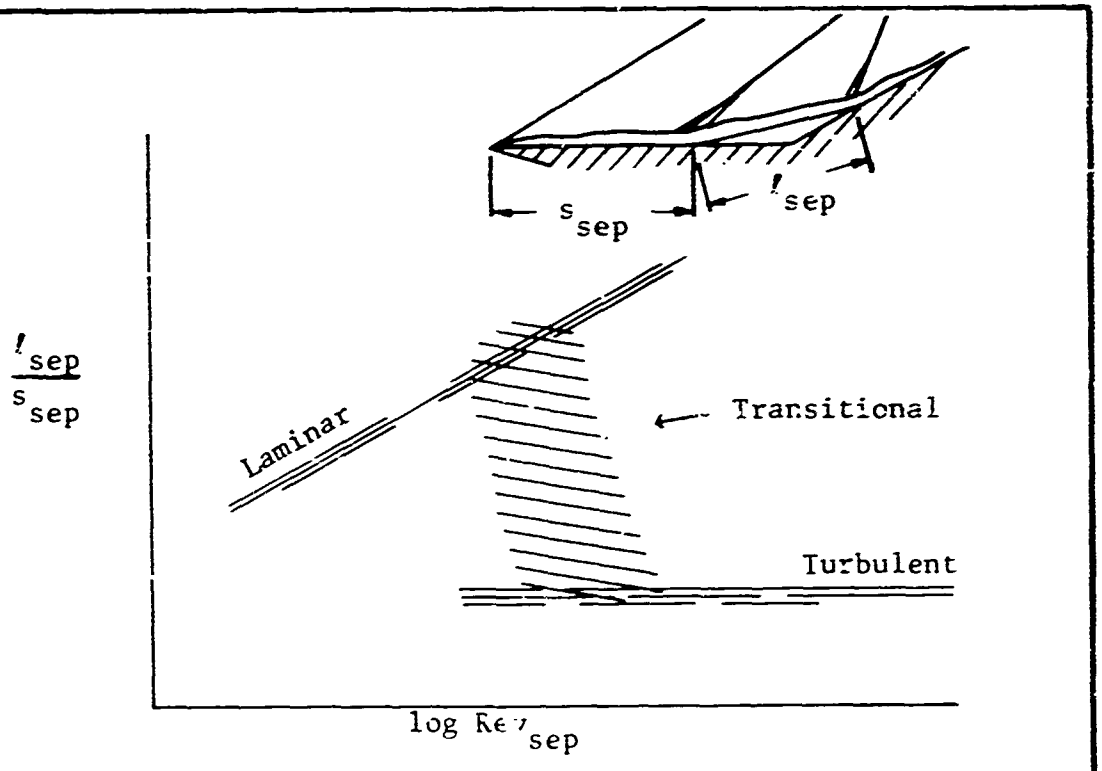

Sketch of Variation of ℓ_{sep} with Rey_{sep} for Laminar, Transitional, and Turbulent Separation for Two Dimensional Flows

The extent of two dimensional separated flow generally increases with Reynolds number* for entirely laminar boundary layers (boundary layers that remain laminar throughout the free shear layer; transition occurring downstream of reattachment). Turbulent boundary layer separation (transition to fully turbulent flow occurring upstream of separation) is much less extensive than laminar separation and is insensitive to Reynolds number (Ref. 1). For transitional separation (transition occurring in the free shear layer downstream of the separation location but at or before reattachment), the extent of separation diminishes rapidly with increasing Reynolds number from the purely laminar value to the turbulent value.

Separation is a relatively strong disturbance to laminar boundary layer flow and causes transition to occur earlier than for attached, undisturbed boundary layers (Refs. 10 and 30). Separation ahead of a fin is a particularly strong disturbance; in virtually all of the current cases, transition to turbulence occurred either in the free shear layer or upstream of the separation point.

Separation lengths were obtained from profile flow photographs, such as those in Figs. 18 and 19, for many unit Reynolds number ($Re_{y_{inch}}$) values. These lengths are plotted in Fig. 20 versus s_{sep}/s_{trans} (distance from plate leading edge to separation location/distance from plate leading edge to calculated transition location for undisturbed boundary layer). The extent of separated flow for transitional separation is greatest for the smallest Reynolds numbers (lowest s_{sep}/s_{trans} values), and decreases with increasing Reynolds number to a fairly constant value of approximately 2 d for turbulent separation ($s_{sep} > s_{trans}$). There is

*$Re_{y_{sep}}$, based on undisturbed flow conditions, and length, s_{sep}, from leading edge to separation location.

a particularly large, unsteady movement of the separation point location and a correspondingly large variation in the length of separation ($2.3\ d > \ell_{sep} > 1.9\ d$) when separation occurs in the vicinity of the undisturbed transition location ($s_{sep} \approx s_{trans}$). (This is the case for $M_\infty = 4$ and $d = 3/4$-inch, cf. Table II and Fig. 17.)

Oil film flow photographs, such as those shown in Fig. 21, were scaled to obtain the separation lines drawn in Fig. 22. For turbulent boundary layer separation ahead of blunt fins, the lines collapse into a narrow band for $2 \leq M_\infty \leq 4$ (Mach 2 data from Sedney, Ref. 62). Within the range of test conditions, turbulent separation appears to be independent of Reynolds number (for $\ell < d$) and insensitive to Mach number (for $2 \leq M_\infty \leq 4$).

Pressure Distributions on Fin Leading Edge

Shimming the 1-inch fin resulted in the dense pressure distribution along the fin leading edge shown in Fig. 23. For $M_\infty = 3$, the peak pressure is approximately 1.5 times as large as the pitot stagnation pressure (p_{o2}) on the fin leading edge. Included in Fig. 23 is the maximum pressure recorded on the plate surface ahead of the fin, which is over 3/4 the stagnation pressure value (over nine times as large as the undistributed pressure on the plate surface). This supports Avduyevskii's (Ref. 17) results that indicate the existence of high velocity streams, in the separated flow region, that impinge on the plate surface.

The curve faired through the Mach 3 data (Fig. 23) is superimposed on the Mach 2.5 and 4 data shown in Fig. 24. The peak pressure for Mach 2.5 is slightly smaller than for Mach 3 and occurs further outboard on the fin; the peak pressure for Mach 4 is larger

than for Mach 3 and occurs closer to the fin foot. The peak to total pressure ratio increases with Mach number. Because of the smaller shock wave angle, the impingement point and location of the peak pressure moves inboard (closer to the plate surface) with increasing Mach number (Ref. 7) (cf. Figs. 15, 18, and 25).

Interaction Flow Field Measurements

The total pressure probe traverses were made by extending one of the probes forward a small distance, recording the pressure measurement and photographing the flow, then extending the same probe forward to a new position, and repeating the process. The pressure measurements stabilized very quickly, because of the relatively high pressure levels, so measurements could be obtained at many locations along each traverse during one tunnel run. The fin was then shimmed, which increased the height of the probe above the plate surface, and a traverse made at the new height station.

Profile flow photographs, such as the shadowgraph shown in Fig. 26, were used as an aid in determining the probe location with respect to the "triple point," the point where the impinging shock wave intersects the fin bow shock. The unsteadiness of the separated flow region caused a shifting of the impinging shock with a resulting change in the triple point location. To minimize the effects of the fluctuating shock position, the probe measurements were referenced to the triple point location. In this manner a more accurate, truer, representation of the interaction flow field was obtained.

Thus, vertical distances above the triple point (z_{tp}; cf. Fig. 26), are indicated for the total pressure traverses shown in Fig. 27. Similar to the pressures measured along the fin leading edge, the total pressures measured during the pitot probe traverses

are nondimensionalized with respect to the free stream flow pitot pressure, p_{o2}.

The traverse taken closest to the plate surface (using the larger probe and no fin shims) has a vertical height of -0.64 d, referenced to the triple point. There is an initial decrease in total pressure as the probe moves forward from the fin leading edge. The total pressure decreases from $0.6\ p_{o2}$ at the fin leading edge to less than $0.4\ p_{o2}$ at $x = -0.2$ d, and then increases to $1.5\ p_{o2}$ as the probe moves forward to $x = -1.0$ d. The probe was behind the separation (impinging) shock for all of the traverses shown in the first part of Fig. 27 ($z_{tp} \leq -0.40$ d). For higher traverses ($z_{tp} \geq -0.34$ d), the probe extends forward, through the separation shock, into the free stream flow ($p = p_{o2}$).

The traverses for $z_{tp} \geq -0.14$ d were made using the smaller probe. Above the triple point, a small drop in pressure was observed just ahead of the fin leading edge ($x \approx -0.05$ d). This can be attributed to the streamlines diverging just ahead of the fin, so that their misalignment with respect to the probe is large just before the flow stagnates on the fin leading edge.

The locations of these traverses with respect to the lambda shock pattern may be determined by comparing the x and z_{tp} values in Fig. 27 with the sketch shown in Fig. 28. The sketch was traced from an enlargement of a microsecond schlieren flow photograph. Comparing this sketch with the numerous flow photographs taken with the probes extended, normal shocks ahead of the probes were observed in the region indicated. No probe bow shocks were observed behind the fin bow shock or behind the rearward "leg" of the lambda shock. The region immediately behind and slightly below the triple point was somewhat obscured in all the probe flow photographs; therefore,

very weak probe bow shocks may have existed in this region although none were visible.

As the larger probe was extended forward in the separated flow region, indicated in Fig. 28, it caused a sudden collapse of the flow field, evidenced by the schlieren flow photographs shown in Fig. 29. The flow separated from the probe and effectively "streamlined" the blunt fin. As shown in Fig. 29, this separated flow was unstable, in one case the probe was extended to $x = -1.0$ d without disturbing the interaction flow, whereas in the other case, at the same probe height above the plate, the probe altered the flow field when extended to $x = -0.8$ d. The region where there was severe probe interference is indicated in Fig. 28.

When the probe altered the flow field, causing the separated flow region to collapse, the resulting bow shock wave from the probe impinged on the fin bow shock wave. In a few of these "off-design" cases, the shock impingement peak pressure on the fin leading edge was recorded. These peak pressures, and the corresponding pressure tap locations, are indicated on the schlieren flow photographs in Fig. 30.

DATA ANALYSIS AND COMPARISONS

Extent of Separation

For fins having heights and diameters greater than the local boundary layer thickness, the extent of separation and the extent of increased loads on the plate surface are proportional to the fin diameter. As indicated in Fig. 20, the separated flow region extends approximately two diameters ahead of the fin ($\ell_{sep} \approx 2$ d) if the boundary layer is turbulent upstream of separation. Many investigators observed similar results ($\ell_{sep} \approx 2$ d) for turbulent separation ahead of fins for a wide range of test conditions. Robertson (Ref. 13) obtained separation lengths of 1.85 d, 2.15 d, and 2.16 d for $M_1 = 1.2$, 1.4, and 1.6, respectively. Waltrup et al. (Ref. 53) obtained $\ell_{sep} = 2.2$ d for $M_1 = 2.2$. Young et al. (Ref. 7), Surber (Ref. 23), and Voitenko et al. (Ref. 28) all obtained separation lengths of approximately 2 d for Mach numbers from 2.5 to 4.5. Winkelmann (Ref. 14) obtained $\ell_{sep} \approx 2.3$ d for $M_1 = 5$. Westkaemper (Ref. 51) obtained an upstream "limit of disturbed flow" (which exceeds ℓ_{sep} as usually defined by approximately 0.5 d. cf. Fig. 11) of approximately 2.6 d, based on data from several sources for Mach numbers from 2 to 21.

Young et al. (Ref. 7), Price and Stallings (Ref. 15), Westkaemper (Ref. 51), and others (e.g., Refs. 17-19 and 26-28) observed that the extent of turbulent separation is apparently insensitive to Mach number, Reynolds number, and boundary layer thickness for a wide range of test conditions, for fin diameters that are larger or comparable to the undisturbed boundary layer thickness.[†] Further, the results are consistent within the range of separation lengths

[†]Zukoski (Ref. 11) indicates that turbulent separation ahead of forward facing steps is independent of Reynolds number and is insensitive to Mach number.

caused by the unsteady movement of the separation point (cf. page 14 and Figs. 11 and 12). Summarizing, for Mach numbers from 1.2 to 21, turbulent boundary layers separate approximately two diameters ahead of the fin leading edge (for fin diameters larger than the undisturbed boundary layer thickness). Because of the unsteadiness of the separated flow, it probably would not be fruitful to attempt to obtain a more precise expression for the extent of turbulent separation ahead of fins.

Laminar or transitional boundary layer separation ahead of a fin is much more extensive than turbulent separation, and depends on both Mach number and Reynolds number. Limited data indicate that the extent of entirely laminar separation ahead of a fin increases with increasing Reynolds number (Rey_{sep}). Laminar separation lengths exceeding six diameters ($\ell_{sep} > 6$ d) have been observed (Ref. 7) for both Mach 3 and Mach 5 flows. However, as noted earlier, separation is a strong disturbance to a laminar boundary layer and causes earlier transition than for attached, undisturbed boundary layers. In virtually all of the present tests, transition occurred either ahead of the separation location (turbulent separation) or in the free shear layer bounding the reverse flow region ahead of the fin (transitional separation). As indicated by the data shown in Fig. 20, the extent of transitional separation diminishes towards the turbulent value ($\ell_{sep} \rightarrow 2$ d) as the separation location approaches the undisturbed boundary layer transition location ($s_{sep} \rightarrow s_{trans}$). Mach number, Reynolds number, and boundary layer thickness effects on the extent of laminar or transitional separation have not been clearly differentiated. As yet, there appear to be no reliable methods for predicting the extent of laminar or transitional separation ahead of blunt fins.

Avduyevskii et al. (Ref. 17), Giagolev (Ref. 18), Voitenko (Refs. 19 and 27), and Panov (Ref. 26) derived on empirical equation for the initial shape of the separation line on the plate surface. The initial shape of the separation lines shown in Fig. 22 are matched fairly well by the elliptic equation. The equation contains two empirical constants, however, and these almost guarantee a good fit for the initial part of the separation line.

Further outboard from the fin ($y > 6$ d), the fin bow shock wave weakens and becomes insufficient to separate the turbulent boundary layer on the plate surface. Korkegi (Ref. 30) observes that at this location the horseshoe vortices curve downstream and proceed in a streamwise direction. In the same paper, Korkegi describes the effects of transition on the separation line shape. As the fin bow shock location moves outboard and downstream, it crosses the location for undisturbed boundary layer transition on the plate surface. At this point, there is an inflection in the separation line shape and, as shown in the following sketch, downstream of this location the transitional separation line approaches the turbulent separation line shape.

The vertical extent of the separated flow can be described partially by reviewing total pressure rake data obtained during our earlier tests (Ref. 7) for the same Mach and Reynolds numbers as for the present tests. Sample total pressure profiles, obtained at several stations along chordwise lines at $y = d$ and 2 d and referenced to the same triple point position (z_{tp}) as used herein, are plotted in Fig. 31. The first profile ($x = -0.67$ d, $y = d$) extends above the reverse flow region and indicates a pitot pressure that is nearly equal to that measured by the single probe

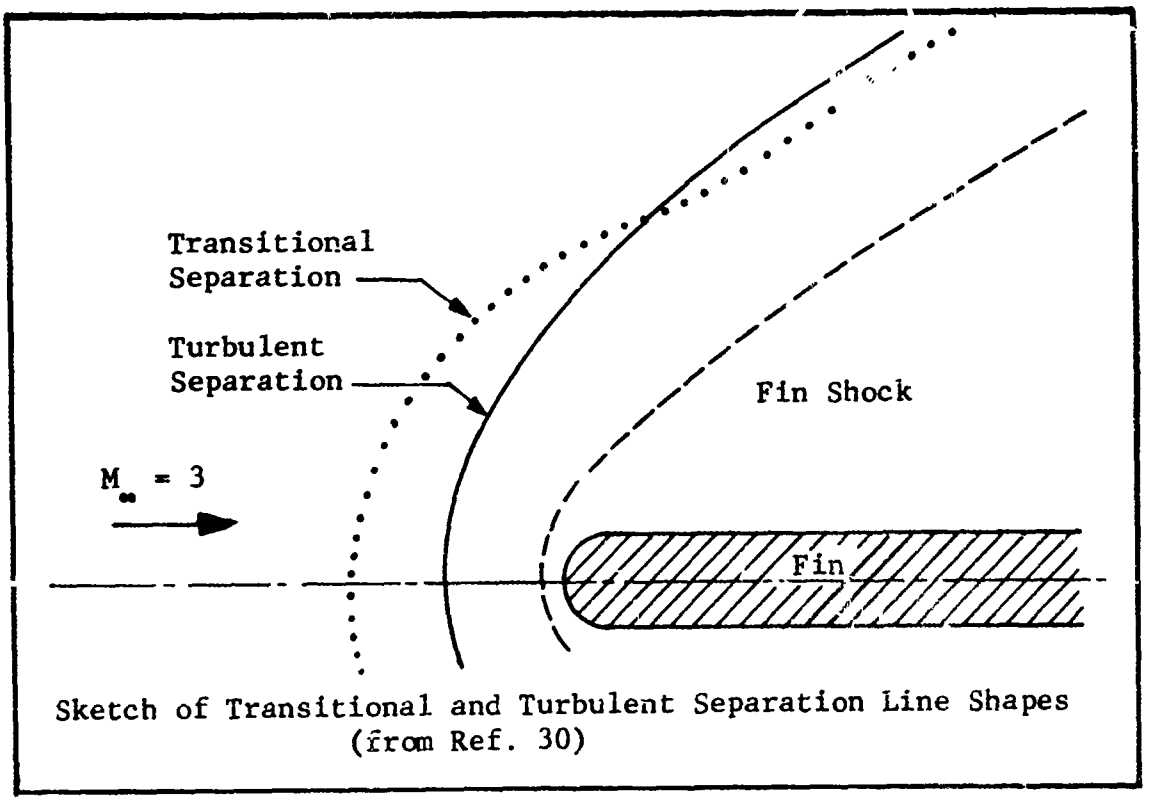

Sketch of Transitional and Turbulent Separation Line Shapes
(from Ref. 30)

for $z_{tp} = -0.40$ d (cf. Figs. 27 and 31). The rake pressures drop substantially as the plate surface is approached, both for $x = -0.67$ d and for $x = +0.50$ d at $y = d$. Two factors cause this: the rake extends further into the reverse flow region (closer to the plate surface) than the single probe measurements, and outboard of the centerline there is a large outward component of the flow (evidenced on the surface by the oil film flow photographs herein), and thus the local streamflow is not aligned with the rake probes. Further aft, at $x = +1.33$ d and $y = d$, the local streamflow is primarily chordwise and the pitot pressure is nearly equal to p_{o2} except near the plate surface. The first profile along the outboard chord ($y = 2$ d) is quite close to the separation line (cf. Fig. 22). The local streamflow is just beginning to turn outboard, and high

total pressures (up to $1.35\ p_{o2}$) are obtained behind the separation shock. Again, the low pitot pressures measured using the rake at the two further downstream stations are indicative primarily of the predominantly outward flow direction at these locations (cf. Fig. 24 of Ref. 7).

Load on Plate Surface

Although we are not familiar with any systematic force measurements of fin-induced loads on an adjacent plate surface, many experimental investigations provide pressure distributions (e.g., Refs. 3-7, 12-19, 24-28, and 55) and these may be used to obtain at least a qualitative understanding of the increased load on the plate surface.

Along the centerline ahead of the fin, the pressure rises to a peak value (cf. Fig. 11) that can be estimated using relations, such as those presented by Sterrett and Emery (Ref. 63), obtained for two dimensional turbulent boundary layer separation:

$$\frac{p_{pk}}{p_1} = \begin{cases} 1 + \dfrac{2.24\ M_1^2}{8 + (M_1 - 1)^2} & \text{for } M_1 \leq 3.4 \\ \text{or} & \\ 0.091\ M_1^2 - 0.05 + \dfrac{6.37}{M_1} & \text{for } M_1 \geq 3.4 \quad . \end{cases} \tag{1}$$

For $M_1 \approx 3$, these relations give a peak pressure rise somewhat greater than the measured values shown in Fig. 11. Voitenko et al. (Ref. 28) also observed peak pressures in their $M_1 = 2.5$ experiments that were somewhat less than those corresponding to two dimensional separation. However, Waltrup et al. (Ref. 53) measured peak

pressures in a Mach 2.2 flow that were in good agreement with those indicated by Eq. (1). Lucero (Ref. 55) points out that the measured peak pressures ahead of a fin are lower than the two dimensional values for Mach numbers greater than about 2.2; for lower Mach numbers, the measured peak pressures agree with the two dimensional values predicted by Eq. (1). Robertson's (Ref. 13) experiments for $M_1 = 1.2$, 1.4, and 1.6 bear this out. Thus, along the centerline, it appears that the pressure rise to the peak value is of the "free interaction" type and can be estimated sufficiently well (to within the scatter caused by the unsteadiness in the flow, cf. Fig. 11), using the relations developed for turbulent separation ahead of forward facing steps. However, as pointed out by Robertson (Refs. 12 and 13), the fluctuating pressure ahead of the fin "may be as large as an order of magnitude greater than those encountered within two dimensional separated flows."

Although the location of laminar boundary layer separation ahead of a fin depends on several parameters, the character of the flow in the vicinity of laminar separation depends only on local flow conditions. Similar to turbulent separation, the pressure rise to a plateau value along the centerline can be calculated using an experession developed for two dimensional laminar boundary layer separation (Ref. 10):

$$\frac{p_{pl}}{p_1} = 1 + 1.22\, M_1^2 \left[(M_1^2 - 1) Rey_{sep} \right]^{-1/4} \quad . \qquad (2)$$

The plateau pressure rise given by Eq. (2) can be used in oblique shock relations to calculate the initial slope of the laminar dividing streamline and impinging shock wave angle.

Pressure distributions outboard on the plate surface generally resemble the one along the centerline. The pressure rises at separation, reaches a peak or plateau value, dips somewhat, and then attains extremely large values in the immediate vicinity of the fin leading edge. These trends are evident in the detailed pressure distributions, obtained by Price and Stallings (Ref. 15), which are plotted in Fig. 32, for turbulent boundary layer separation. As one would expect, the peak pressures diminish in intensity and move aft for the further outboard stations. Downstream of the separation line, there are substantial overpressures on the plate surface that persist many diameters downstream of the fin leading edge. The data presented in Fig. 32 are for a relatively thick boundary layer (three times as thick as the fin), but show the same trends as do surface pressure data presented by other investigators (e.g., Refs. 5-7, 13, and 28).

The maximum pressure on the plate surface recorded during our tests was nine times the undisturbed value for $M_\infty = 3$ (cf. Fig. 13). Waltrup et al. (Ref. 53) observed pressures, near the fin foot, of 6 p_1 for $M_\infty = 2.2$, and Meyer (Ref. 43) measured pressures approaching 10 p_1 immediately ahead of a blunt protuberance for $M_\infty = 4.25$. These values approach the pitot total pressure values. Further, because of the extreme pressure gradients (cf. Fig. 32), it is doubtful that the maximum peak pressure was measured during any test.

The very large pressures and pressure gradients lead to intense heating rates on the plate surface in the immediate vicinity of the fin foot. This intense heating is evident in photographs showing the burnt section of the X-15 fuselage in the vicinity of the ventral fin (cf. Ref. 1), and the severe burn marks on a fin-plate model (cf. Ref. 21). Kaufman et al. (Ref. 20) measured

heating rates near the fin foot that were 10 times larger than the undisturbed plate heating rates for $M_\infty = 8$, and Couch et al. (Ref. 22) measured heating rates ahead of a blunt protuberance that were eight times larger than the undisturbed values on the plate surface for Mach 4.44. Avduyevskii et al. (Ref. 17) and Voitenko (Ref. 19) indicate the possibility of still higher heating rates due to impingements on the plate surface of supersonic streams embedded in the separated flow region. Unfortunately, the details of the flow in this region are still unknown and detailed experimental data are quite sparse; therefore the maximum heating rates on the plate surface in the vicinity of the fin foot are still largely a matter of conjecture.

Shock Impingement

Pressures and heat transfer rates 10 times larger than stagnation point values have been measured in local regions on blunt leading edges in the vicinity of shock impingement (Refs. 20, 21, and 33-46). The magnitude of these peak values depends on the strength of the impinging shock, leading edge geometry, and flow conditions. As yet, there are no satisfactory analytical methods for accurately predicting the peak values for a particular interaction. The effects of various parameters on the peak loads can be described, however, at least qualitatively, and the maximum attainable values can be estimated.

As noted on page 6, the type of shock impingement that causes the most severe heating and largest pressure gradients results when shock waves corresponding to 10- to 20-degree flow deflections impinge on unswept fins (cf. Fig. 5 and Ref. 35, p. 45). Swept leading edges result in a different type of interaction with much

lower peak to stagnation line pressure and heating rate ratios (Refs. 21, 33-36, and 47-50). Different types of interactions than that shown in Fig. 5 occur for impinging shocks corresponding to flow deflection angles less than 10 or greater than 20 degrees (Refs. 33-36). These also result in less severe heating and pressure ratios (Refs. 39-42). Francis (Ref. 41) observed maximum amplification factors for deflection angles "between 10 and 15 degrees."

The pressure rise associated with turbulent boundary layer separation, as given by Eq. (1), corresponds to flow deflection angles between 10 and 15 degrees for all Mach numbers between 1.6 and 20. Thus, in accord with the results mentioned above, turbulent boundary layer separation ahead of an unswept fin results in the most severe type of shock impingement. Indeed, in those instances when there are two distinct shock impingements on a blunt leading edge (e.g., Refs. 20, 21, 45, and 46), the more severe peak heating is associated with the separated-boundary-layer induced shock impingement near the fin or wing root (cf. sketch). In these instances, the flow passes first through the leading edge shock and then is further compressed by the shock wave emanating from the separated flow region ahead of the fin or wing. Kaufman et al. (Ref. 20) and Rogers (Ref. 46) observed inboard peak heating rates up to twice as large as the outboard peak heating rates caused by impingement of the

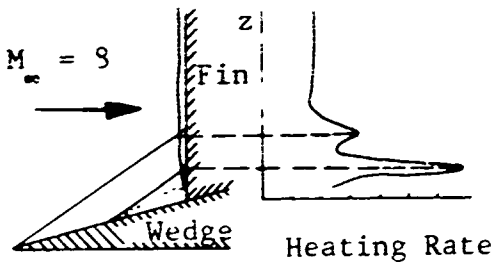

Sketch of Double Shock Impingement and Resulting Heat Transfer Distribution (from Ref. 20)

shock wave from the leading edge of the model. Nestell (Ref. 37) also observed that self-induced shock impingement usually results in the more severe peak heating rates. However, for very thick boundary layers relative to the fin diameter or height, the effects of separation induced shock impingement are less severe and are somewhat masked within the thick boundary layer (Refs. 14, 15, 38, and 51-56).

For fins that are thicker than the local undisturbed boundary layer, the location of the peak pressure and heating rate on the fin leading edge can be estimated crudely by calculating where the separation shock impinges on the fin bow shock (cf. Figs. 26 and 28). The peak pressure on the leading edge usually occurs slightly inboard of (below) this location (Refs. 7 and 51). In the present experiments, the peak pressure on the fin leading edge occurred within 0.1 d of the triple point location (cf. Fig. 33).

Pitot Pressure Profiles

The probe total pressure data (Fig. 27) were crossplotted to obtain the total pressure profiles shown in Fig. 33. The shock locations, from Fig. 28, are superimposed on the profiles to serve as a location reference for the profiles. For example, at the first profile station ($x = -0.90$ d), the impinging shock crosses the station at $z_{tp} = -0.33$ d, and the pressure begins to increase in the region below the shock. Because of severe probe interference (cf. Fig. 28), there were too few points to complete the first three profiles ($-0.90\ d \leq x \leq -0.80\ d$). The total pressure values are indicated for the lowest probe position ($z_{tp} = -0.64$ d), and dashed lines are drawn from these values through the region of probe interference.

The impingement shock crosses the station $x = -0.75\ d$ at $z_{tp} = -0.24\ d$. The pressure begins to increase in the vicinity of the shock, attains a maximum value of $p = 1.56\ p_{o2}$ in the region below the shock, and then decreases as the reverse flow region is approached (cf. Figs. 28 and 33). The maximum measured pressure is slightly less than the calculated value ($p = 1.62\ p_{o2}$) for the flow behind (below) the impingement shock; we attribute this difference to an expansion of the flow downstream of the impingement shock.

The calculated value was arrived at (as described below) neglecting viscous losses and assuming a straight dividing streamline between the reverse flow region and the flow behind the impingement shock. Careful examination of the profile flow photographs (e.g., Figs. 3, 12, and 26) reveals that the dividing streamline appears to bend downward, presenting a convex shape to the separated flow and thereby causing it to expand. An expansion of just 1.7 degrees would reduce the calculated pitot pressure value to the measured value. The expansion of the separated flow is also reflected in the decrease of the surface pressure from $2.5\ p_1$ at $x = -1.40\ d$ to $1.85\ p_1$ at $x = -0.75\ d$ (cf. Fig. 11).

The maximum pressure in the separated flow region is further reduced for the further downstream profiles. At $x = -0.40\ d$, the maximum pressure is $1.48\ p_{o2}$; this corresponds to a further expansion of 2.0 degrees from the value at station $x = -0.75\ d$. From Fig. 11, the surface pressure is a minimum, approximately $1.5\ p_1$, at $x = -0.40\ d$. The lower portions of the downstream profiles extend further below the dividing streamline than for the upstream profiles (cf. Figs. 28 and 33). At $x = -0.40\ d$, the minimum pitot pressure is $0.55\ p_{o2}$ at $z_{tp} = -0.64\ d$; this point is in the shear layer, well below the dividing streamline.

In comparison to the larger probe diameter (shown in the first part of Fig. 33), the pressure gradients along the profiles are quite steep. Most of the pressure rise across the impingement shock occurs within one larger probe diameter.

The profiles between the fin leading edge and bow shock ($0 \geq x \geq -0.35$ d) exhibit a local peak pressure that falls within the narrow jet-type flow region sketched in Fig. 28. The width of this region is comparable to the smaller probe diameter (shown in the third part of Fig. 33). The pitot pressure along the profile at $x = -0.20$ d starts to rise at $z_{tp} = +0.06$ d, reaches a maximum ($p = 1.50\ p_{o2}$) at $z_{tp} = -0.08$ d, drops to $1.40\ p_{o2}$ at $z_{tp} = -0.12$ d, decays to $1.20\ p_{o2}$ at $z_{tp} = -0.47$ d, and then drops to $0.37\ p_{o2}$ at $z_{tp} = -0.64$ d.

A unique feature of the profile immediately ahead of the fin leading edge, at $x = -0.05$ d, is the decreased pressure above the triple point location. The pressure measured by the pitot probe was less than p_{o2} for $z_{tp} > 0.03$ d; the pitot pressure was approximately equal to $0.86\ p_{o2}$ for $0.06\ d < z_{tp} < 0.24\ d$, and then approached p_{o2} for larger z_{tp} values; whereas on the fin leading edge ($z_{tp} = 0$), the pressure remains larger than p_{o2} for all positive z_{tp} values. We attribute this to the local flow being severely deflected (probe misalignment) just before stagnating on the leading edge. The local pressure peaks and dips along the fin leading edge resemble those plotted by Edney (Ref. 35, page 46) and attributed to local expansions and compressions in the vicinity of impingement of the jet on the leading edge.

Flow Field Calculations

The flow field in the center plane ahead of the fin can be reasonably well approximated by using two dimensional oblique shock

relations. If one assumes a straight dividing streamline, the turbulent separation peak pressure rise for $M_\infty = 3$ is (Eq. (1)) $p = 2.68\ p_1$. Oblique shock relations then give the corresponding flow deflection angle (14.2 degrees), the impinging shock angle (31.4 degrees), the Mach number of the separated flow (2.30), and the pitot total pressure of the separated flow ($p_{op} = 1.62\ p_{o2}$). Part of this separated flow passes through another oblique shock wave, which emanates from the triple point (cf. Fig. 5), and forms a small jet flow embedded in the subsonic flow region behind the fin bow shock (cf. Figs. 5 and 28). Requiring the jet flow direction and pressure to be the same as the flow direction and pressure behind the bow shock, oblique shock relations are solved iteratively to obtain the initial directions of the dividing streamline and shock wave that emanate from the triple point. These directions, 10.3 and 39.3 degrees with respect to the free stream direction, are plotted in Fig. 34, and the Mach number, static pressure, and pitot pressure values are indicated for each flow region.

The expansion of the separated flow, described on page 32, reduces the separated flow deflection from 14.2 to 10.5 degrees in the vicinity of the triple point. As shown in Fig. 34b, this results in a greater jet flow deflection (dividing streamline angle of 17.2 degrees and shock wave angle of 45.7 degrees with respect to the free stream). These values are considerably closer to the measured values obtained from schlieren photographs (19.5 and 51.5 degrees, respectively, cf. Fig. 34c). The measured deflection angle ($19.5^\circ + 10.5^\circ = 30.0^\circ$) with respect to the separated flow) just exceeds the maximum value (29.5°) for the weak attached shock wave solution for Mach 2.48 flow. Therefore, the shock emanating from the triple point is a strong shock for the separated flow and substantially reduces the total pressure in the

jet flow. The maximum measured pitot pressure ($1.50\ p_{o2}$) in the jet flow is much less than the value calculate for the weak shock solution ($2.01\ p_{o2}$); the measured pressure corresponds to a Mach 0.93 jet flow (cf. Fig. 34).

Edney et al. (Ref. 34) also observed a greater jet flow deflection than calculated using the inviscid analysis. They attribute the additional 2 to 3 degrees deflection to the displacement thickness growth of the viscous shear layer at the edge of the jet flow. Although a displacement correction of 2 to 3 degrees brings the values calculated inviscidly into good agreement with the measured values (for the present Mach 3 experiments as well as for the Mach 6 and 20 experiments conducted by Edney et al.), this displacement correction is, unfortunately, purely empirical. For the present case, shown in Fig. 34, the calculated displacement growth of the free shear layer is quite small, less than one degree.[†]

The flow field calculations in the vicinity of the triple point, described above, are just part of the calculations required to determine the conditions throughout the extent of the embedded jet flow. Referring to Fig. 5, if the initial flow in the jet is supersonic, then another shock wave emanates from the point "Q". The shock wave emanating from this point, similar to the one from the triple point, is solved by requiring the pressure and direction of the jet flow to equal those in the subsonic flow region below the jet. The remainder of the flow is solved using characteristics up to the normal shock in the jet. The flow in this embedded jet is thus compressed through many weak shock waves and, therefore, as noted by Hains and Keyes (Ref. 33), "the total

[†]Similar profile, integral equations derived by Wilbur Hankey, Aerospace Research Laboratories, September 1971, private communication.

pressure remains high right up to the body surface." This becomes increasingly important for higher Mach number flows.

Hains and Keyes also point out that the peak pressure and heating rate depend strongly on the entire bow shock pattern. The number of oblique shocks in the jet flow, and hence the peak pressure experienced on the fin leading edge, depend on the location of the point "Q" (Fig. 5), and this location is indeterminate (cf. page 6). An upper limit to the peak pressure can be calculated by assuming isentropic compression of the jet flow downstream of the shock wave emanating from point "Q". However, this can be considerably larger than the total pressure downstream of a normal shock wave in the jet flow, particularly at higher Mach numbers. The location of this normal shock wave, the location of the point "Q", and an accurate determination of the jet flow deflection at the triple point, are still required before this problem can be considered solved. Further, Reynolds number effects are expected to be important for the shear layers bounding the embedded jet flow.

Probe Generated Shock Impingement

As mentioned on page 21, the probe generated shock impingement led to particularly large peak pressures on the fin leading edge, and a substantially different interaction flow field than that resulting from shock impingement caused by boundary layer separation (cf. Figs. 29 and 30). The probe shock wave impinges on the fin bow shock, and the reflected shock wave apparently impinges on the fin leading edge. No bow shock is visible ahead of the lower portion of the fin (the portion behind the probe shock) for these cases (Fig. 30). The flow is similar, in some aspects, to the flows over blunt axisymmetric bodies with spikes protruding from their leading edges, which were investigated many years ago by

Bogdonoff and Vas (Ref. 64) and several others. They observed that the flow separated from the leading edge of the spike, for spike lengths comparable to the body diameter, and reattached near the shoulder of the blunt body. This effectively streamlined the blunt body and greatly reduced its drag (Ref. 64). They also observed an instability of the flow, similar to that shown in Fig. 2b.

Comparable to the spike-body results, we postulate that the flow separated from the probe leading edge, formed a conical region of reverse flow, and reattached on the fin leading edge. Part of the flow above this conical "dead air" region passes through the strong shock wave emanating from the triple point and stagnates on the fin leading edge. In Fig. 30, it appears that the jets that form behind the triple point are deflected slightly upward in these cases. The probe shock wave angles were measured and oblique shock relations were used to calculate flow field parameters in the vicinity of the triple point, similar to the flow field calculations described above. For these cases, the calculated maximum pitot pressures in the jet flows vary from $1.7\ p_{o2}$ to $1.9\ p_{o2}$. Although these approximate the maximum pressures measured on the fin leading edge (cf. Fig. 30), the interaction flow does not match any of those categorized by Edney et al. (Refs. 34-36), and only very limited data were obtained for these "off-design" cases. No further conclusions should be drawn concerning probe-generated shock impingement without a more thorough analysis of this type of interaction flow field.

CONCLUSIONS AND RECOMMENDATIONS

"Self-induced" shock impingement, caused by turbulent boundary layer separation ahead of blunt fins, results in a complex, three dimensional, viscous-inviscid interaction flow field. The pressure rise across the fin bow shock causes the boundary layer to separate from the adjacent surface ahead of the fin. The separated flow region is composed of horseshoe shaped vortices that scavenge part of the oncoming stream flow and spiral downstream very rapidly. Shock waves emanate from the separation location and impinge on the fin bow shock, resulting in a lambda-type shock interaction pattern in the plane of symmetry ahead of the fin. A small jet of relatively high energy flow is formed where the two shocks intersect, and impinges on the fin leading edge.

The major effects of the interaction are an increased load on the surface and intense pressures and heating rates in small regions on the fin leading edge and on the surface in the immediate vicinity of the fin leading edge. The extent of separated flow ahead of the fin is proportional to the fin diameter for fins that are thicker than the local undisturbed boundary layer. Turbulent boundary layer separation occurs approximately two diameters ahead of the fin and is insensitive to Mach number, Reynolds number, and boundary layer thickness for a very wide range of test conditions (Mach numbers from 1.2 to 21). Laminar boundary layer separation is considerably more extensive than turbulent separation, and depends on Mach number and Reynolds number. The pressure rises are similar to those ahead of forward facing steps and approach the two dimensional laminar plateau or turbulent peak pressure values.

Although the extent of separation and pressure distributions on the plate surface have been obtained from many experiments, no systematic force measurements or calculations have been made to determine the over-all increased load on the plate caused by the interaction. For turbulent separation, this increased load is expected to scale with fin diameter (for $d > \delta$) and simply be a function of Mach number. Limited force tests would serve as a comparison for integrating existing pressure distributions, and thus be most useful in determining a relationship for the increased load.

The separated flow ahead of the fin is highly unstable. The oscillation of the separation point about its mean position, and the fluctuating pressures ahead of the fin, are an order of magnitude greater than for two dimensional separated flows. The amplitude of the oscillation of the separation point is particularly large when separation occurs in the vicinity of transition for the undisturbed boundary layer.

The vortices bring high energy stream flows into proximity with the surface, resulting in extremely high pressures and heating rates on the surface in the immediate vicinity of the fin foot. In this small region, surface pressures approaching the pitot pressure of the free stream flow, and heating rates exceeding 10 times the undisturbed surface values, have been measured. Because of the extreme gradients, more detailed pressure and heat transfer measurements are required to determine the maximum peak pressures and heating rates that can occur in this region.

Shock impingement caused by turbulent boundary layer separation ahead of unswept fins generally results in the type of interaction that leads to the greatest pressure and heat transfer rate

amplifications on the fin leading edge. It is important to include the convex shape of the dividing streamline, which results in an expansion of the separated flow, in calculating the direction of the slip line emanating from the triple point. In the present Mach 3 experiments, the measured slip line was displaced 2 degrees from its inviscidly calculated position. This displacement was just sufficient to result in a strong shock wave from the triple point with attendant large pressure losses in the embedded jet flow. It would be extremely valuable to repeat the experiments at a higher free stream Mach number to ensure having an attached, weak shock emanating from the triple point, and hence, an initially supersonic embedded jet flow.

Although features of the interaction are understood fairly well, and upper limits for the maximum attainable pressures can be ascribed using an inviscid analysis, the measured peak pressures are substantially less than these calculated values. The reduction has been attributed to viscous effects, but as yet there is no rational theory that adequately accounts for these effects. The experiments recommended in this section, along with a careful review of existing data from other sources, are suggested as an approach to developing empirical corrections to the inviscid analysis. The resulting engineering method could be used reliably to predict accurately the peak pressures and heating rates caused by self-induced shock impingement resulting from turbulent boundary layer separation.

REFERENCES

1 Korkegi, R., "Survey of Viscous Interactions Associated with High Mach Number Flight," AIAA Journal, Vol. 9, No. 5, May 1971.

2 Ryan, B., Summary of the Aerothermodynamic Interference Literature, Naval Weapons Center TN4061-160, April 1969.

3 Kaufman, L. II, Meckler, L., and Hartofilis, S., "An Investigation of Flow Separation and Aerodynamic Controls at Hypersonic Speeds," J. Aircraft, Vol. 3, No. 6, November 1966.

4 Kaufman, L. II, et al., An Investigation of Hypersonic Flow Separation and Control Characteristics, AFFDL TR 64-174, January 1965.

5 Kaufman, L. II, Pressure Distributions and Oil Film Photographs for Mach 5 Flows Past Fins Mounted on a Flat Plate, ASD-TDR 63-755, September 1963.

6 Kaufman, L. II and Meckler, L., Pressure and Heat Transfer Measurements at Mach 5 and 8 for a Fin Flat Plate Model, ASD-TDR 63-235, April 1963.

7 Young, F., Kaufman, L. II, and Korkegi, R., Experimental Investigation of Interactions between Blunt Fin Shock Waves and Adjacent Boundary Layers at Mach Numbers 3 and 5, ARL 68-0214, December 1968.

8 Uselton, J., Fin Shock/Boundary-Layer Interaction Tests on a Flat Plate with Blunted Fins at M_∞ = 3 and 5, AEDC TR 67-113, June 1967.

9 Lucas, E., Investigation of Blunt Fin-Induced Flow Separation Region on a Flat Plate at Mach Numbers 2.5 to 4.0, AEDC TR 70-265, January 1971.

10 Hill, W. Jr., A Comparison of Theory and Experiment for Laminar Separation Ahead of a Compression Corner at Supersonic and Low Hypersonic Speeds, Grumman Research Department Report RE-401, December 1970.

11 Zukoski, E., "Turbulent Boundary-Layer Separation in Front of a Forward-Facing Step," AIAA Journal, Vol. 5, No. 10, October 1967.

12 Robertson, J., Characteristics of the Static and Fluctuating Pressure Environments Induced by Three Dimensional Protuberances at Transonic Mach Numbers, NASA CR 102269, June 1969.

13 Robertson, J., Fluctuating Pressures Induced by Three Dimensional Protuberances, Wyle Laboratories Report WR-70-10, April 1970.

14 Winkelmann, A., Flow Visualization Studies of a Fin Protuberance Partially Immersed in a Turbulent Boundary Layer at Mach 5, NOL TR 70-93, May 1970.

15 Price, E. Jr. and Stallings, R. Jr., Investigation of Turbulent Separated Flows in the Vicinity of Fin-Type Protuberances at Supersonic Mach Numbers, NASA TND-3804, February 1967.

16 Couch, L., Flow-Field Measurements Downstream of Two Protuberances on a Flat Plate Submerged in a Turbulent Boundary Layer at Mach 2.49 and 4.44, NASA TND-5297, July 1969.

17 Avduyevskii, V. et al., The Physical Properties of a Flow in the Separation Region for the Three-Dimensional Interaction of the Boundary Layer with a Shock Wave, RAE Library Translation 1342, January 1969.

18 Glagolev, A., Zubkov, A., and Panov, Yu, A., Supersonic Flow over an Obstacle in the Form of a Gas Jet on a Plate, Johns Hopkins University, APL Translation 2155, July 1968.

19 Voitenko, D., The Existence of Supersonic Zones in Three-Dimensional Separated Flow Regions, RAE Library Translation 1302, May 1968.

20 Kaufman, L. II, Leng, J., and Johnson, A., Exploratory Tests Using Temperature-Sensitive Paints to Obtain Hypersonic Heat Transfer Data on Spheres and on Fin-Plate Models, Grumman Research Memorandum RM-487, September 1970.

21 Hiers, R. and Loubsky, W., Effects of Shock-Wave Impingement on the Heat Transfer on a Cylindrical Leading Edge, NASA TND-3859, February 1967.

22 Couch, L., Stallings, R. Jr., and Collins, I., Heat-Transfer Measurements on a Flat Plate with Attached Protuberances in a Turbulent Boundary Layer at Mach Numbers of 2.49, 3.51, and 4.44, NASA TND-3736, December 1966.

23 Surber, T., "Heat Transfer in the Vicinity of Surface Protuberances," Journal of Spacecraft and Rockets, Vol. 2, No. 6, November 1965, pp. 978-980.

24 Truitt, R., "Hypersonic Turbulent Boundary Layer Interference Heat Transfer in Vicinity of Protuberances," AIAA Journal, Vol. 3, No. 9, September 1965, pp. 1754-175[illegible].

25 Burbank, P., Newlander, D., and Collins, I., Heat Transfer and Pressure Measurements on a Flat Plate Surface and Heat Transfer Measurements on Attached Protuberances in a Supersonic Turbulent Boundary Layer at Mach Numbers of 2.65, 3.51, and 4.44, NASA TND-1372, December 1962.

26 Panov, Yu, A , Shape of the Separated Flow Region Caused by Supersonic Flow Past a Cylindrical Obstacle, Moskovskii Universitet, Vestnik, Seriia I-Matematika-Mekhanika, January 1969.

27 Voitenko, D., Influence of Mach Number on Flow in a Three-Dimensi nal Separated Flow Region, Johns Hopkins University, APL-CLB 3T-567, September 1968.

28 Voitenko, D., Zubkov, A., and Panov, Yu, A., Supersonic Gas Flow Past a Cylindrical Protuberance on a Plate, Johns Hopkins University, APL Translation TG 230-T515, January 1967.

29 Thomas, J., Flow Investigation about a Fin Plate Model at a Mach Number of 11.26, ARL Report 67-0188, September 1967.

30 Korkegi, R., "Effect of Transition on Three-Dimensional Shock-Wave/Boundary-Layer Interaction," AIAA Journal, Vol. 10, No. 3, March 1972.

31 Goldman, R., Morkovin, M., and Schumacher, R., "Unsteady Control Surface Loads of Lifting Re-Entry Vehicles at Very High Speeds," AIAA Journal, Vol. 6, No. 1, January 1968, pp. 44-50.

32 Holden, M., "Shock Wave-Turbulent Boundary Layer Interaction in Hypersonic Flow," AIAA Paper 72-74, January 1972.

33 Hains, F. and Keyes, J., "Shock Interference Heating in Hypersonic Flows," AIAA Paper 72-78, January 1972.

34 Edney, B., Bramlette, T., Ives, J., Hains, F., and Keyes, J., Theoretical and Experimental Studies of Shock Interference Heating, Bell Aerospace Company Report 9500-920-195, October 1970.

35 Edney, B., Anomalous Heat Transfer and Pressure Distributions on Blunt Bodies at Hypersonic Speeds in the Presence of an Impinging Shock, Aeronautical Research Institute of Sweden Report 115, February 1968.

36 Edney, B., "Effects of Shock Impingement on the Heat Transfer around Blunt Bodies," AIAA Journal, Vol. 6, No. 1, January 1968.

37 Bushnell, D., Effects of Shock Impingement and other Factors on Leading-Edge Heat Transfer, NASA TND-4543, April 1968.

38 Newlander, R., Effect of Shock Impingement on the Distribution of Heat Transfer Coefficients on a Right Circular Cylinder at Mach Numbers of 2.65, 3.51, and 4.44, NASA TND-642, 1961.

39 Knox, E., Measurements of Shock-Impingement Effects on the Heat Transfer and Pressure Distributions on a Hemicylinder Model at Mach Number 19, AEDC TR 65-245, November 1965.

40 Ray, A. and Palko, R., An Investigation of the Effects of Shock Impingement on a Blunt Leading Edge, AEDC TR 65-153, July 1965.

41 Francis, W., "Experimental Heat-Transfer Study of Shock Impingement on Fins in Hypersonic Flow," AIAA J. of Spacecraft, Vol. 2, No. 4, July 1965, pp. 630-632.

42 Siler, L. and Deskins, H., Effect of Shock Impingement on the Heat Transfer and Pressure Distributions on a Cylindrical Leading Edge Model at Mach Number 19, AEDC TDR 64-228, November 1964.

43 Meyer, R., Rocket Experiments on the Heat Transfer to a Protuberance and to a Cavity, National Research Council of Canada, NAE LR-509, July 1968.

44 Carter, H. and Carr, R., Free-Flight Investigation of Heat Transfer to an Unswept Cylinder Subjected to an Incident Shock and Flow Interference from an Upstream Body at Mach Numbers up to 5.50, NASA TND-988, October 1961.

45 Kessler, W., Reilly, J., and Sampatcos, E., Hypersonic Shock Wave Interaction and Impingement, McDonnell Douglas Report E0427, July 1971.

46 Rogers, C., Experimental Investigation of Leading-Edge Shock Impingement and Interaction Heating on a 1/80 Scale Model of a NASA Straight Wing Orbiter Configuration at Mach Numbers 8 and 16, CAL Report AA-2977-Y-1, August 1971.

47 Fontenot, J. Jr., "A Method of Estimating the Effect of Shock Interaction on Stagnation Line Heating," AIAA Journal, Vol. 3, No. 3, March 1965, pp. 562-564.

48 Jones, R., Heat Transfer and Pressure Investigation of a Fin-Plate Interference Model at a Mach Number of 6, NASA TND-2028, 1964.

49 Beckwith, I., Experimental Investigation of Heat Transfer and Pressure on a Swept Cylinder in the Vicinity of its Intersection with a Wedge and Flat Plate at Mach Number 4.15 and High Reynolds Numbers, NASA TND-2020, 1964.

50 Rhudy, J., Hiers, R., and Pippey, J., Pressure Distribution and Heat Transfer Tests on Two Fin-Flat Plate Interference Models and Several Blunt Leading Edge Delta Wing Models, AEDC TN60-168, September 1960.

51 Westkaemper, J., "Turbulent Boundary-Layer Separation Ahead of Cylinders," AIAA Journal, Vol. 6, No. 7, July 1968.

52 Sykes, D., "The Supersonic and Low Speed Flows Past Circular Cylinders of Finite Length Supported at One End," Journal of Fluid Mechanics, Vol. 12, Part 2, March 1962, pp. 367-387.

53 Waltrup, P., Hall, D., and Schetz, J., "Flow Field in the Vicinity of Cylindrical Protuberances on a Flat Plate in Supersonic Flow," AIAA J. of Spacecraft, Vol. 5, No. 1, January 1968.

54 Miller, W., Pressure Distributions on Single and Tandem Cylinders Mounted on a Flat Plate in Mach Number 5.0 Flow, APL/JHU Report CR-25, (University of Tex.Report DRL-538), June 1966.

55 Lucero, E., Turbulent Boundary Layer Separation Induced by Three Dimensional Protuberances, Johns Hopkins University APL Report TG 1094, January 1970.

56 Whitehead, A. Jr., Flow Field and Drag Characteristics of Several Boundary Layer Tripping Elements in Hypersonic Flow, NASA TND 5454, October 1969.

57 AEDC Staff, Test Facilities Handbook, AEDC, 8th ed., December 1969.

58 Pate, S. and Schueler, C., "Radiated Aerodynamic Noise Effects on Boundary-Layer Transition in Supersonic and Hypersonic Wind Tunnels," AIAA Journal, Vol. 7, No. 3, March 1969.

59 Eckstrom, D., Engineering Analysis of Boundary Layers and Skin Friction on Bodies of Revolution at Zero Angle of Attack, Lockheed Missiles and Space Corporation Report LMSC/805162, May 1965.

60 Moretti, G., Inviscid Blunt Body Shock Layers, PIBAL Report 68-15, June 1968.

61 Hayes, W. and Probstein, R., "Hypersonic Flow Theory - I - Inviscid Flows," Academic Press, New York, 2nd ed., 1966.

62 Sedney, R., Private Communication, Research Institute for Advanced Studies, Martin Marietta Corporation, August 1970.

63 Sterrett, J. and Emery, J., Extension of Boundary-Layer Separation Criteria to a Mach Number of 6.5 by Utilizing Flat Plates with Forward-Facing Steps, NASA TND-618, 1960.

64 Bodgonoff, S. and Vas, I., "Preliminary Investigations of Spiked Bodies at Hypersonic Speeds," Jr. Aero/Space Sciences, Vol. 26, No. 2, February 1959.

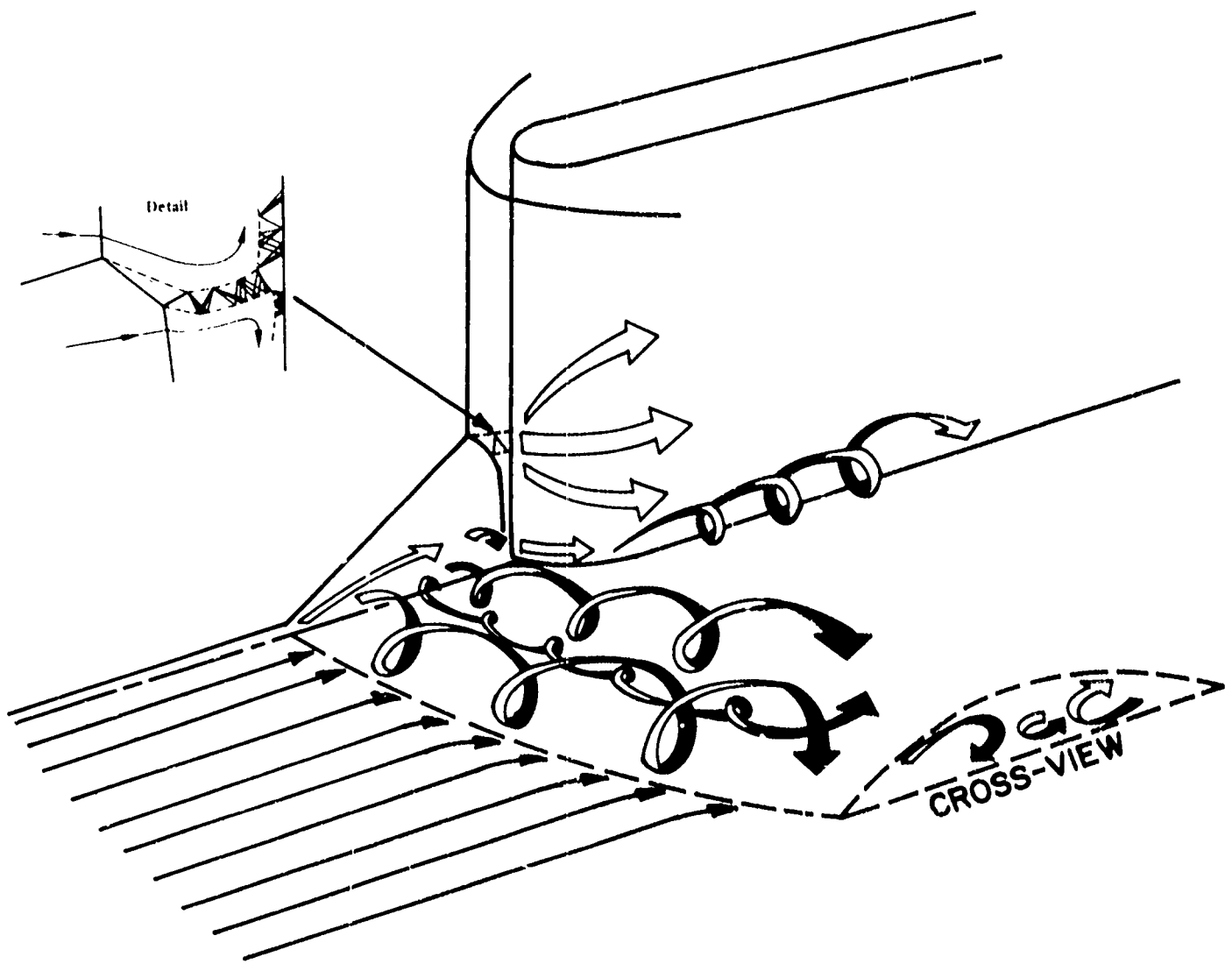

Fig. 1 Sketch of Interaction Flow Field

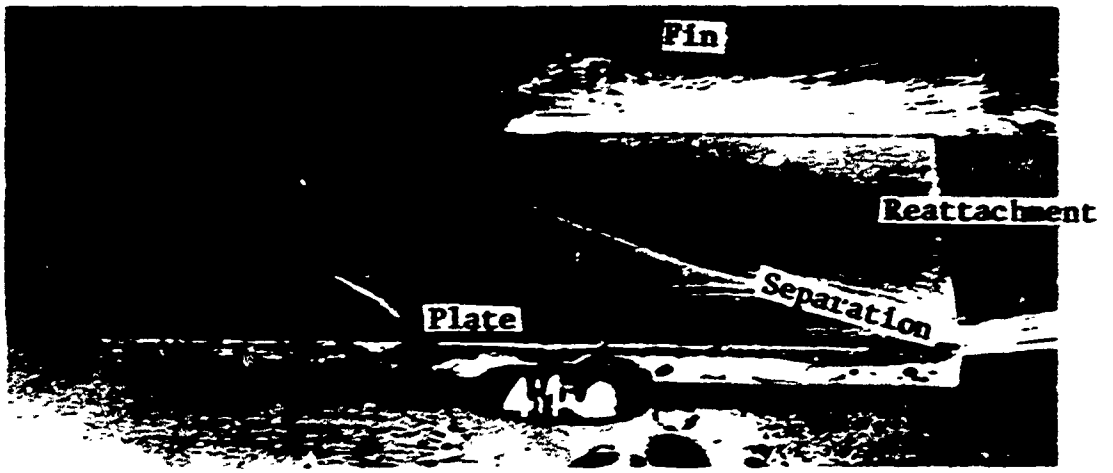

a) Over-all View

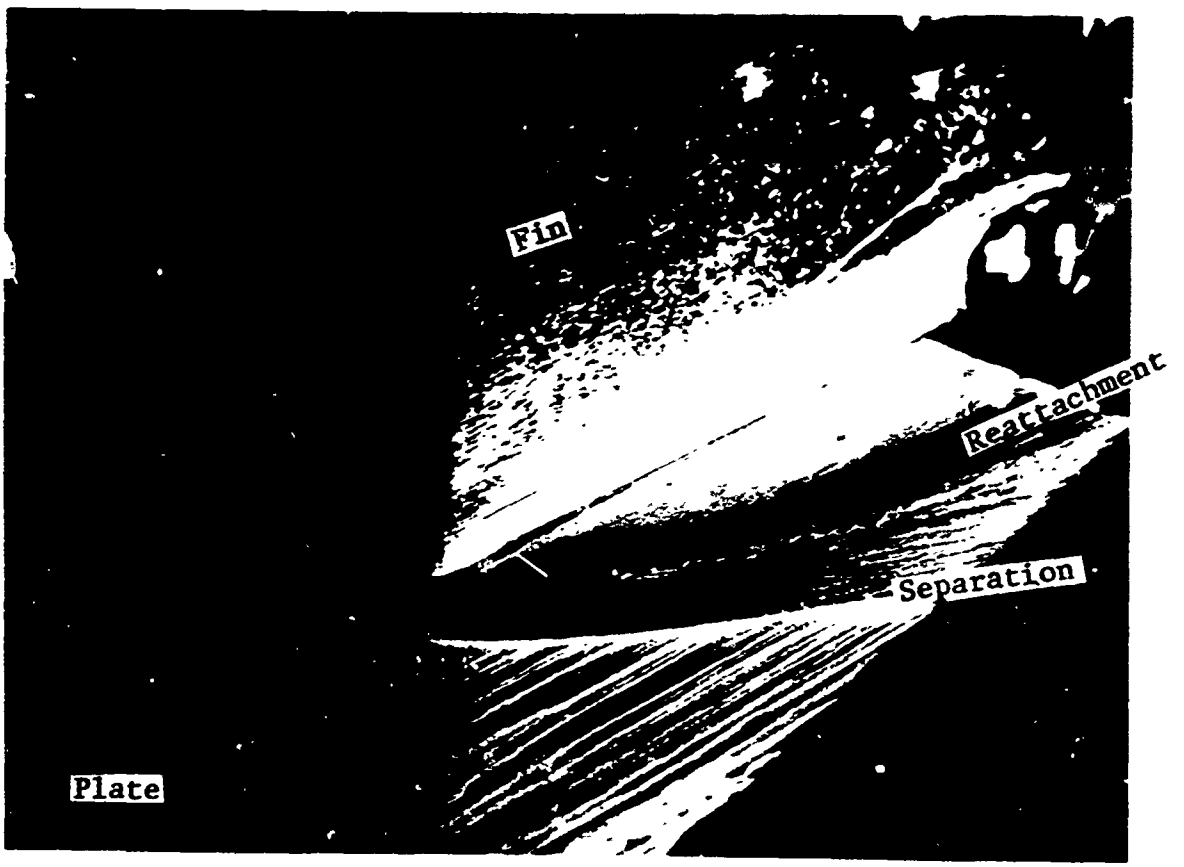

b) Closeup of Region Near Fin Foot

Fig. 2 Oil Film Flow Photographs; $M_\infty = 4$, d = 3/8

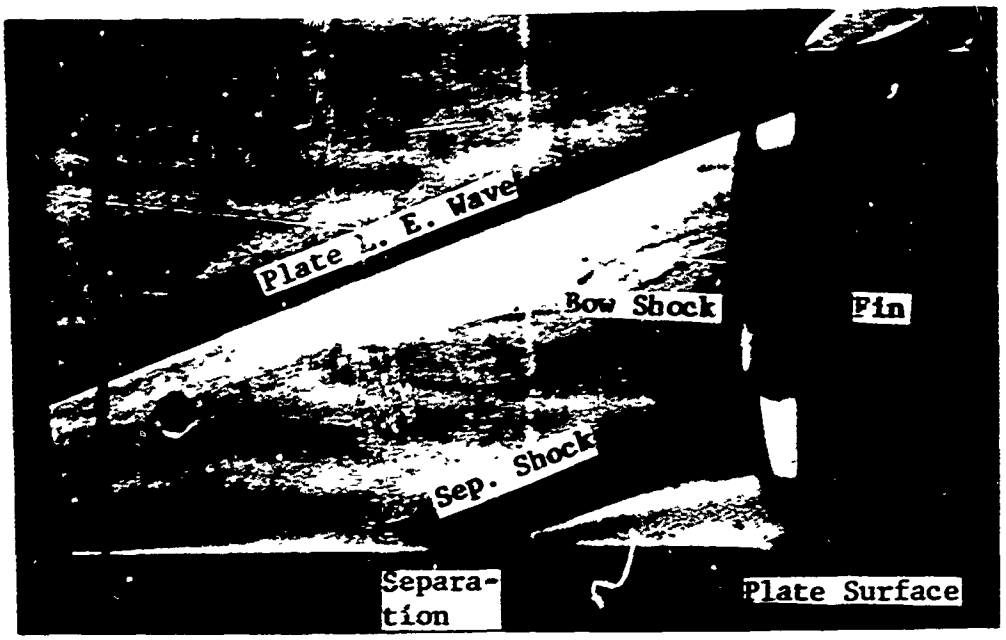

a) Schlieren Photograph

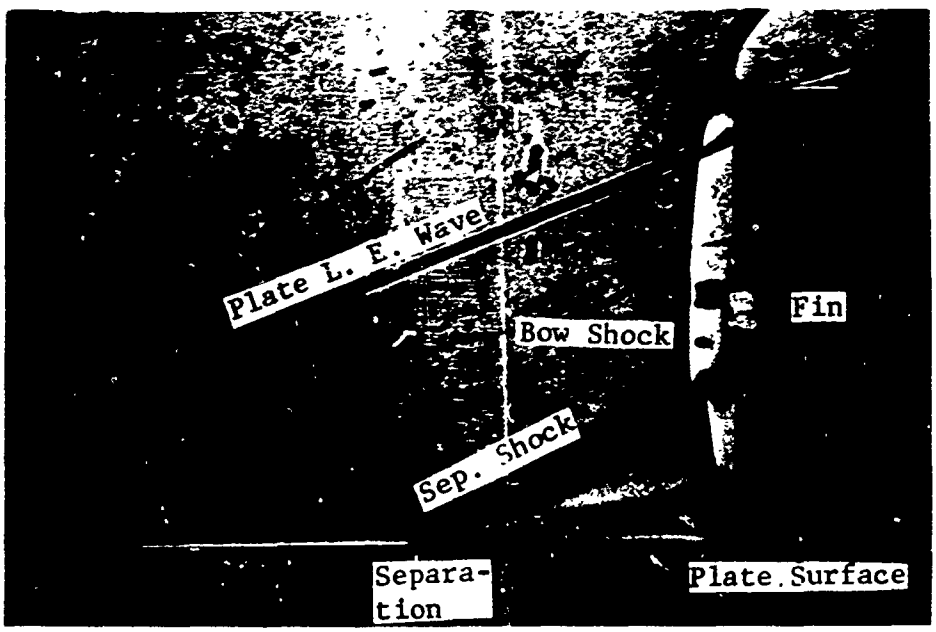

b) Shadowgraph Photograph

Fig. 3 Profile Flow Photographs, One Millisecond Exposure, $M_\infty = 3$, d = 1

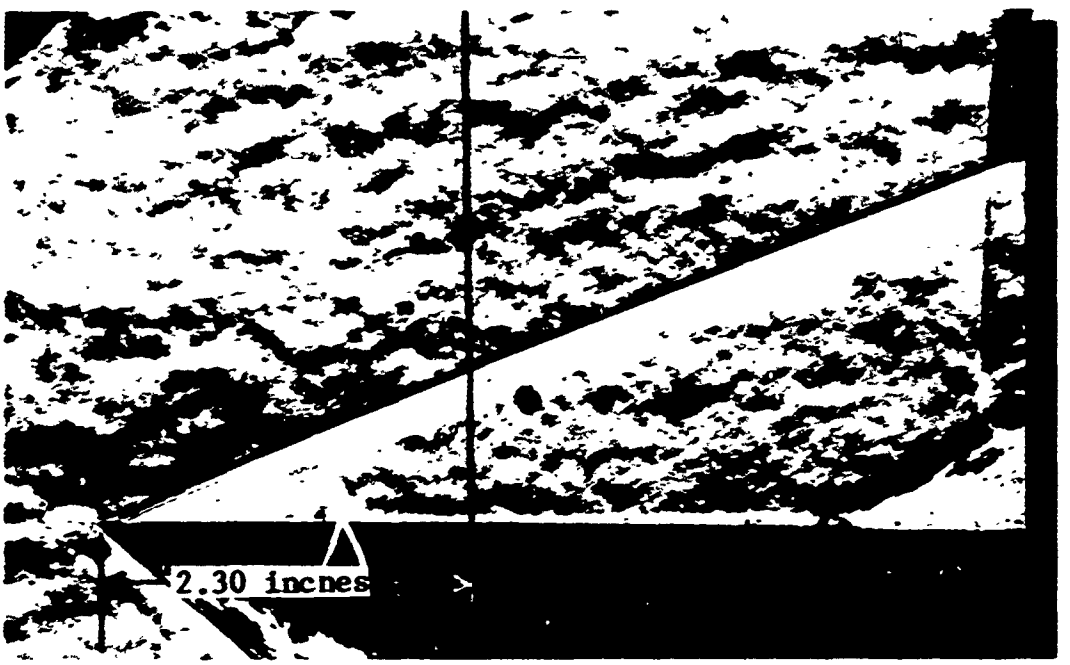

a) Flow Photograph

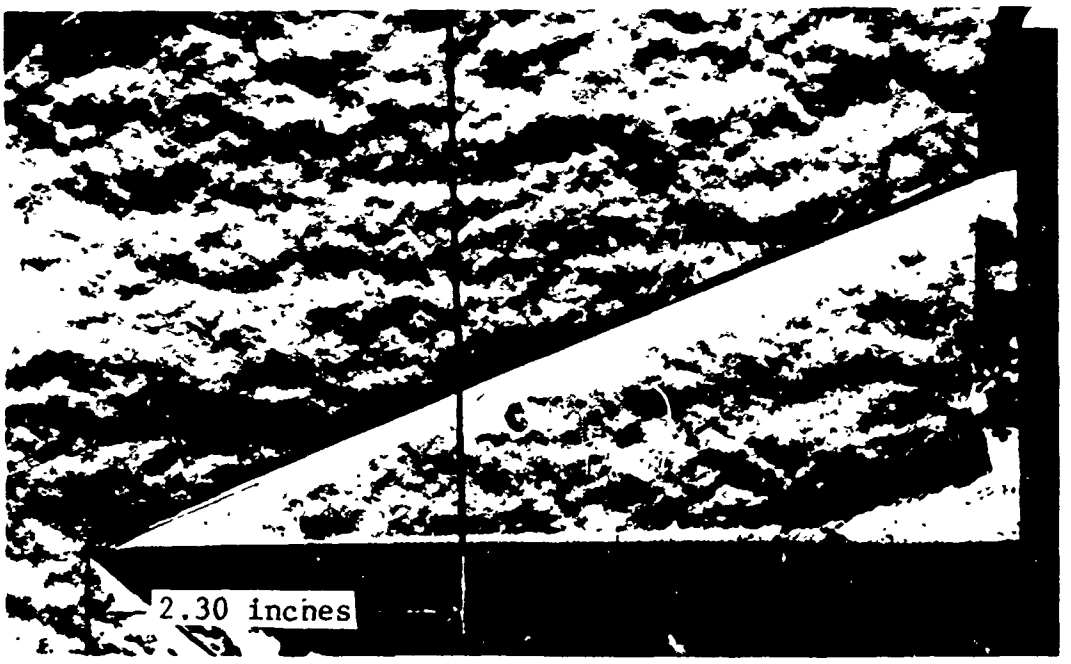

b) Photograph Taken a Few Seconds After That Shown in a) Above

Fig. 4 Schlieren Flow Photographs Taken a Few Seconds Apart During Same Tunnel Run; One Microsecond Exposure, $M_\infty = 3$, $d = 3/4$, Fin L.E. 5.73 inches Downstream of Plate L.E.

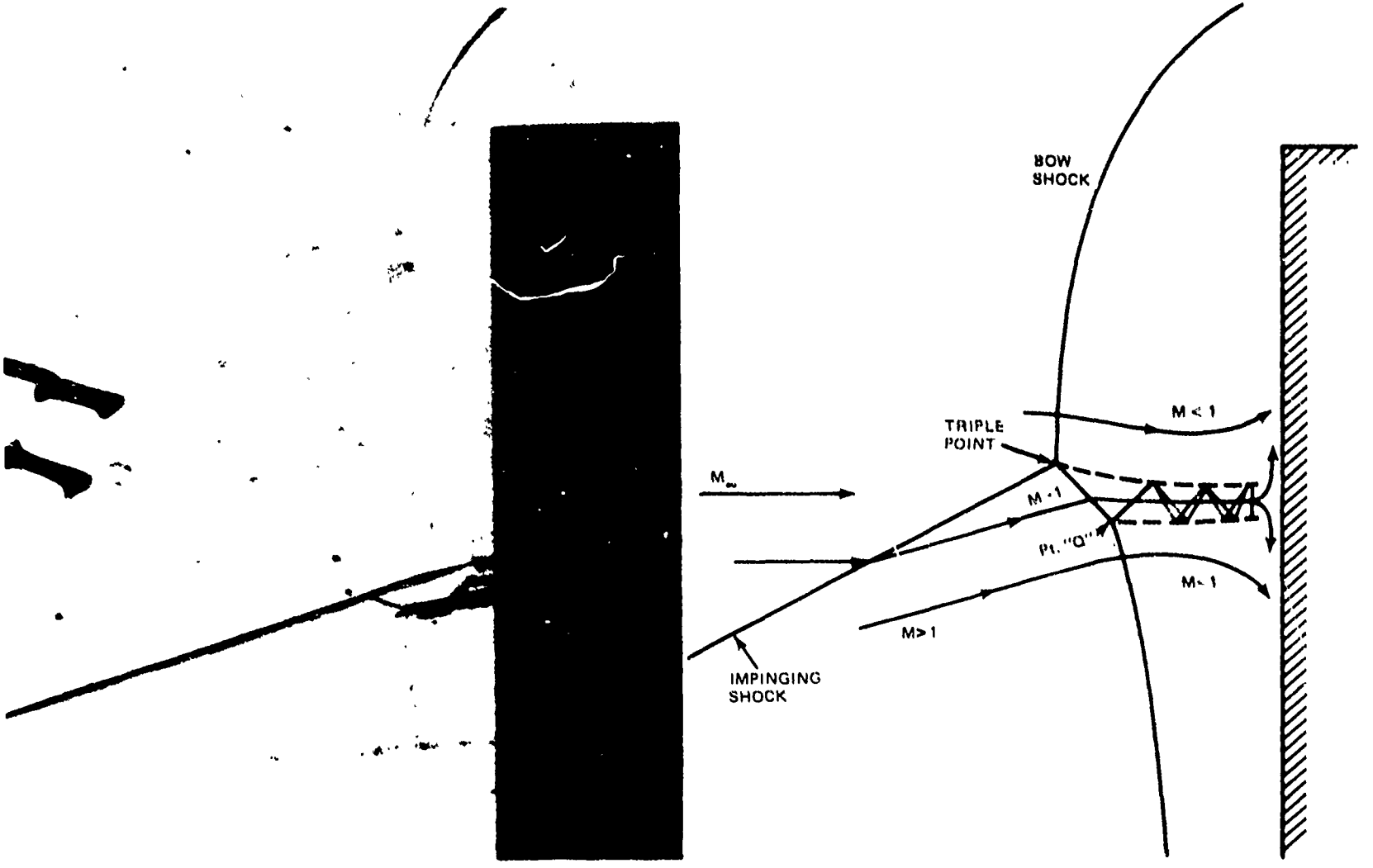

Fig. 5 Schlieren Flow Photograph and Sketch Showing Details of Shock Impingement Region; $M_\infty = 4.6$, from Edney (Ref. 35)

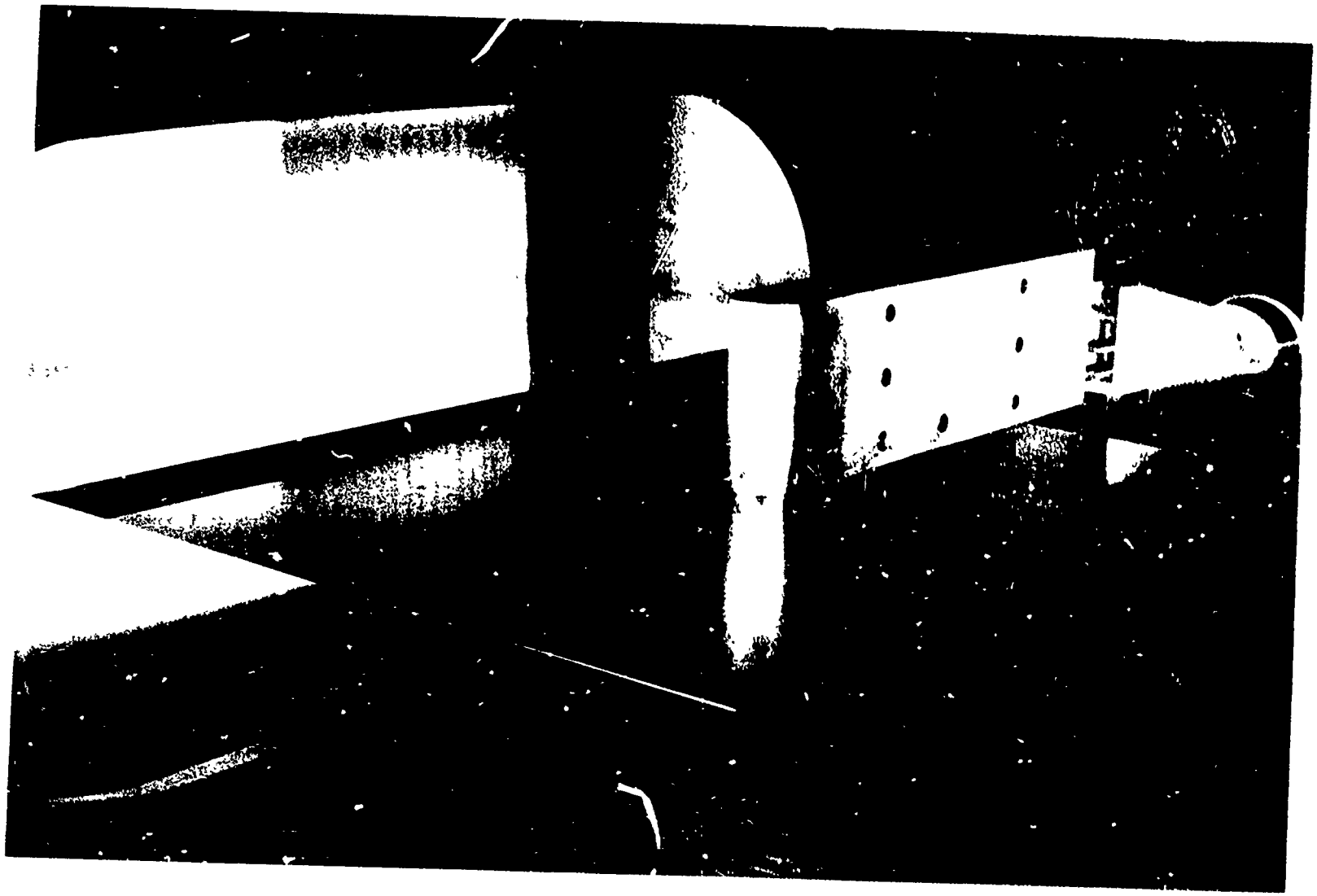

Fig. 6 Photograph of Model with Larger Probe Extended

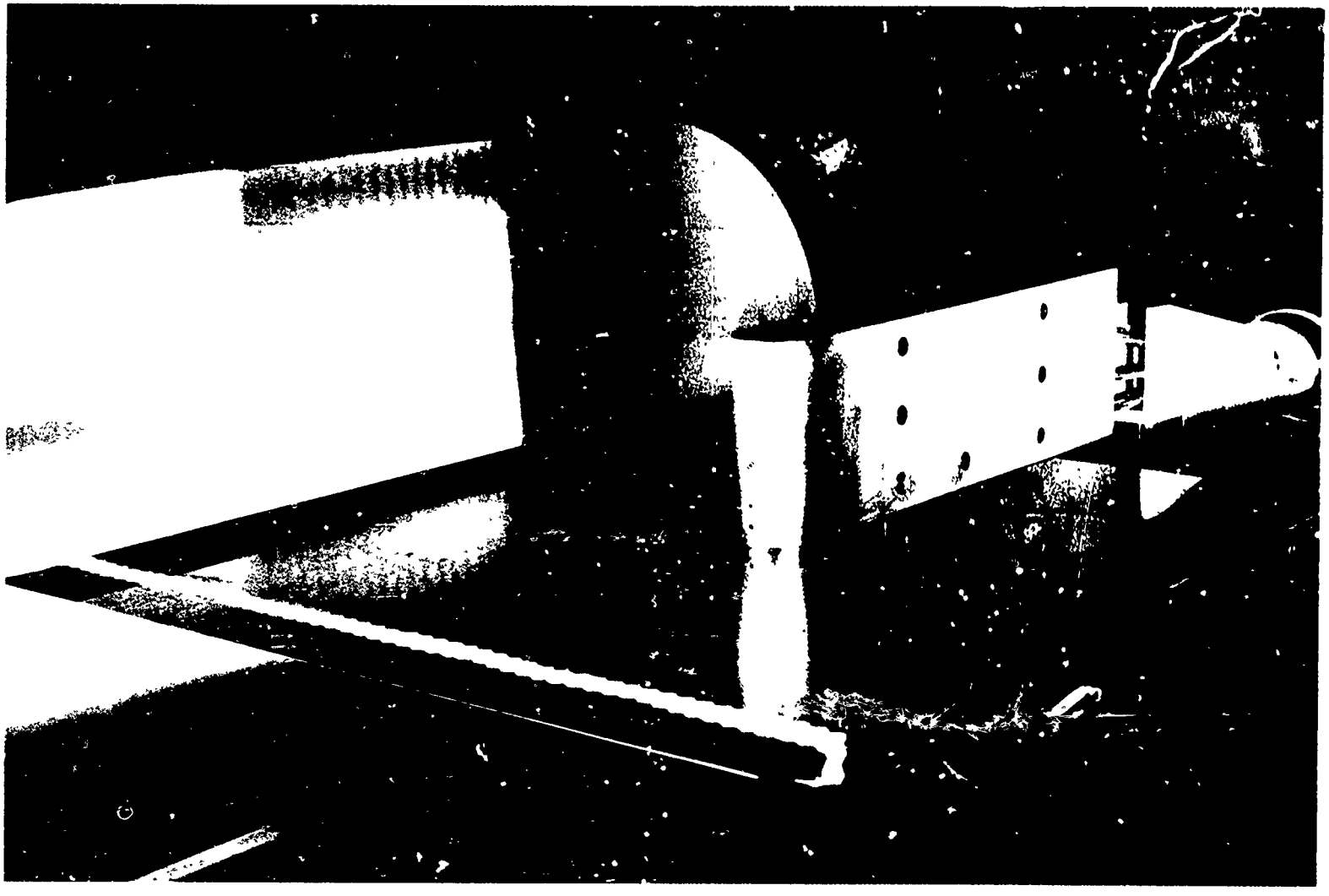

Fig. 7 Photograph of Mcdel with Boundary Layer Trip

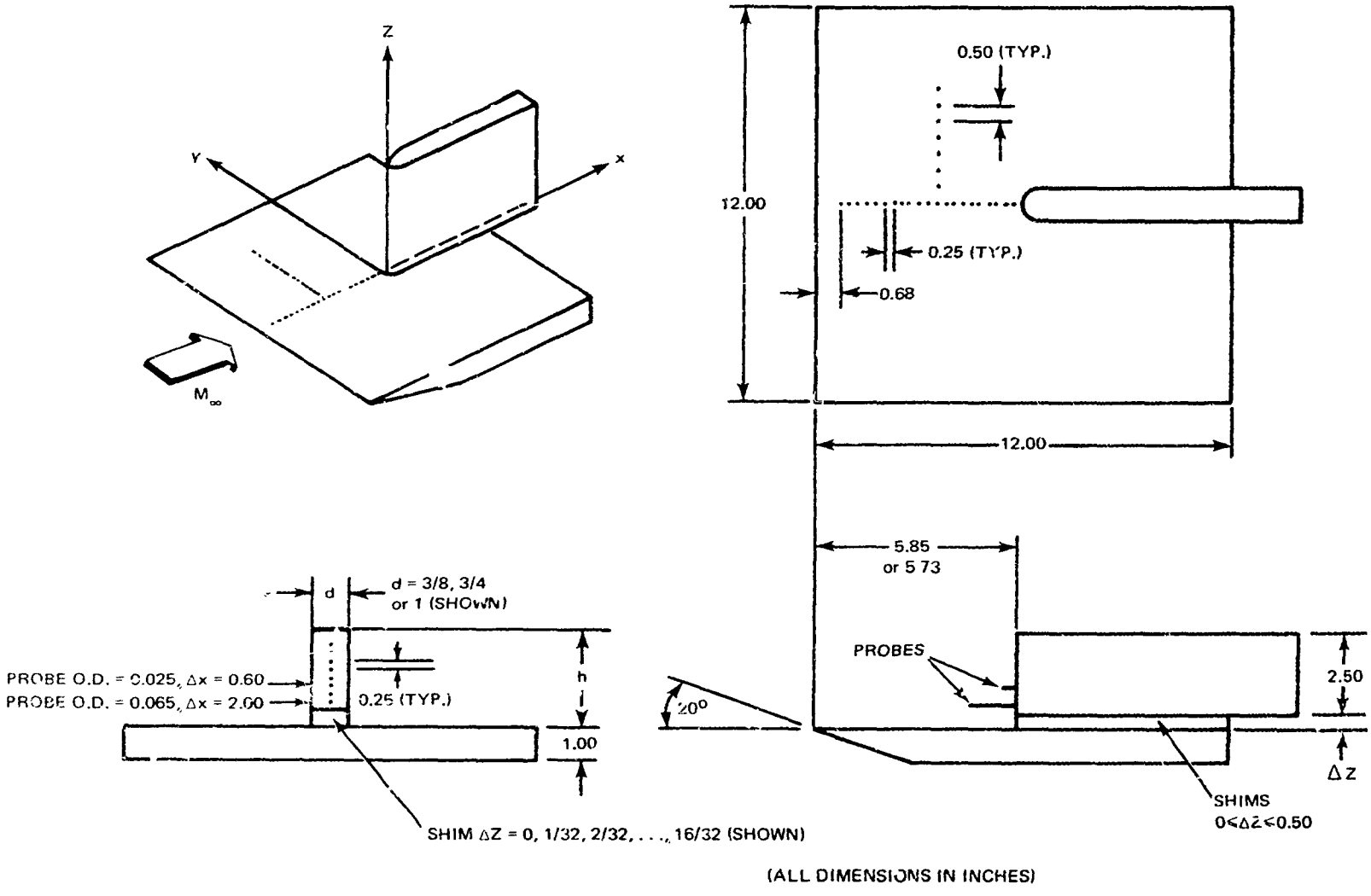

Fig. 8 Sketch of Model and Coordinate System

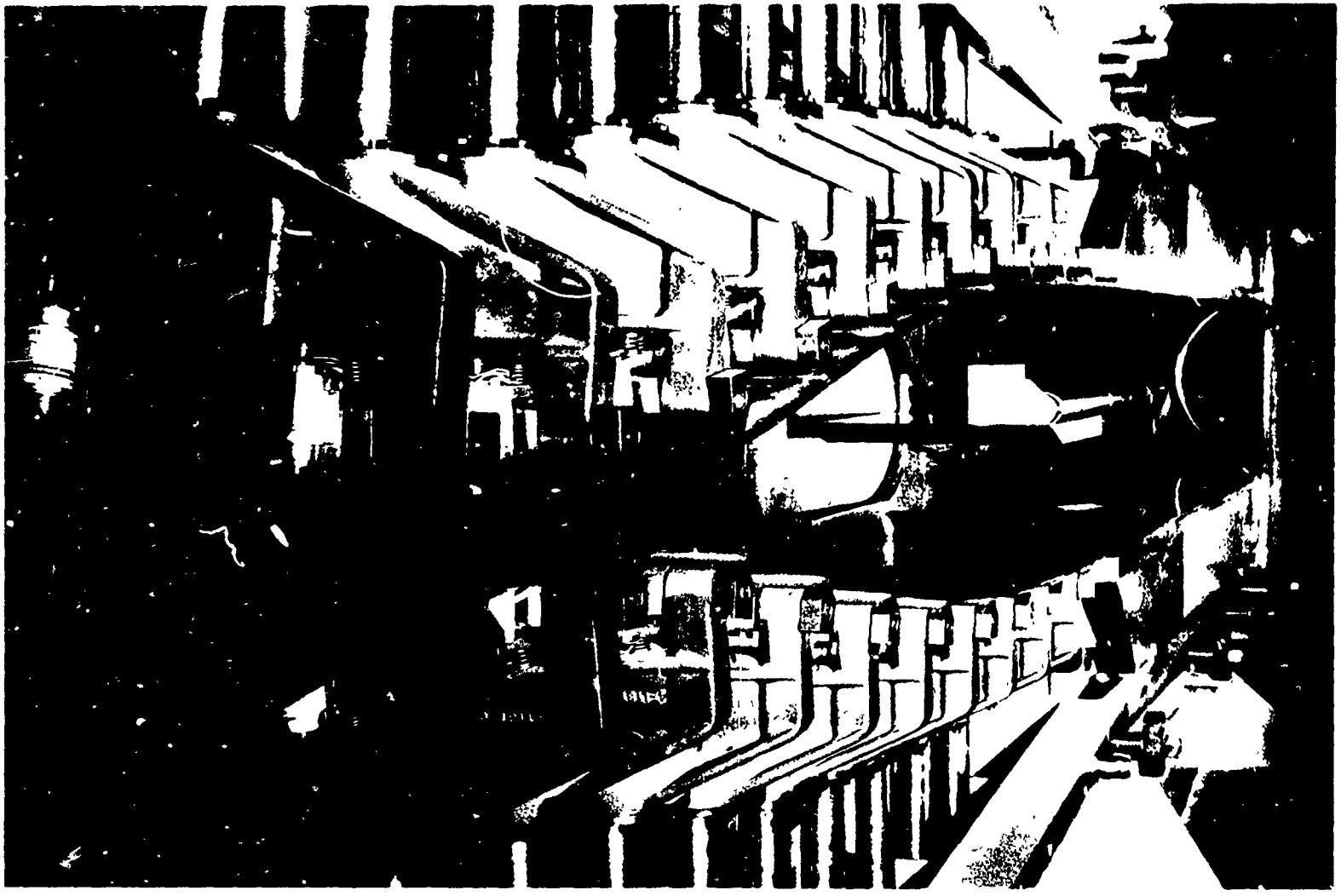

Fig. 9 Photograph of Tunnel Nozzle, Set for $M_\infty = 4$, and Model Mounted in Test Section

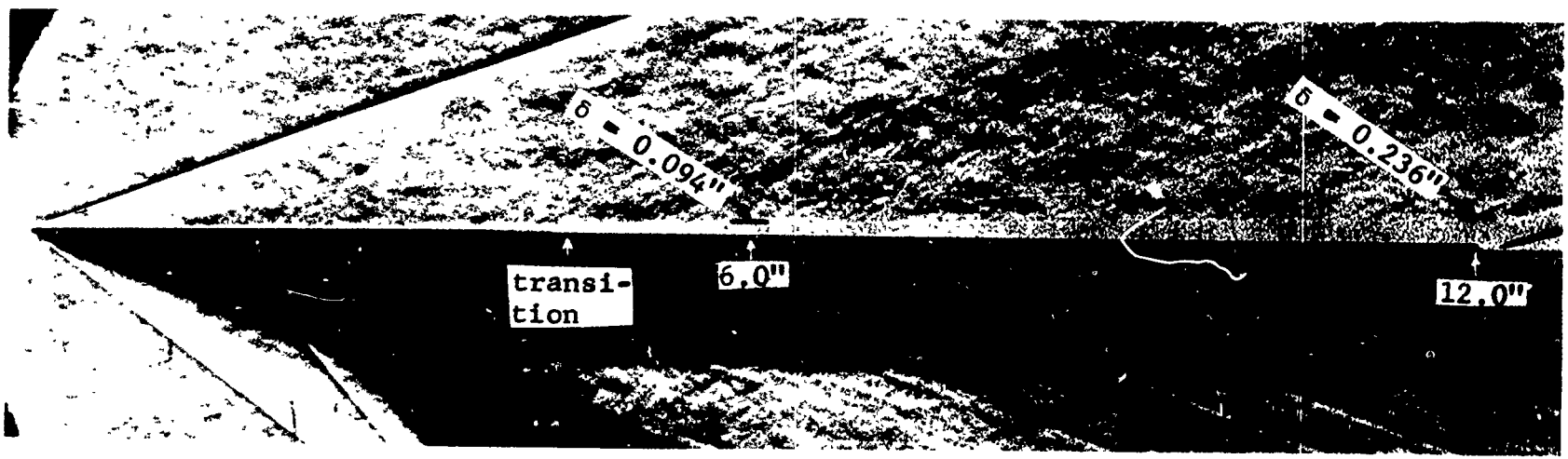

Fig. 10 Schlieren Flow Photograph of Flat Plate with No Fin;
$M_\infty = 3$, $Rey_{inch} = 400{,}000$

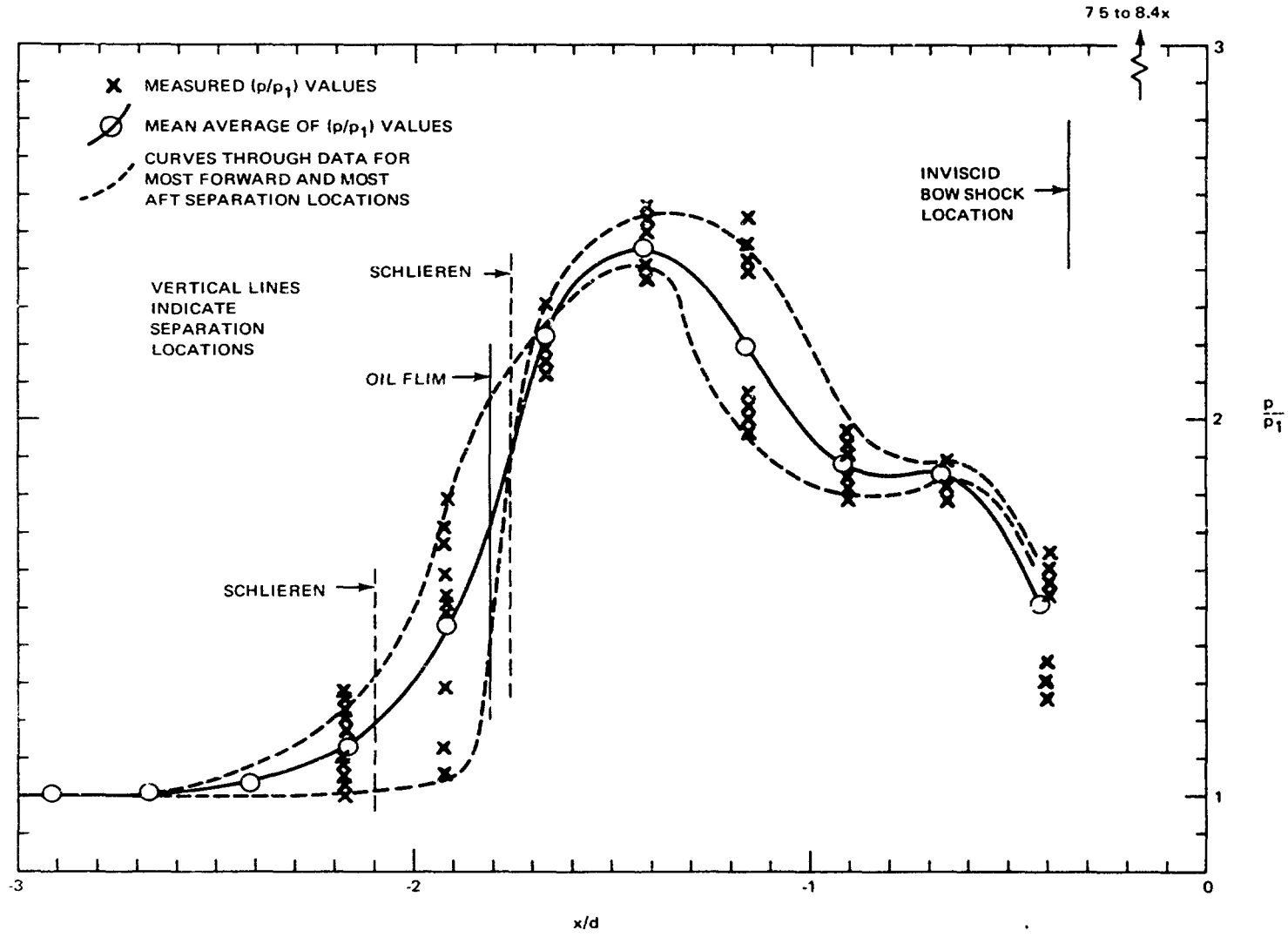

Fig. 11 Surface Pressure Distribution Ahead of Fin
$M_\infty = 3$, d = 1, $Rey_{inch} = 800{,}000$

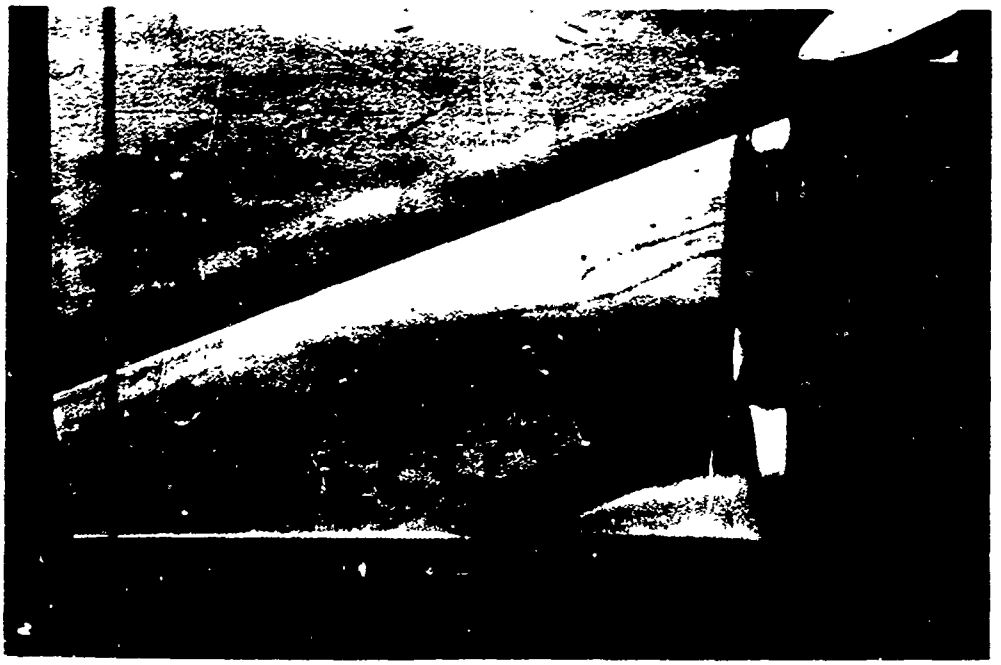

a) Furthest Aft Separation Location Photographed

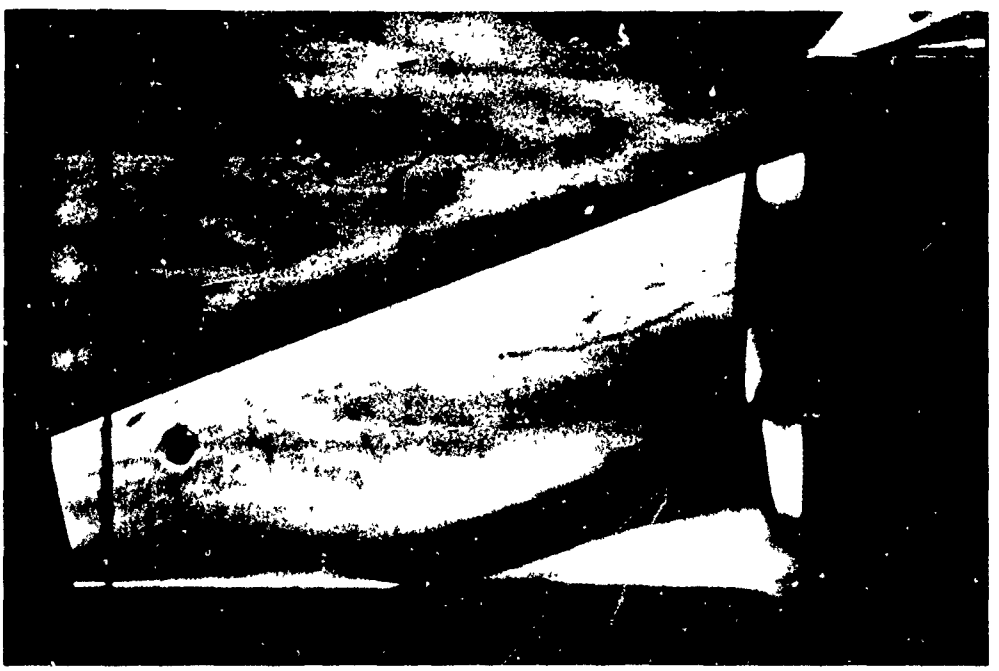

b) Furthest Forward Separation Location Photographed

Fig. 12 Schlieren Flow Photographs Showing Variation of Separation Length During Same Tunnel Run; $M_\infty = 3$, $d = 1$, $Rey_{inch} = 800,000$

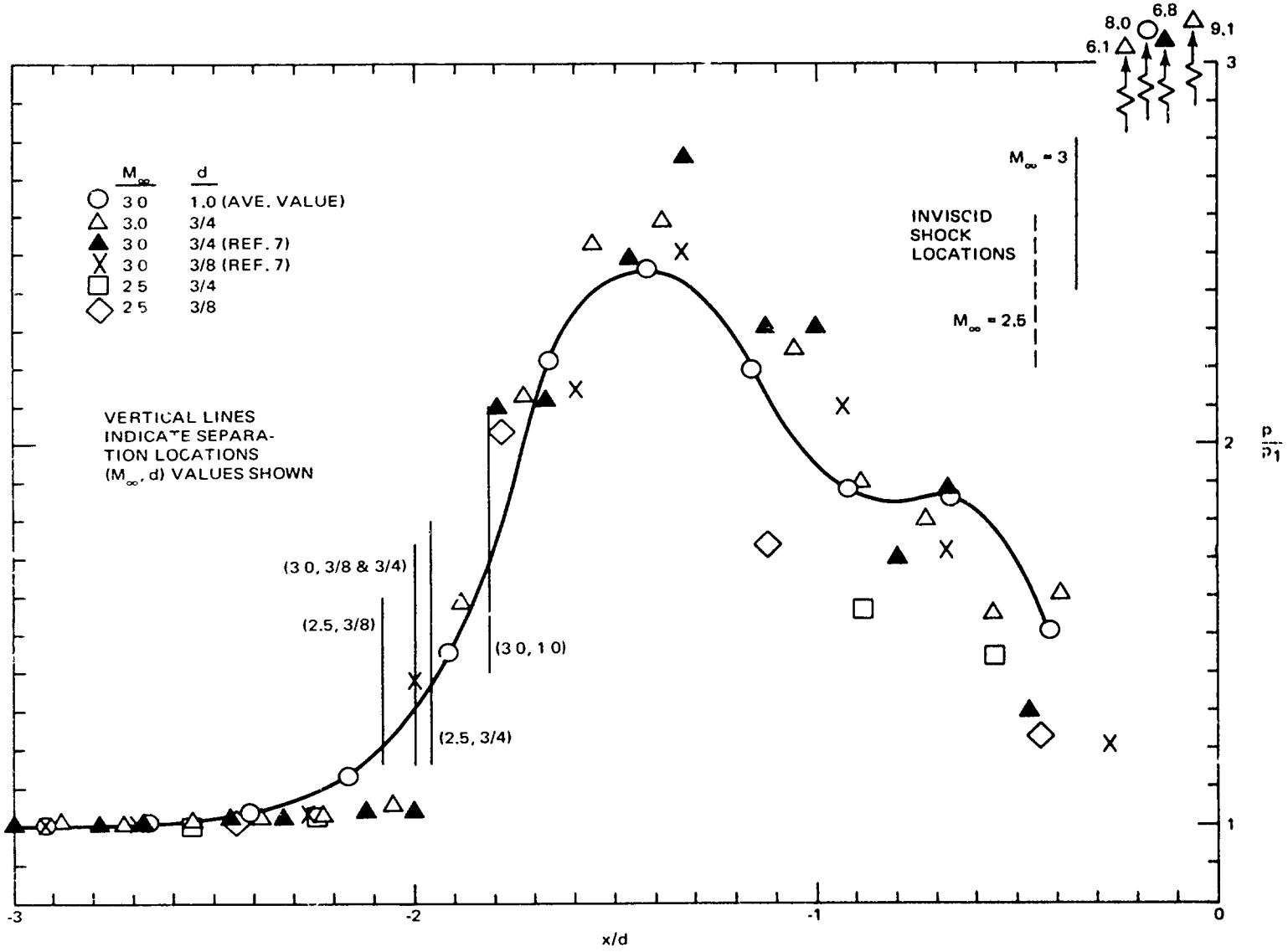

Fig. 13 Surface Pressure Distributions Ahead of Fins;
M_∞ = 2.5 & 3.0, Re_{yinch} = 800,000

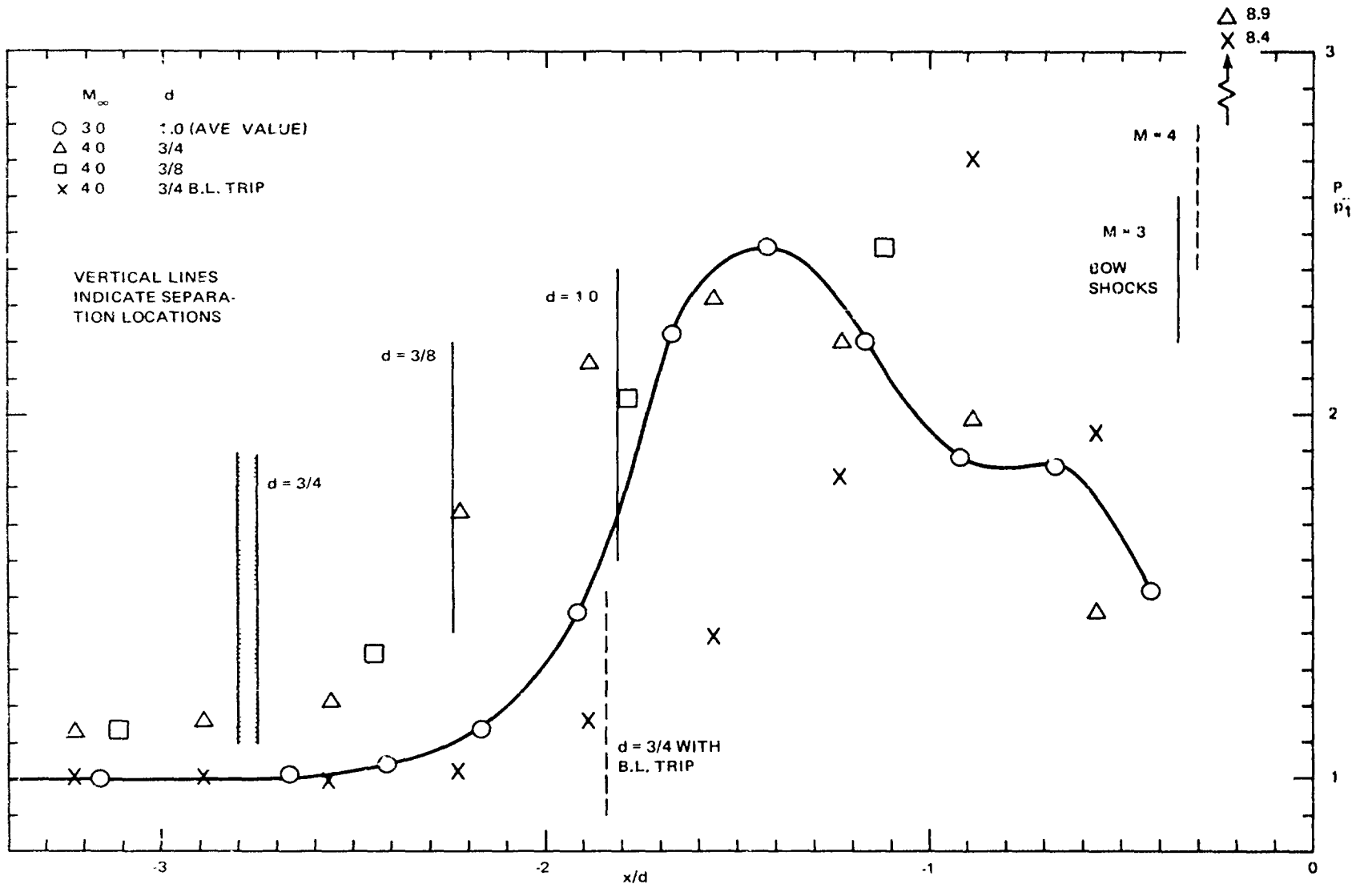

Fig. 14 Surface Pressure Distributions Ahead of Fins; M_∞ = 3 & 4

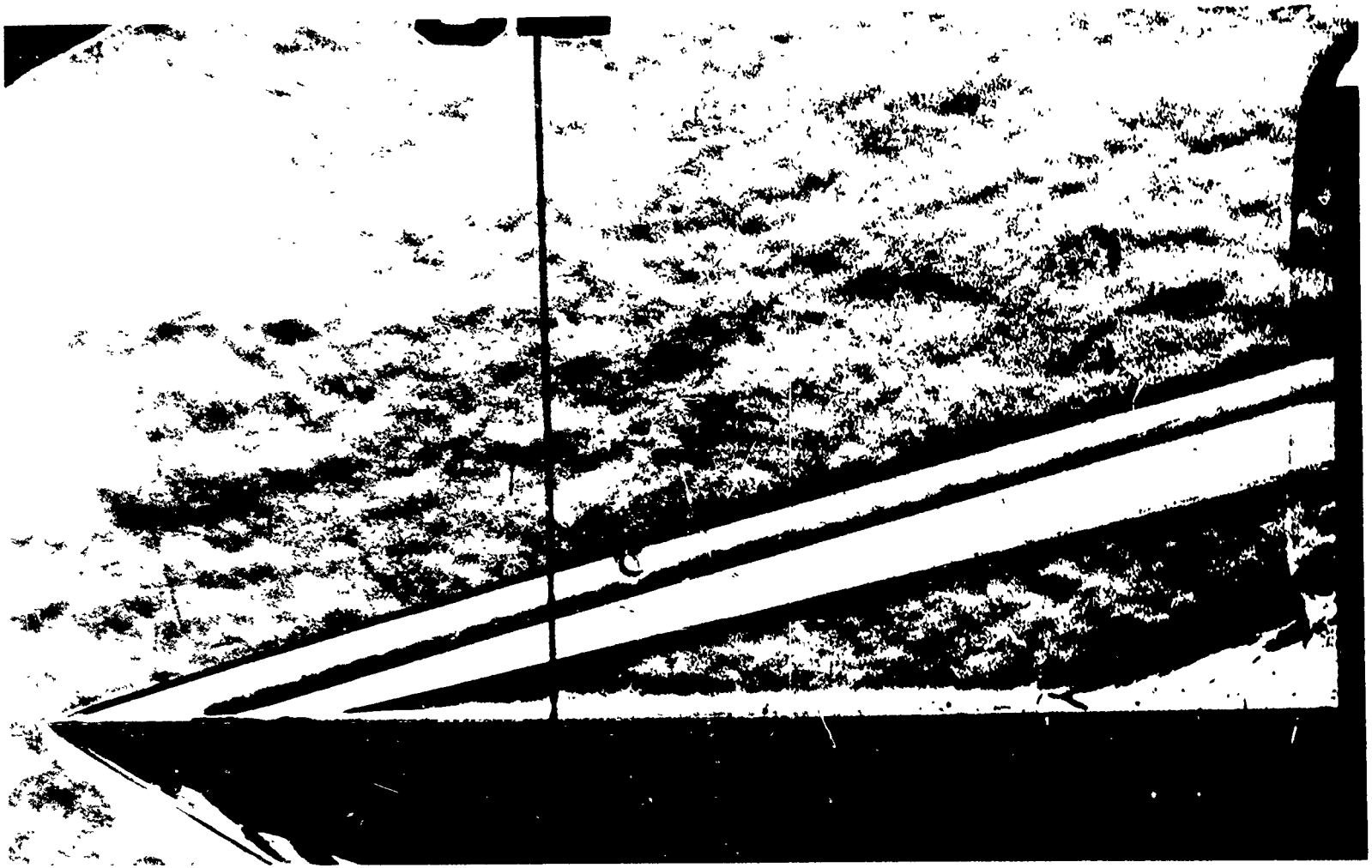

Fig. 15 Schlieren Flow Photograph Showing Boundary Layer Trip Effects;
$M_\infty = 4$, $d = 3/4$, $Rey_{inch} = 470{,}000$

Fig. 16 Oil Film Flow Photograph, Transitional Separation; $M_\infty = 4$, d = 3/4, $Rey_{inch} = 470{,}000$

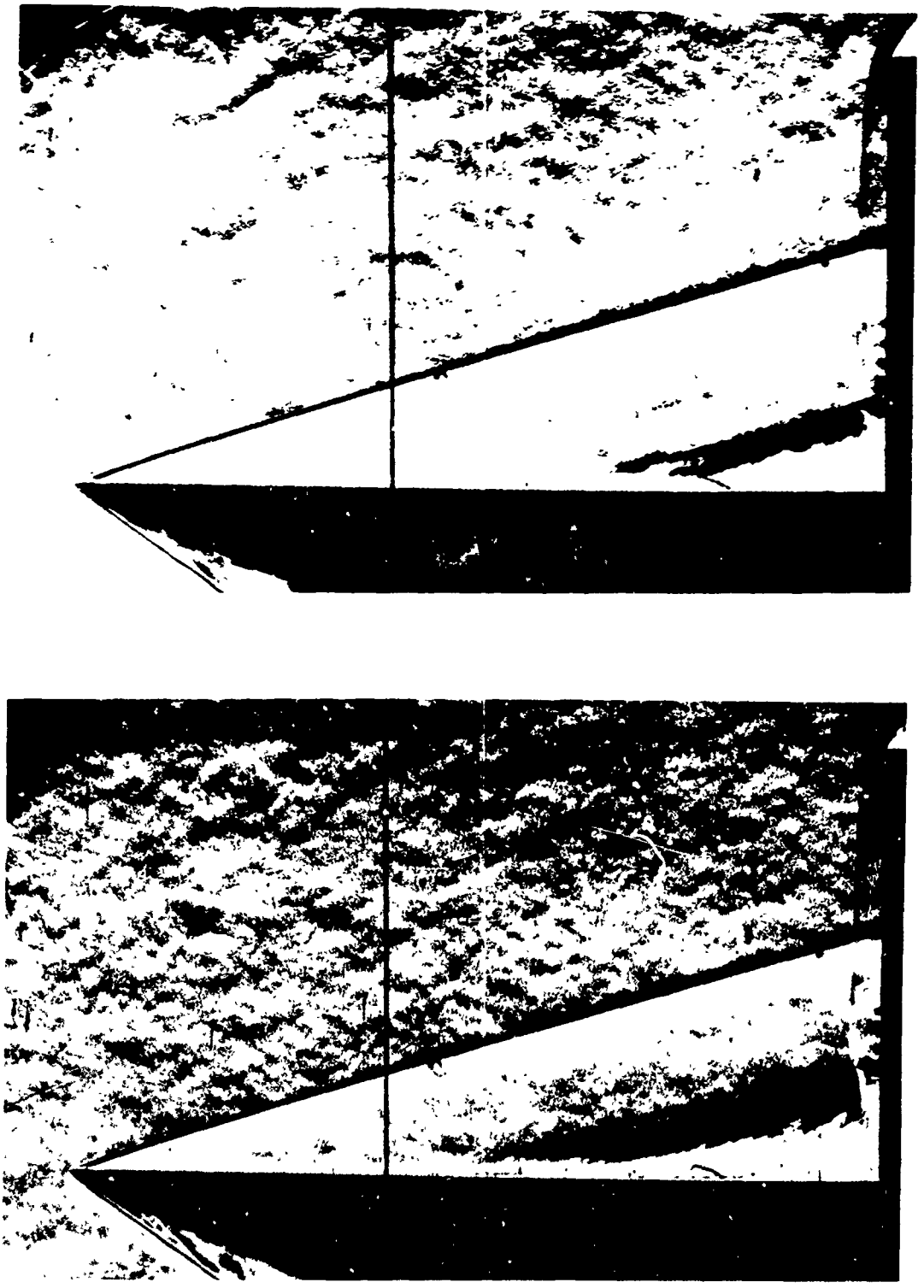

Fig. 17 Schlieren Flow Photographs Showing Extreme Variation of Separation Length During Same Tunnel Run for Transitional Separation; $M_\infty = 4$, $d = 3/4$, $Rey_{inch} = 470{,}000$

a) Rey_{inch} = 400,000

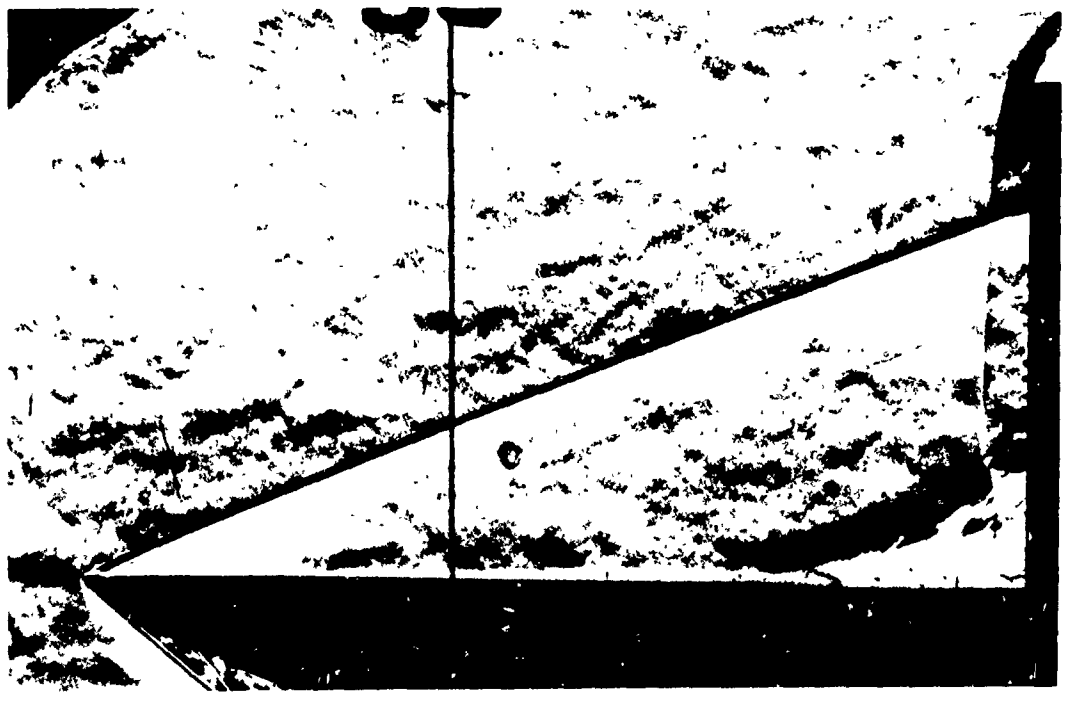

b) Rey_{inch} = 530,000

Fig. 18 Schlieren Flow Photographs Showing Variation of Separation Length with Reynolds Number; M_∞ = 3, d = 3/4 (sheet 1 of 2)

c) Rey_{inch} = 670,000

d) Rey_{inch} = 800,000

Fig. 18 Schlieren Flow Photographs Showing Variation of Separation Length with Reynolds Number; M_∞ = 3, d = 3/4 (sheet 2 of 2)

a) Rey_{inch} = 130,000

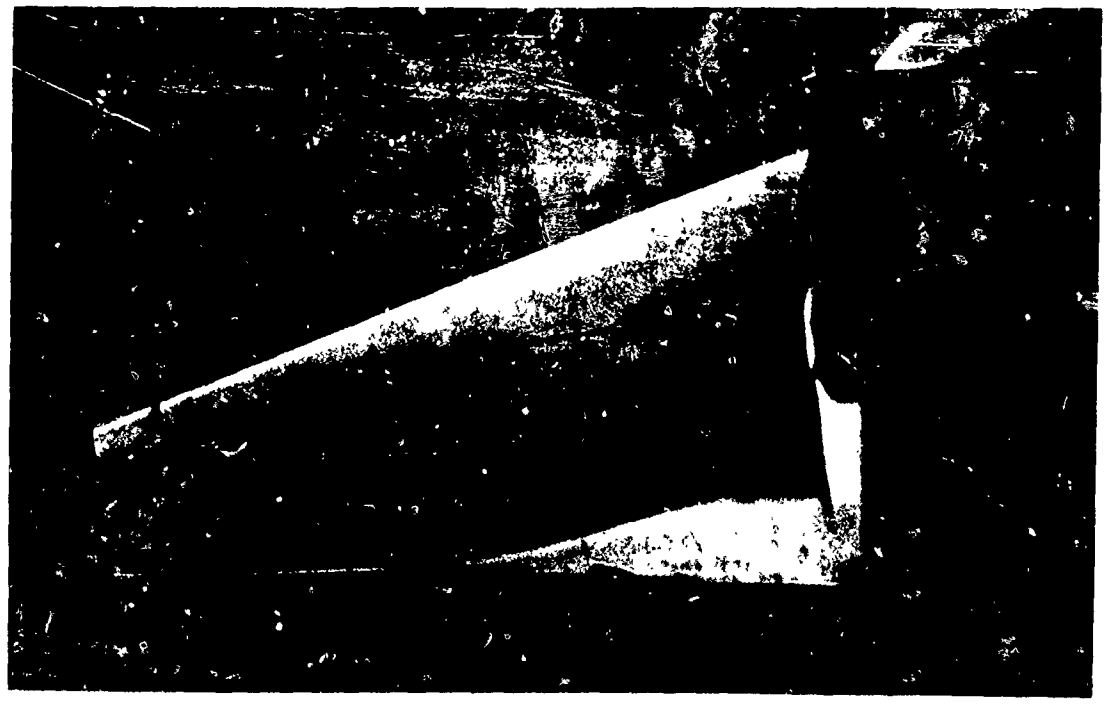

b) Rey_{inch} = 270,000

Fig. 19 Schlieren Flow Photographs Showing Variation of Separation Length with Reynolds Number; M_∞ = 3, d = 1 (sheet 1 of 3)

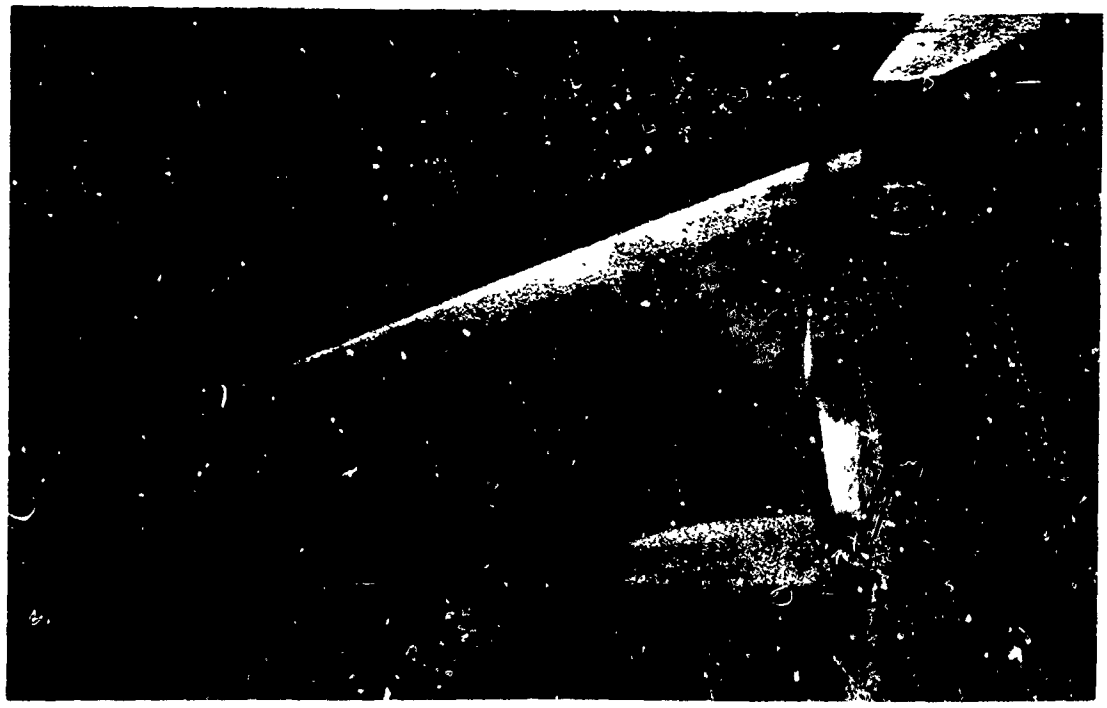

c) Rey_{inch} = 400,000

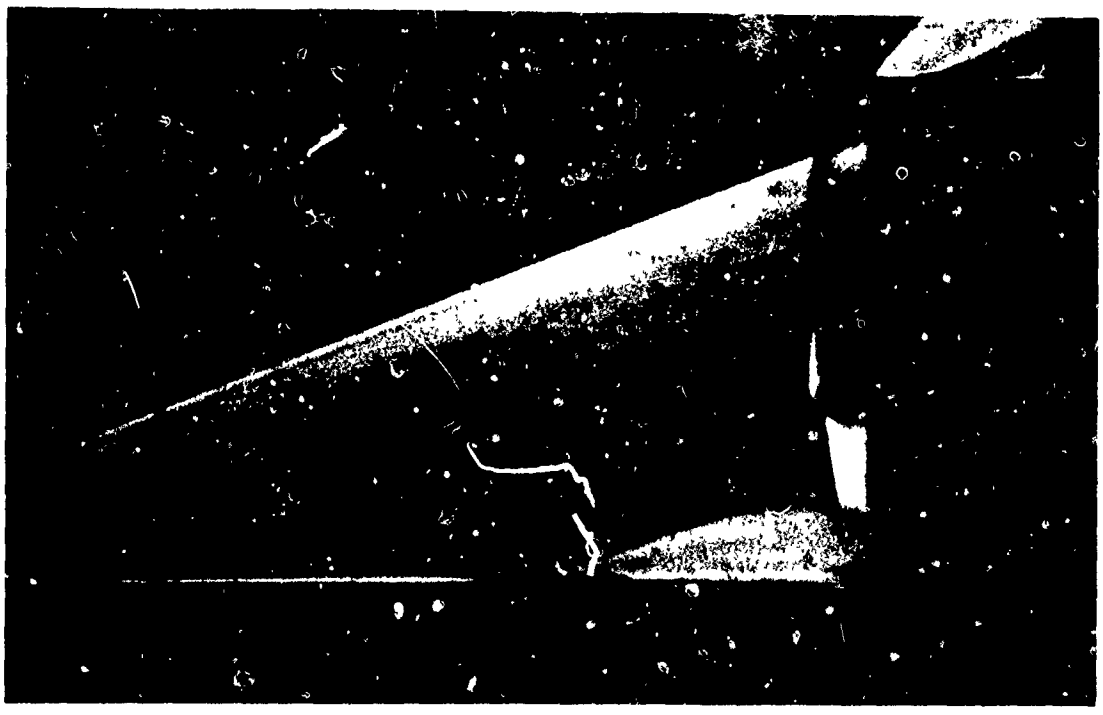

d) Rey_{inch} = 530,000

Fig. 19 Schlieren Flow Photographs Showing Variation of Separation Length with Reynolds Number; M_∞ = 3, d = 1 (sheet 2 of 3)

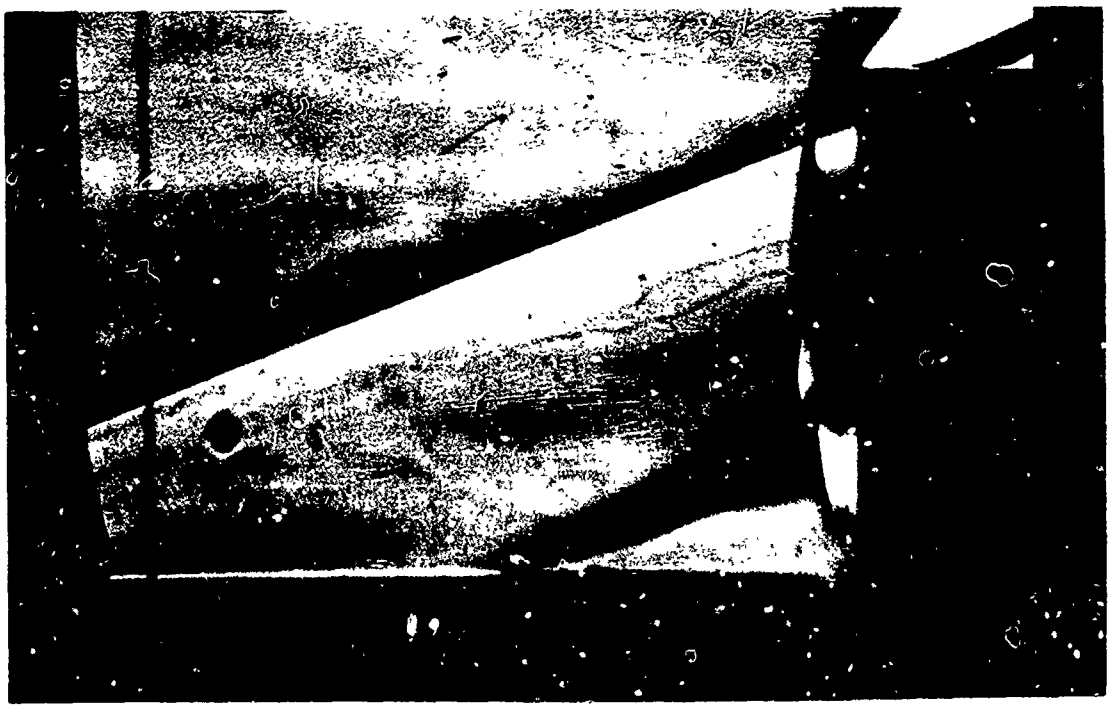

e) Rey_{inch} = 670,000

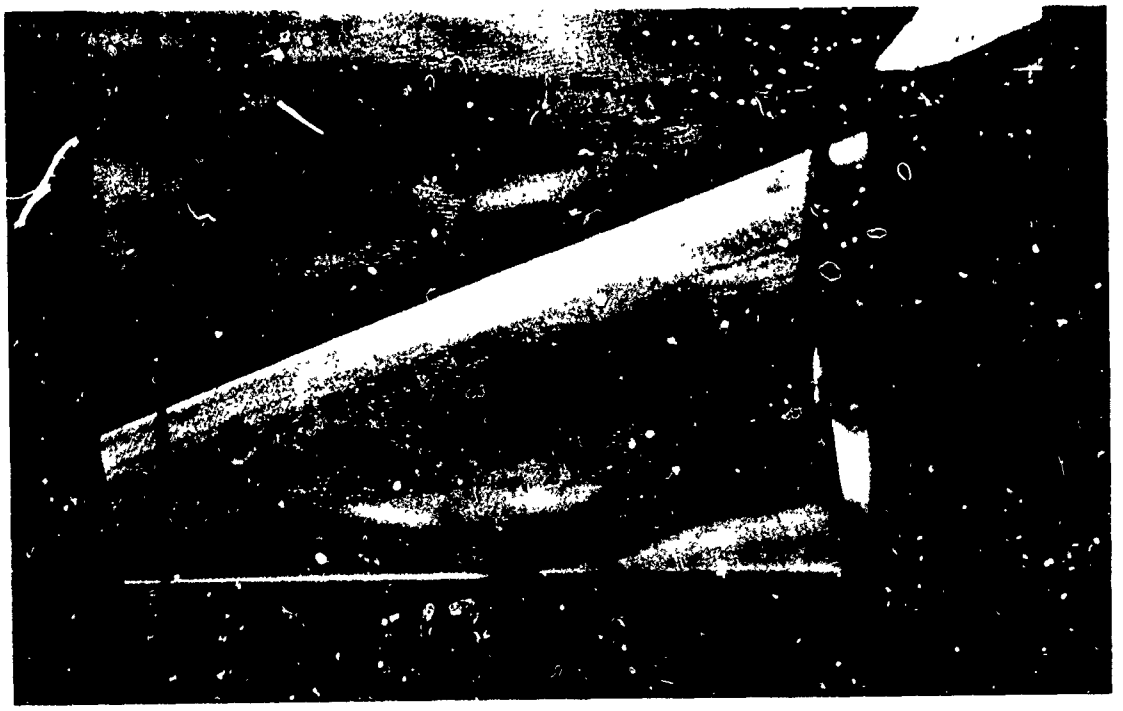

f) Rey_{inch} = 800,000

Fig. 19 Schlieren Flow Photographs Showing Variation of Separation Length with Reynolds Number; M_∞ = 3, d = 1 (sheet 3 of 3)

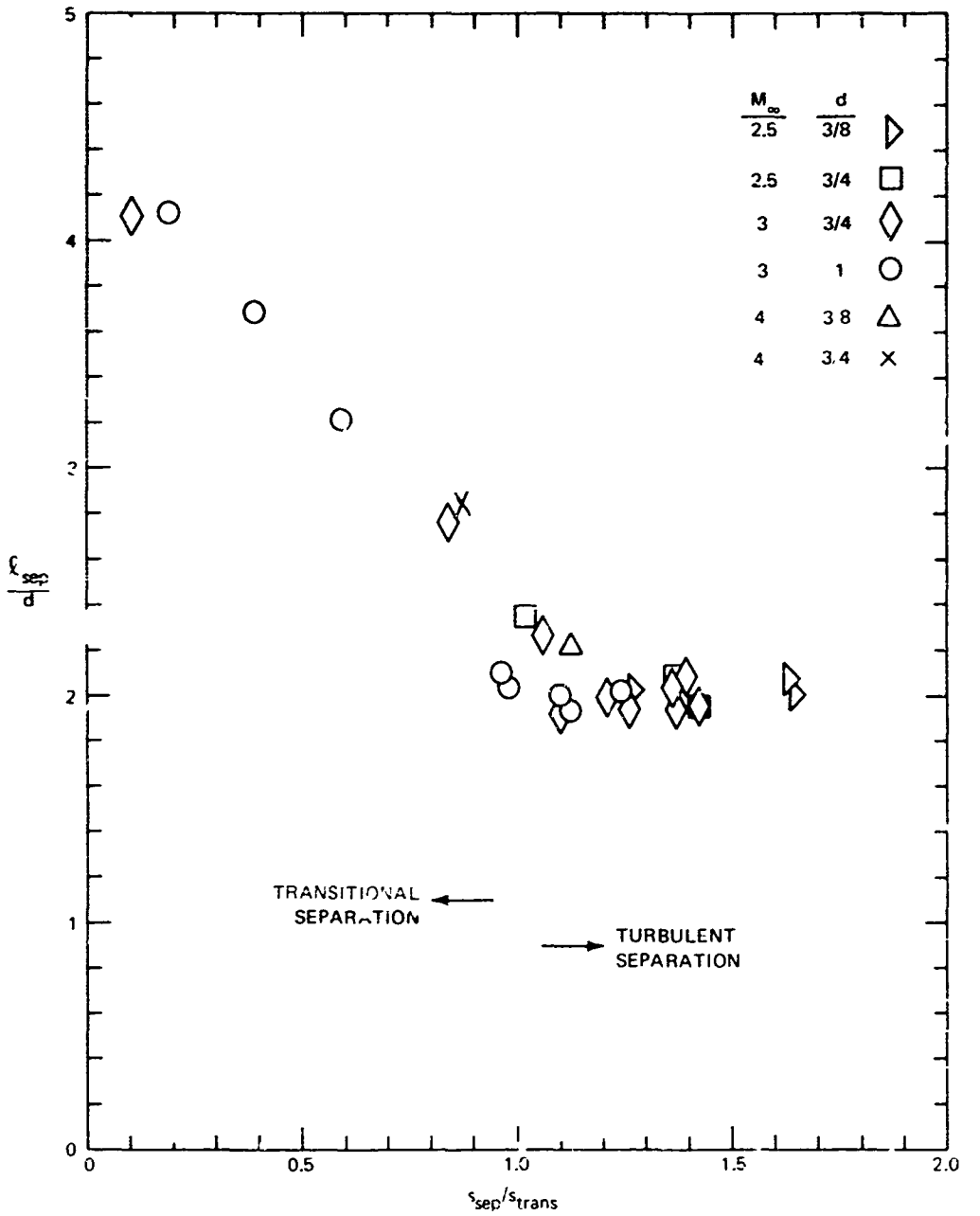

Fig. 20 Dependence of Separation Length on the Character of the Boundary Layer at Separation

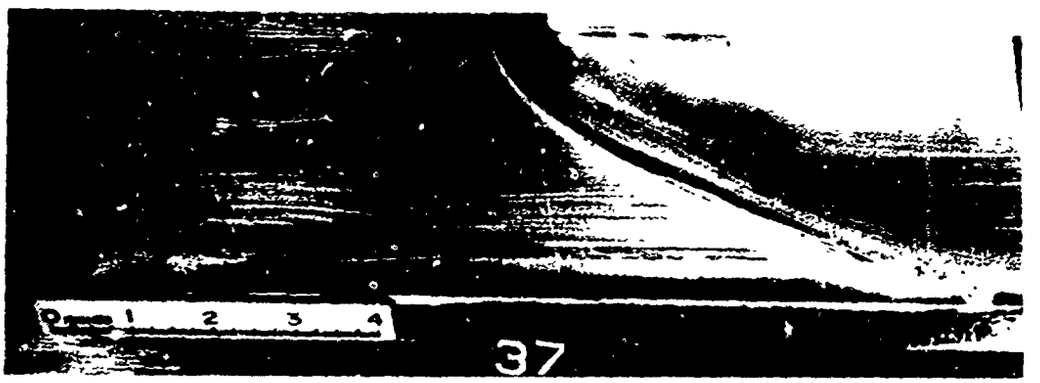

a) $M_\infty = 2.5$, $d = 3/8$, $Rey_{inch} = 800{,}000$

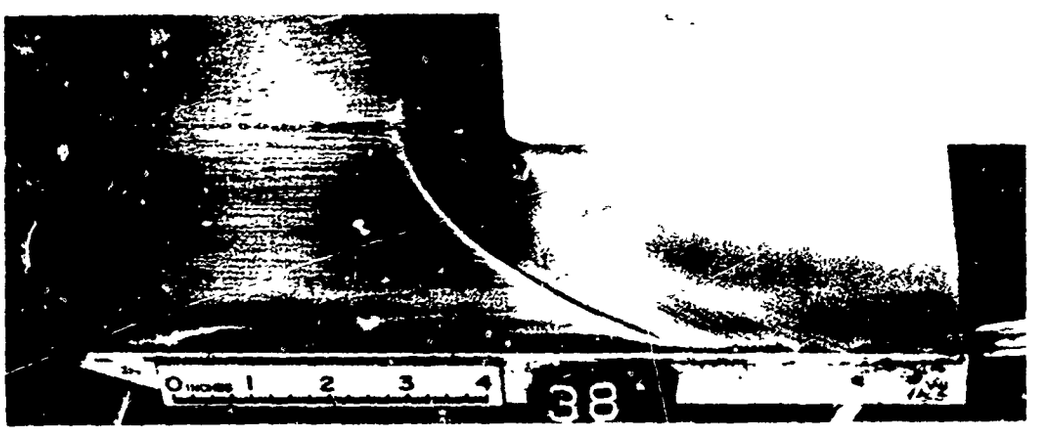

b) $M_\infty = 2.5$, $d = 3/4$, $Rey_{inch} = 800{,}000$

c) $M_\infty = 3.0$, $d = 1$, $Rey_{inch} = 800{,}000$

Fig. 21 Oil Film Flow Photographs

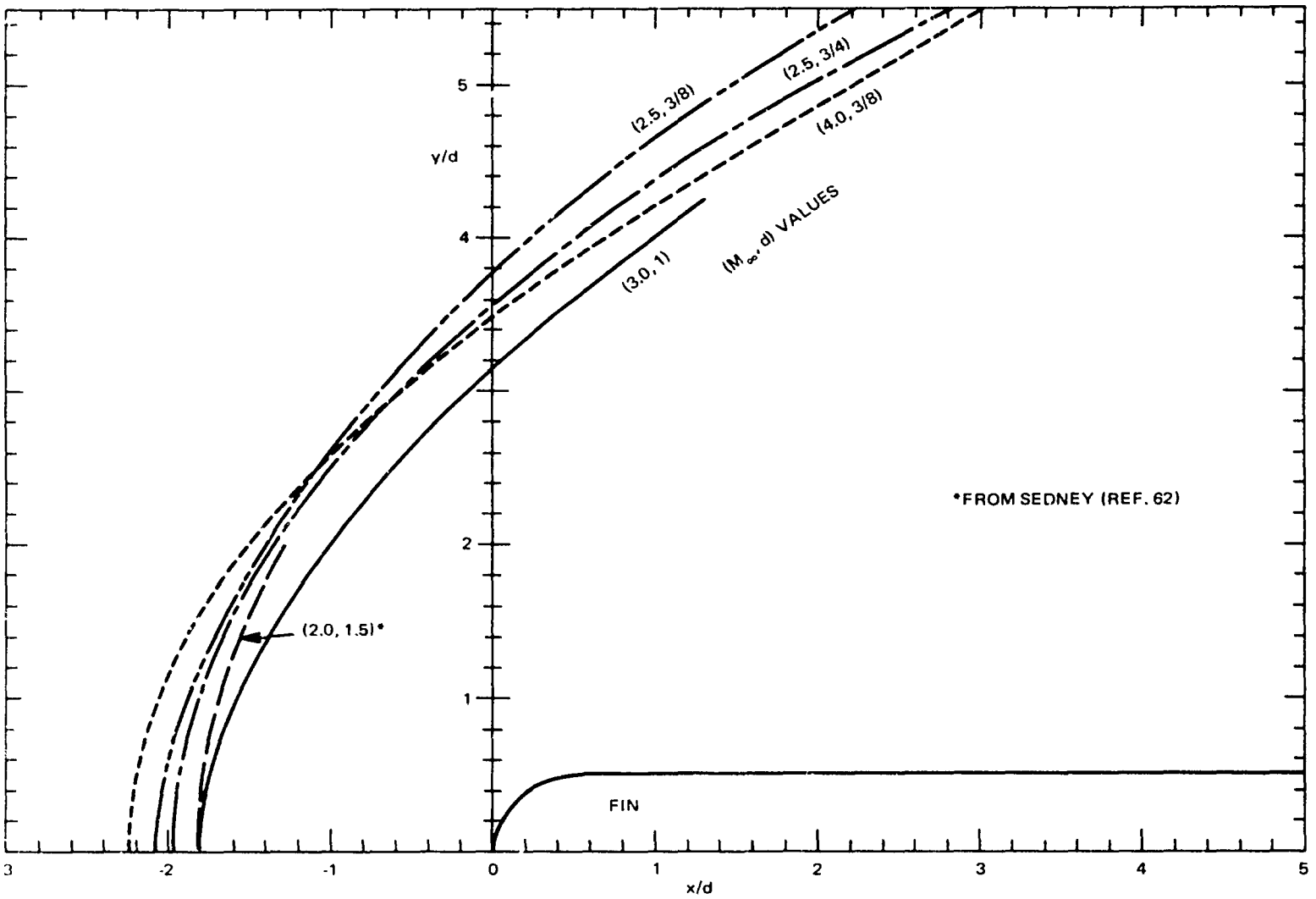

Fig. 22 Separation Line Locations on Flat Plate Surface Scaled from Oil Film Flow Photographs

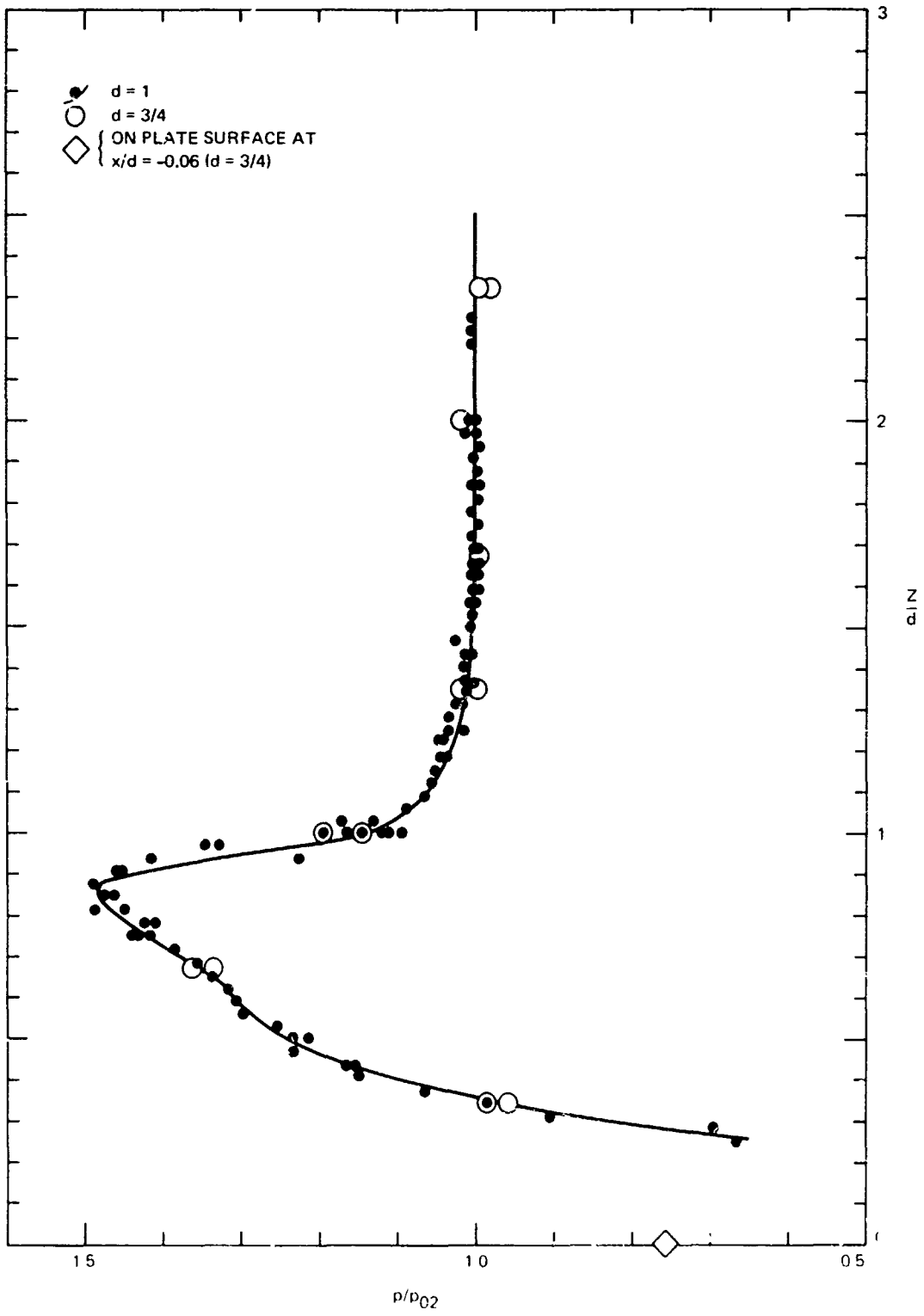

Fig. 23 Pressure Distributions Along Fin Leading Edges; $M_\infty = 3$

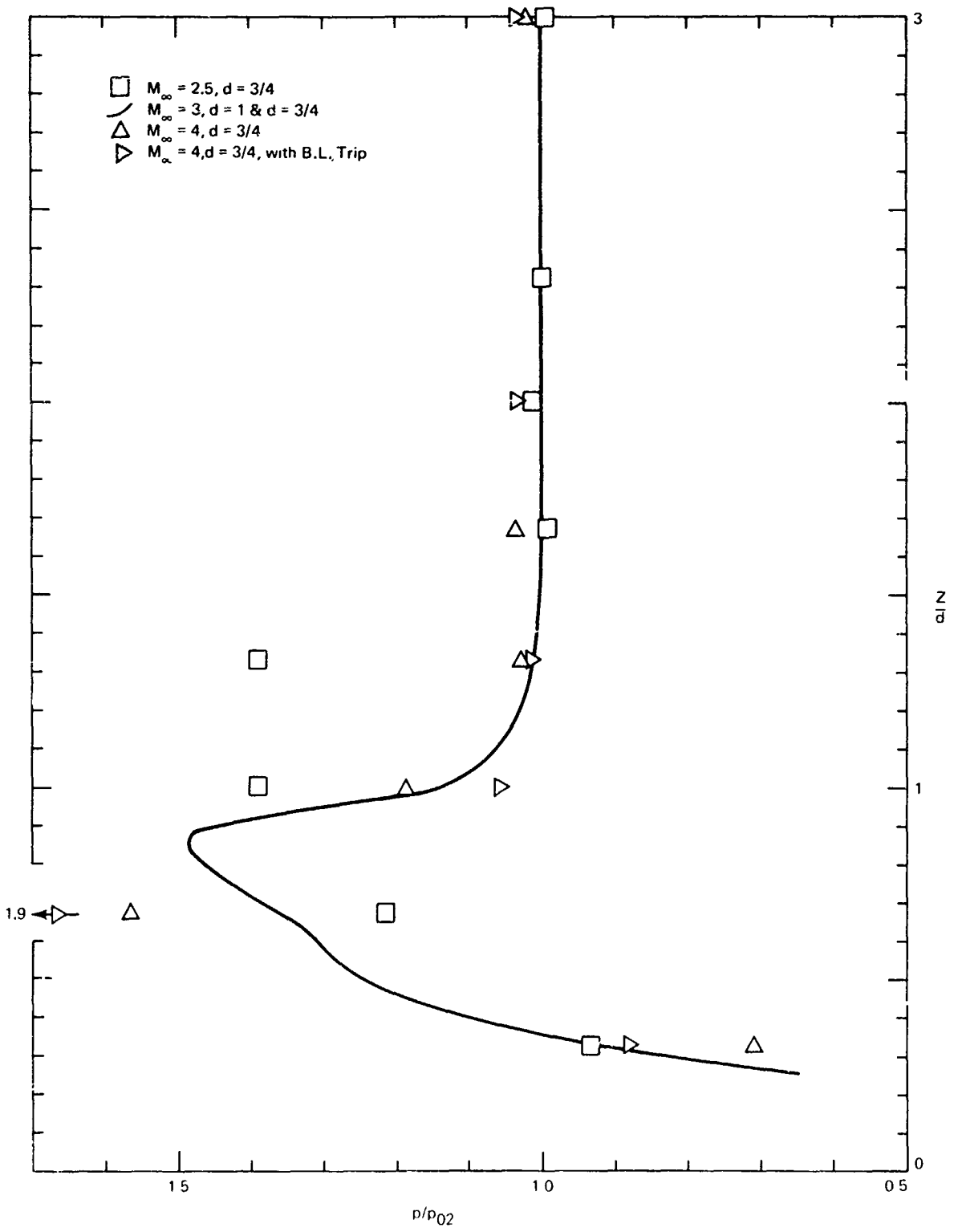

Fig. 24 Pressure Distributions Along Fin Leading Edges; M_∞ = 2.5, 3 & 4

Fig. 25 Schlieren Flow Photograph; $M_\infty = 2.5$, d= 3/4, $Rey_{inch} = 800{,}000$

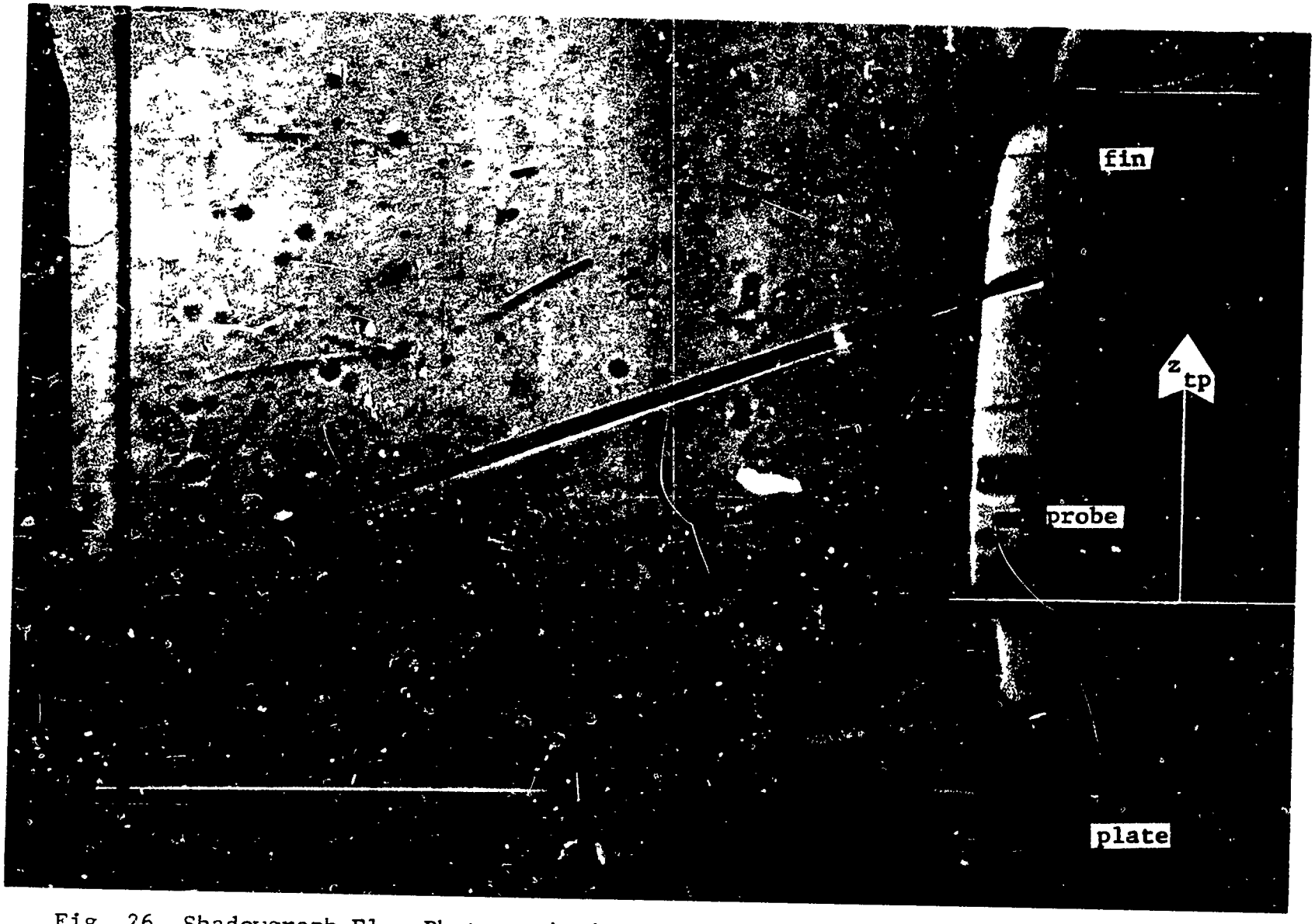

Fig. 26 Shadowgraph Flow Photograph Showing z_{tp} (Vertical Distance Measured from "Triple Point"); Smaller Probe Extended 0.2 inch at $z_{tp} = 0.35d$, $M_\infty = 3$, $d = 1$, $Rey_{inch} = 800{,}000$

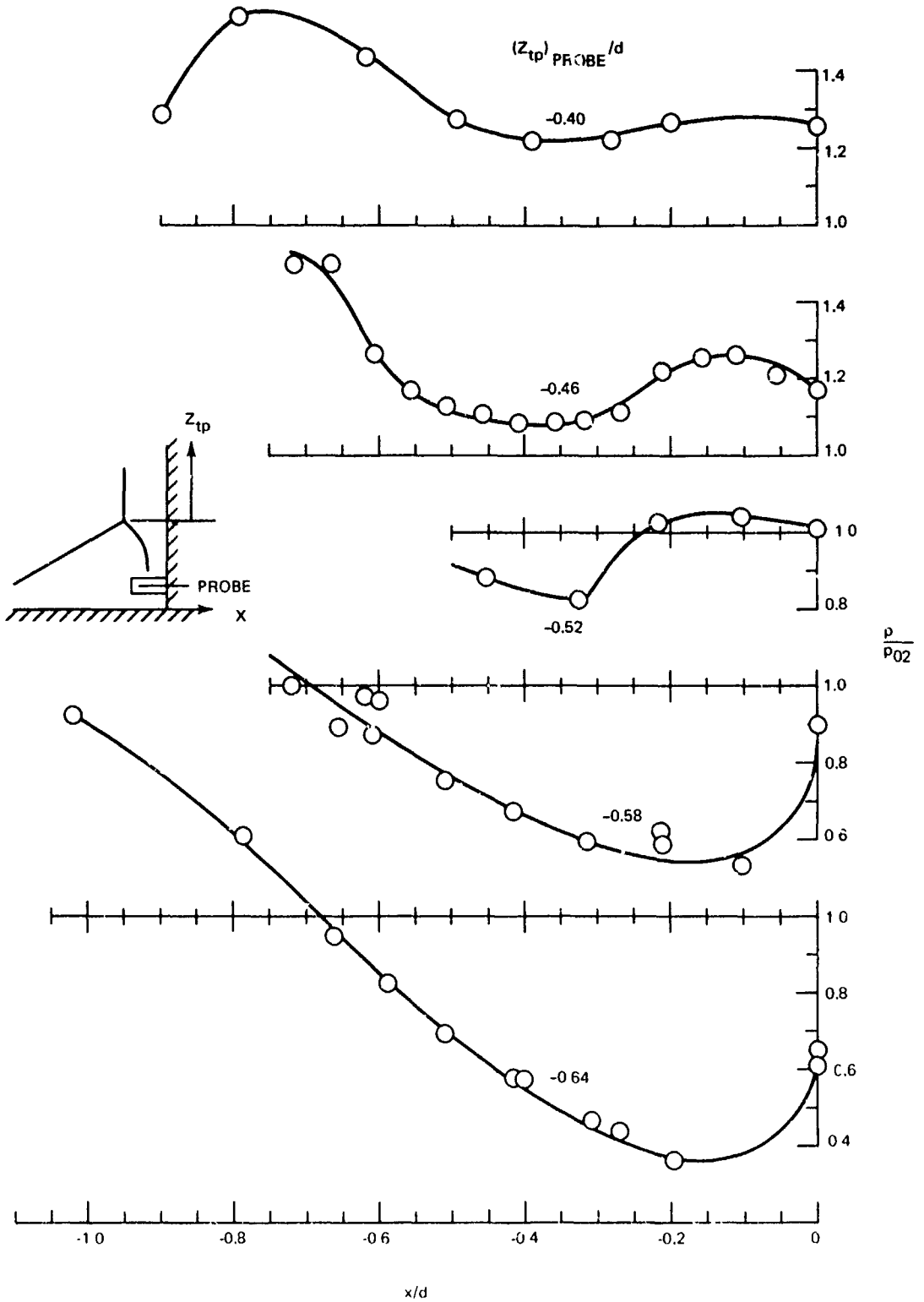

Fig. 27 Probe Total Pressure Measurements (Sheet 1 of 4)

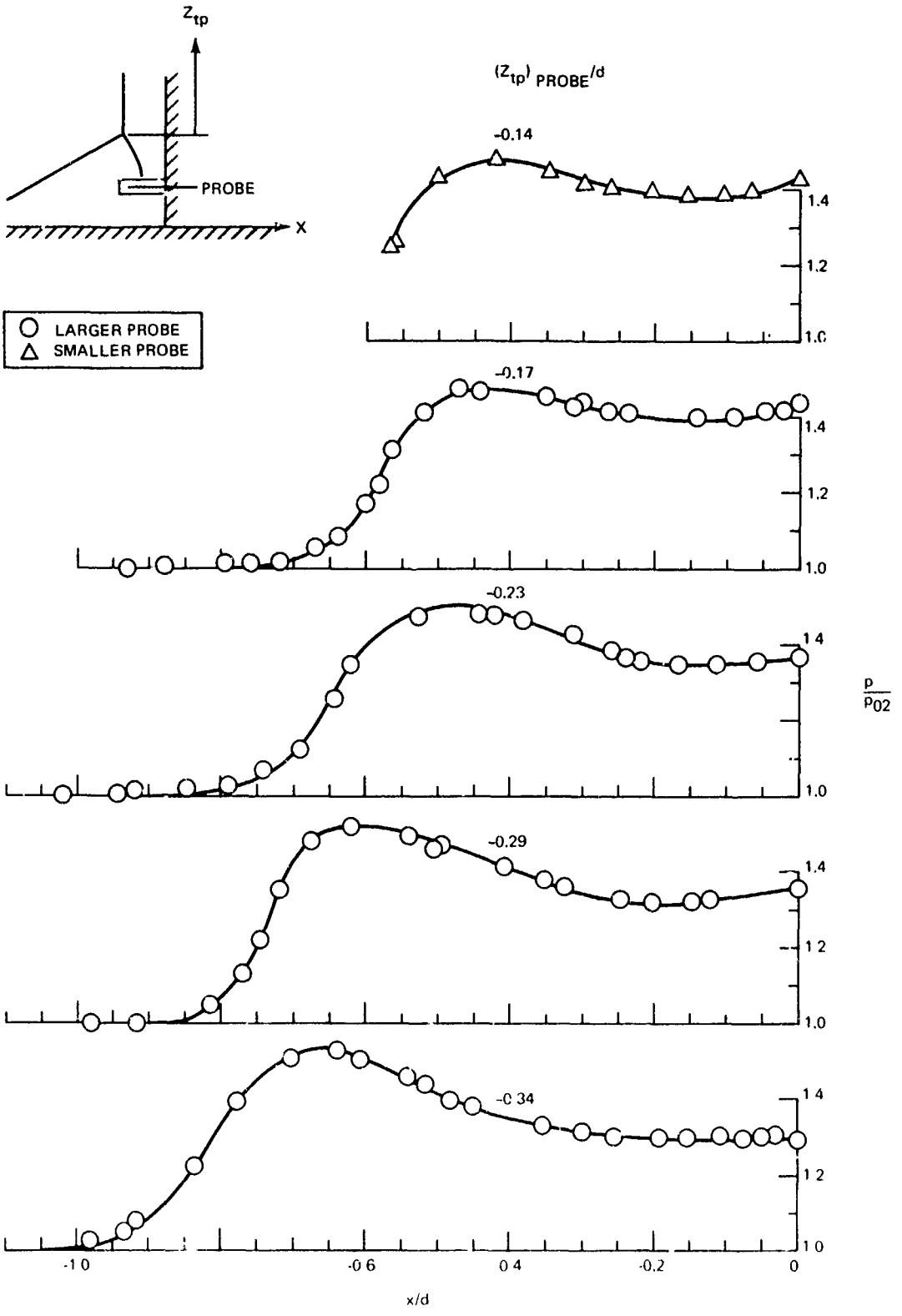

Fig. 27 Probe Total Pressure Measurements (Sheet 2 of 4)

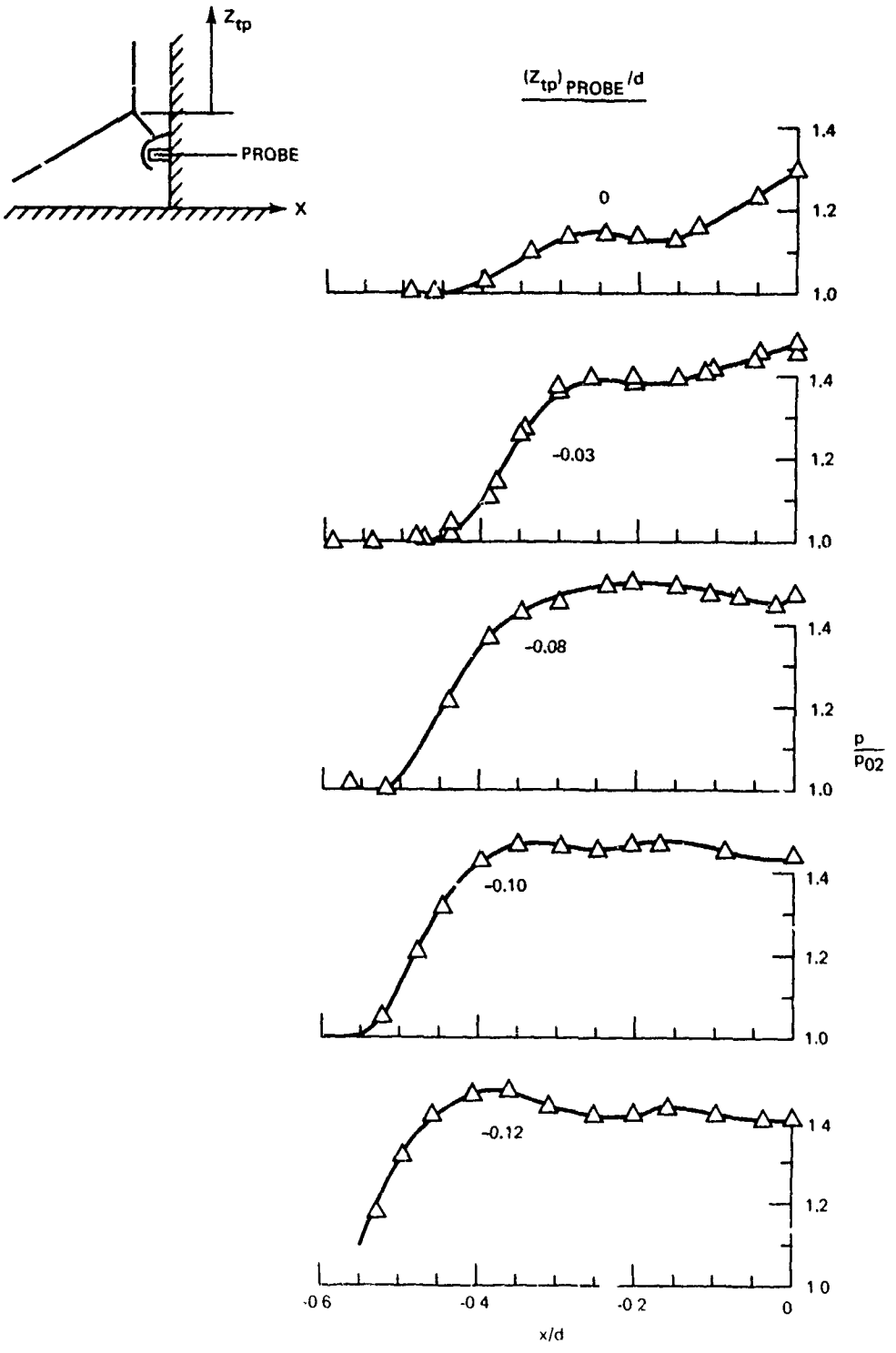

Fig. 27 Probe Total Pressure Measurements (Sheet 3 of 4)

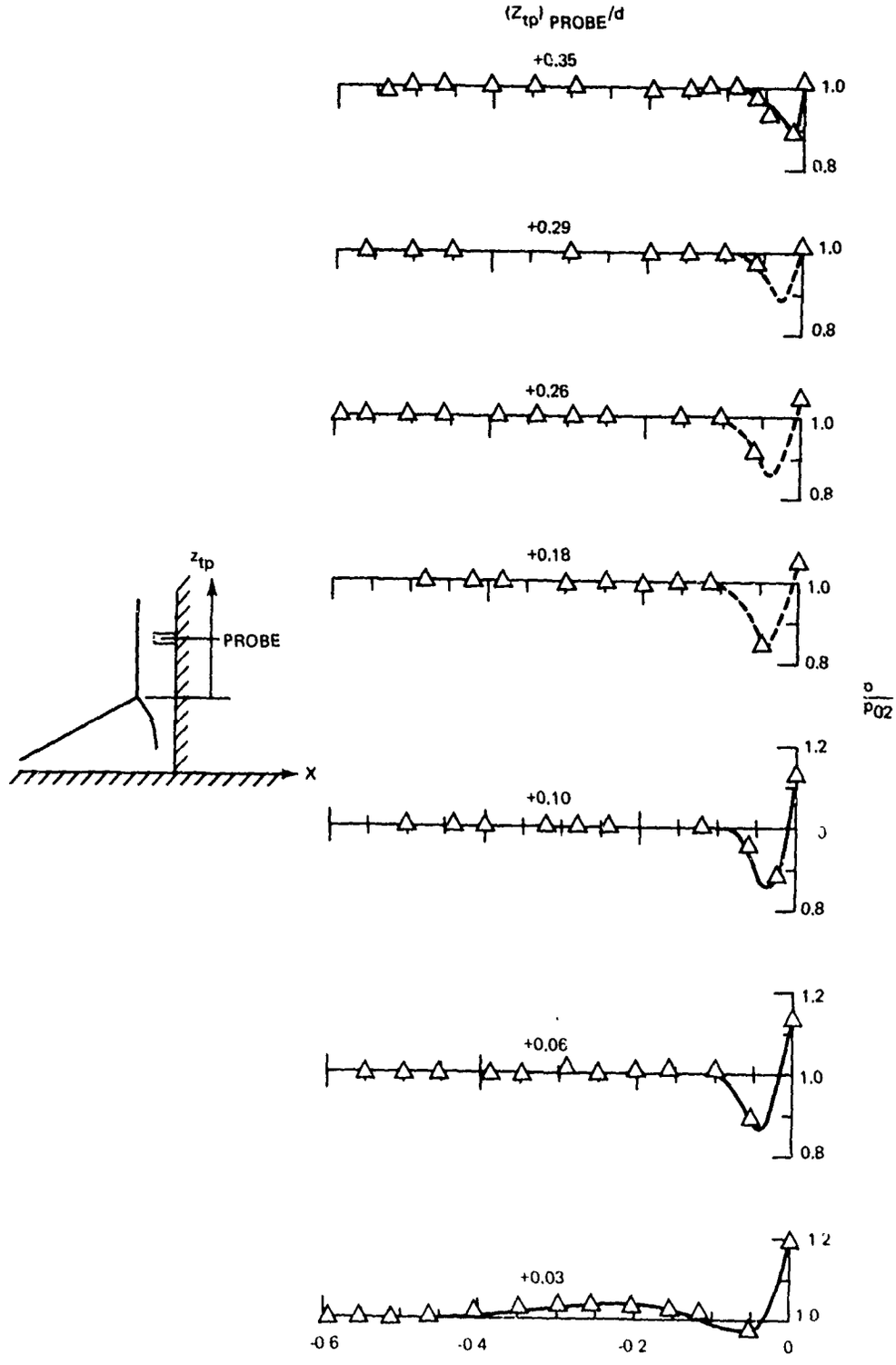

Fig. 27 Probe Total Pressure Measurements (Sheet 4 of 4)

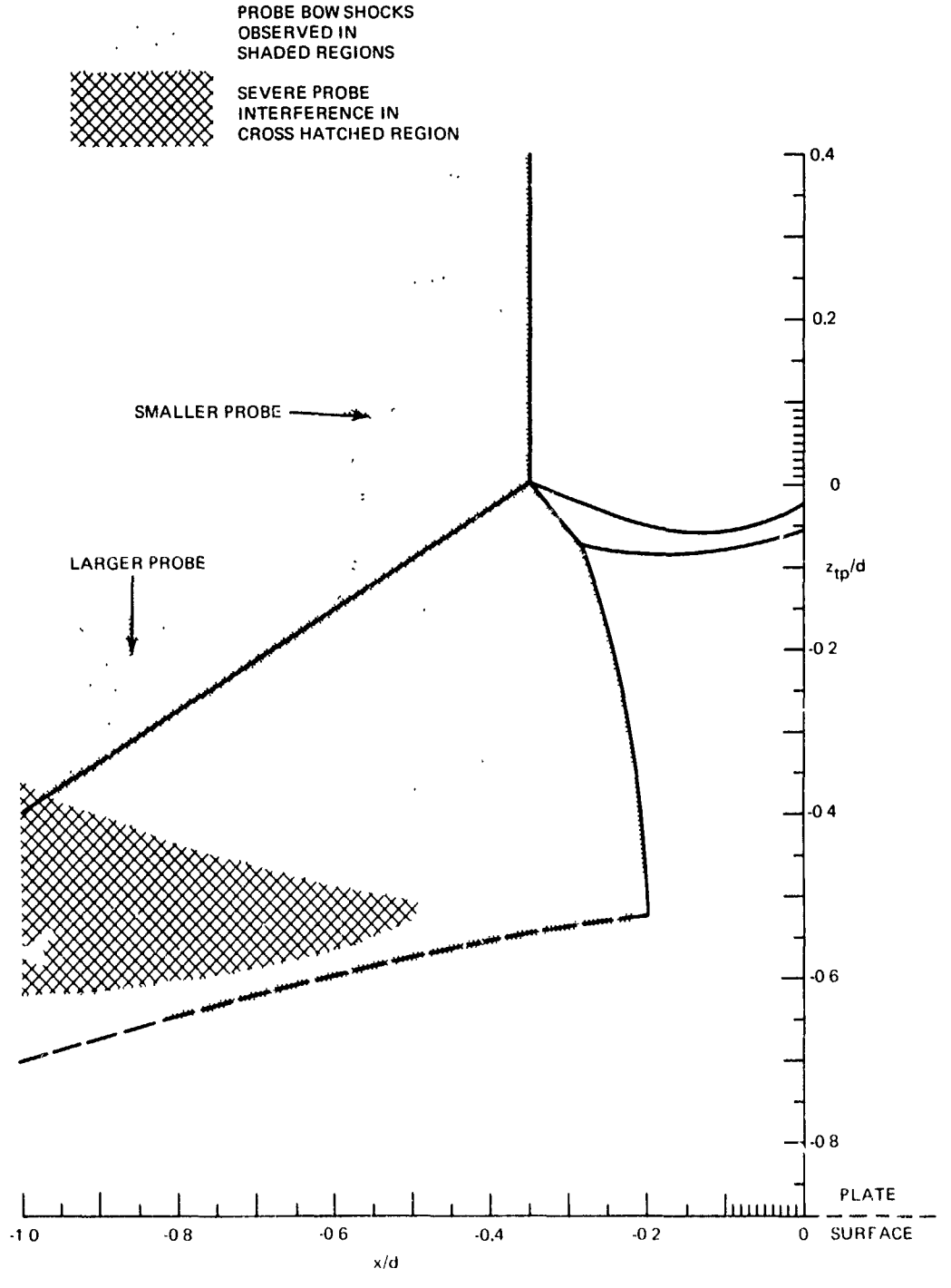

Fig. 28 Sketch of Interaction Flow Field, Scaled from a Microsecond Schlieren Flow Photograph, Showing Lambda Shock Pattern; $M_\infty = 3$, $d = 1$, $Rey_{inch} = 800,000$

a) $(x/d)_{probe}$ = -1.00, little interference

b) $(x/d)_{probe}$ = -0.78, severe interference

Fig. 29 Schlieren Flow Photographs Showing Unstable Probe Interference Effects; M_∞ = 3, d = 1, Rey_{inch} = 800,000

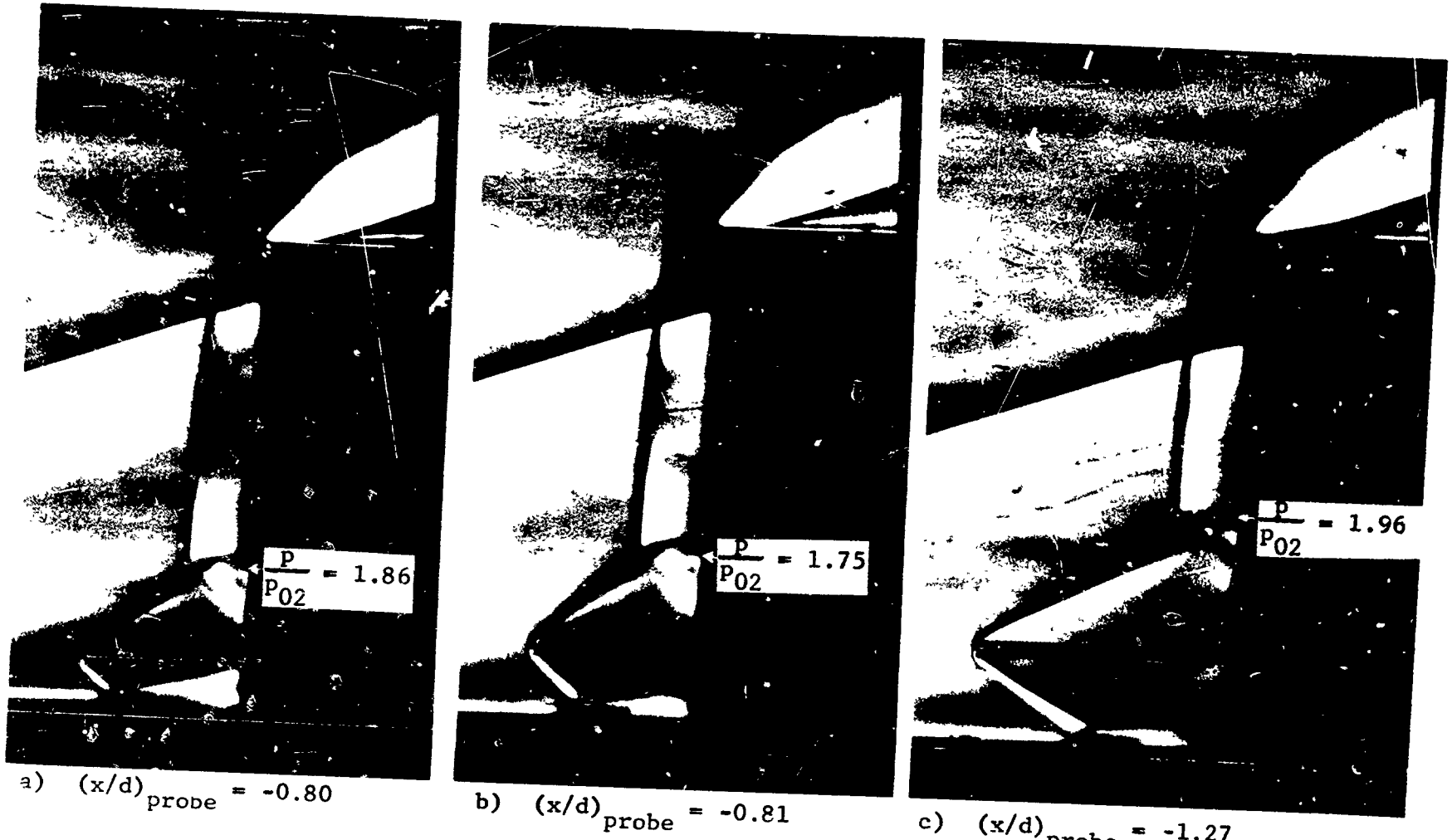

a) $(x/d)_{probe} = -0.80$ b) $(x/d)_{probe} = -0.81$ c) $(x/d)_{probe} = -1.27$

Fig. 30 Schlieren Flow Photographs Showing Probe Induced Shock Impingement; $M_\infty = 3$, $d = 1$, $Rey_{inch} = 800,000$

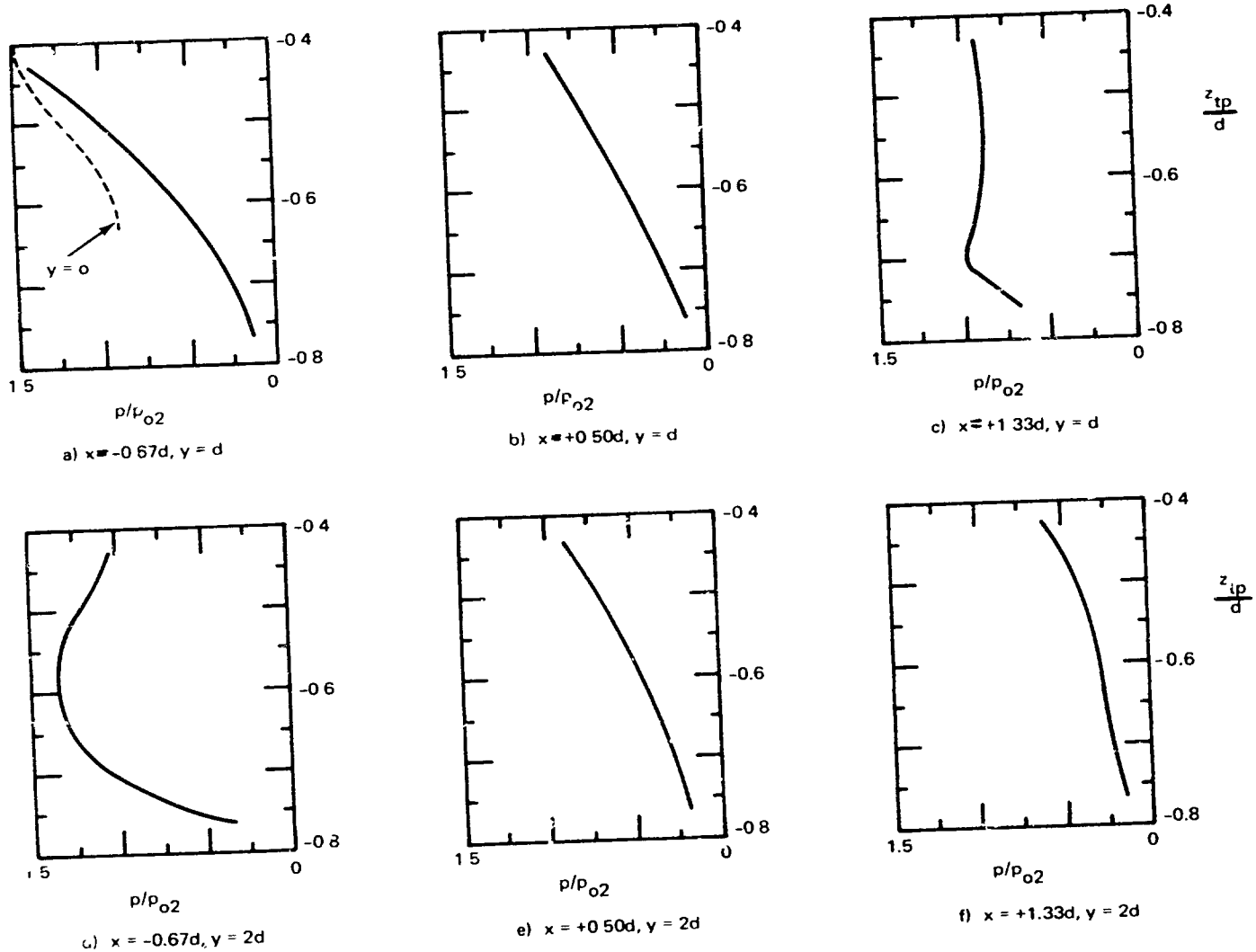

Fig. 31 Rake Total Pressure Profiles Along Outboard Stations y = d and y = 2 d (Data from Ref. 7); M_∞ = 3, d = 3/4, Rey_{inch} = 800,000

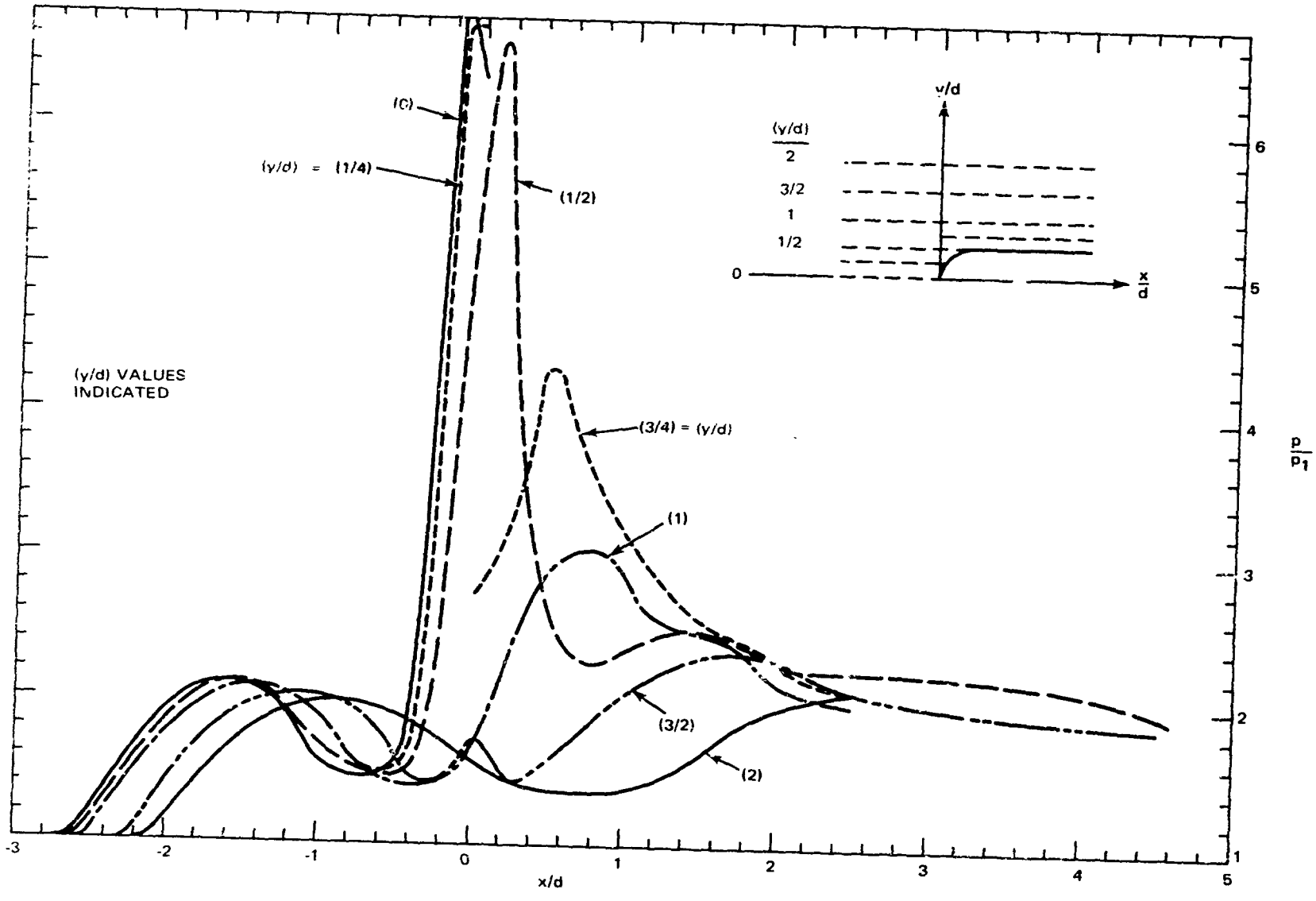

Fig. 32 Chordwise Pressure Distributions on Plate (Data from Price and Stallings, Ref. 15); $M_\infty = 4.44$, Thick Turbulent Boundary Layer, $\delta = 3$ d

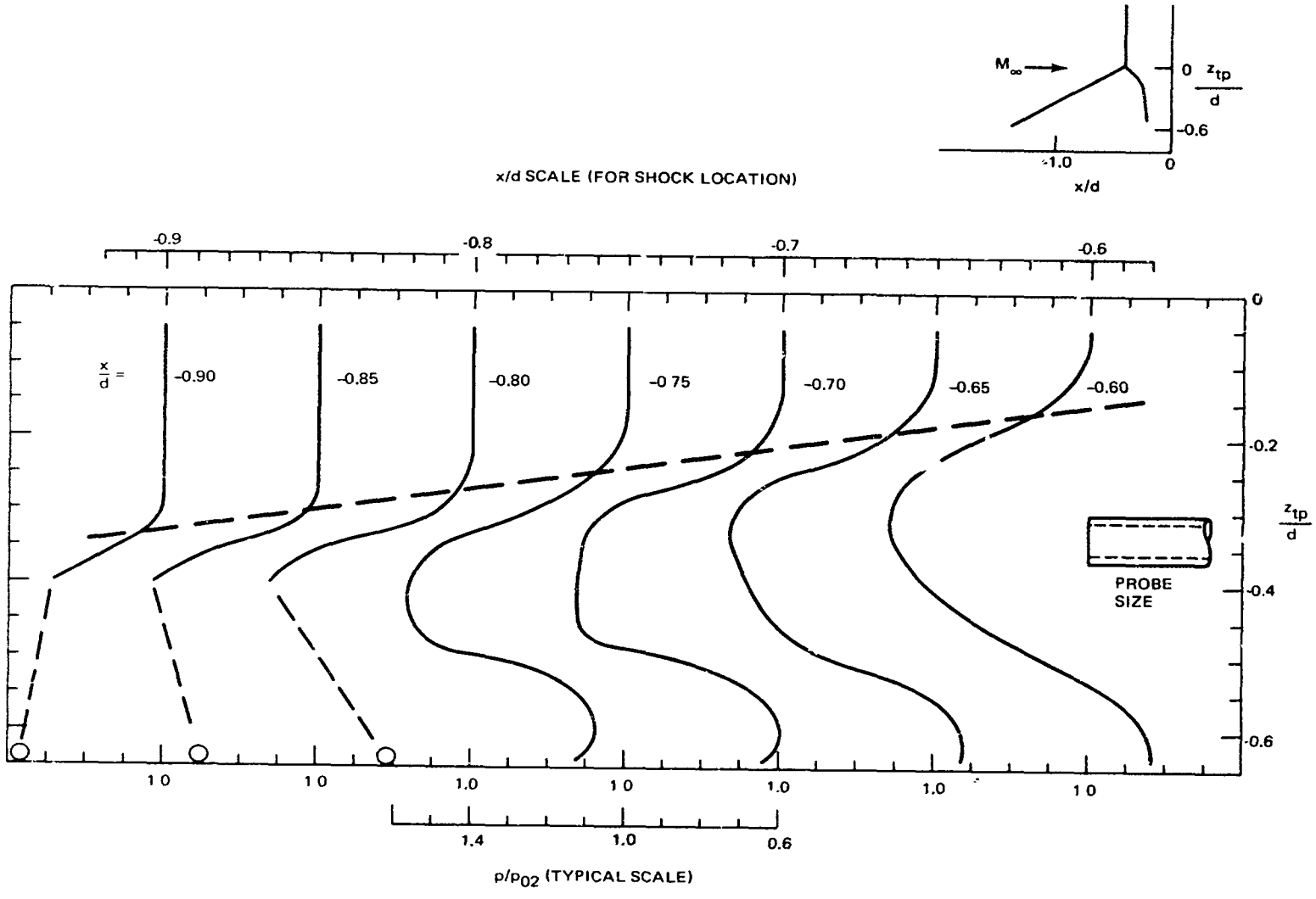

Fig. 33 Probe Total Pressure Profiles in Centerplane Ahead of Fin (Sheet 1 of 3)

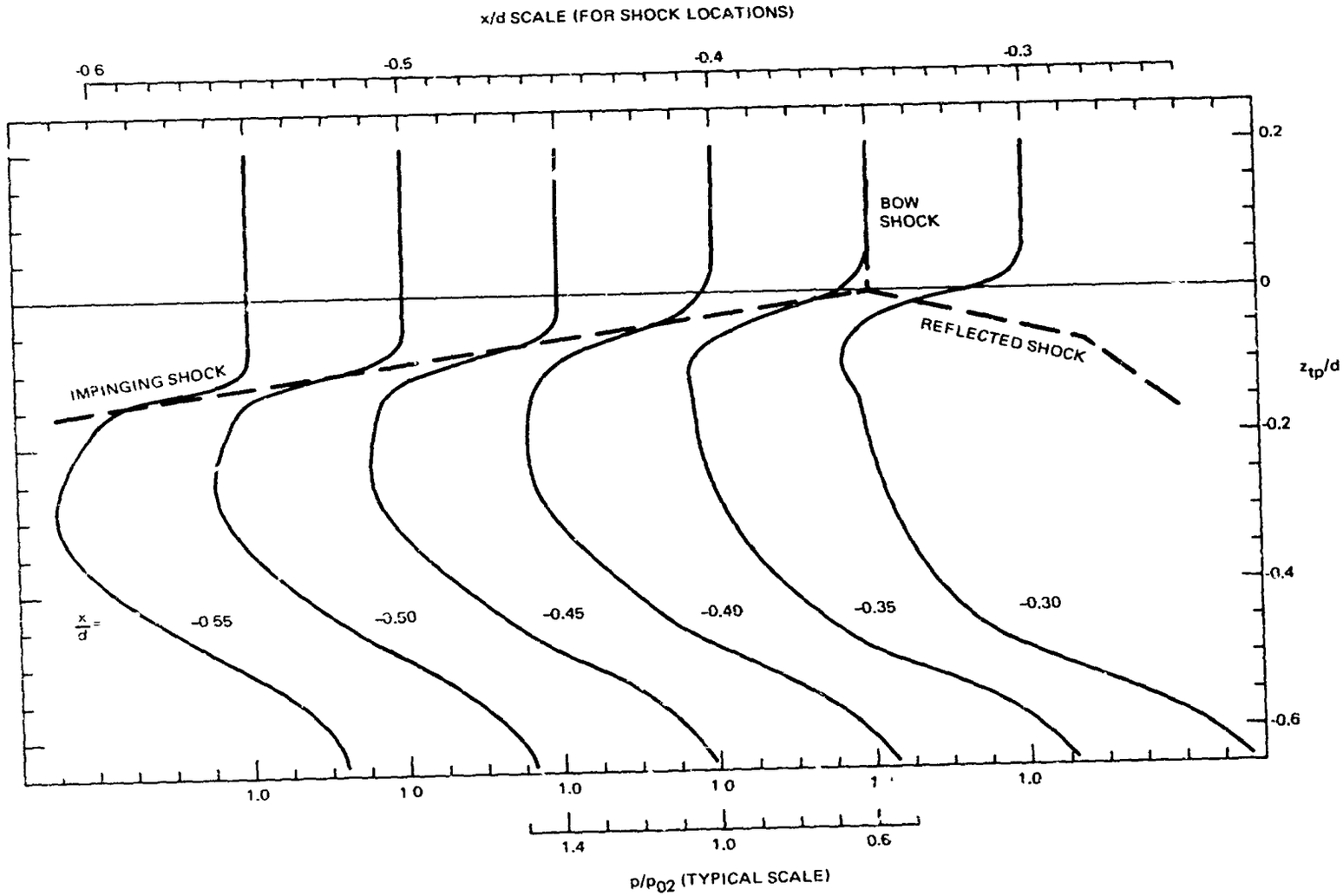

Fig. 33 Probe Total Pressure Profiles in Centerplane Ahead of Fin (Sheet 2 of 3)

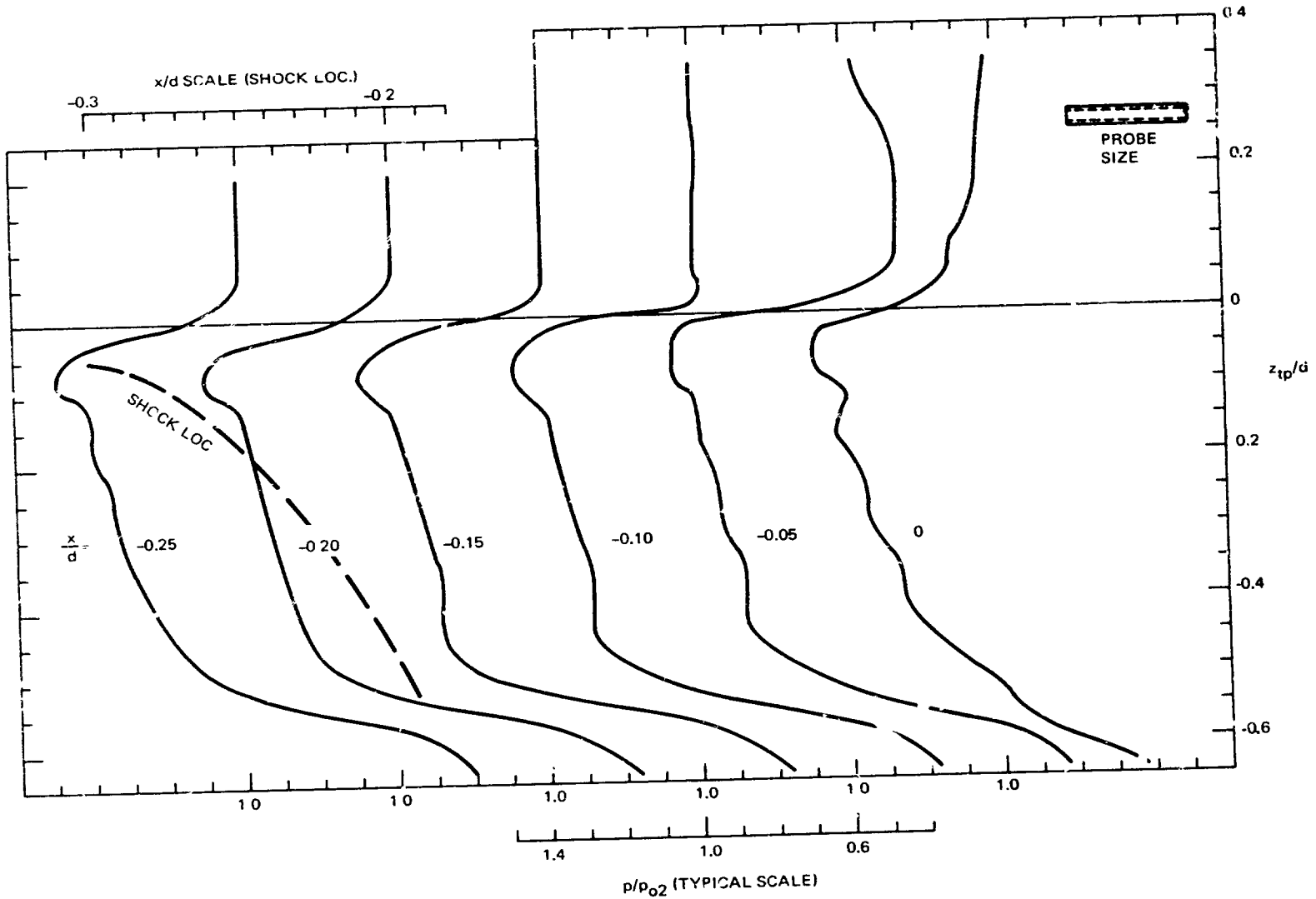

Fig. 33 Probe Total Pressure Profiles in Centerplane Ahead of Fin (Sheet 3 of 3)

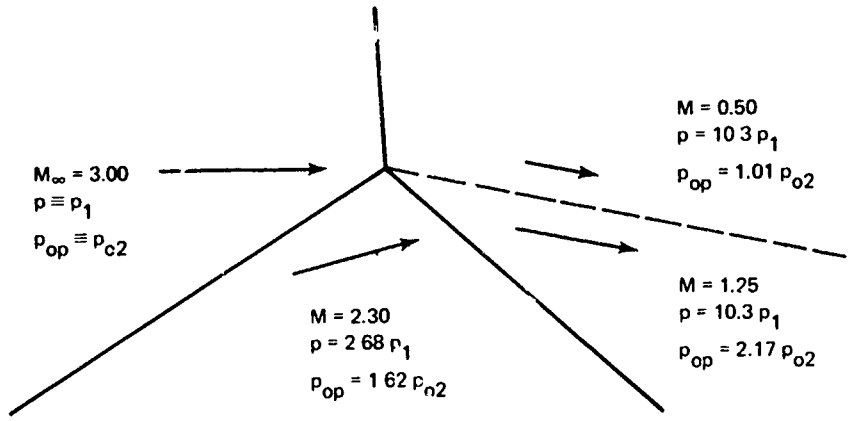

a) CALCULATED FOR 14.2° FLOW DEFLECTION

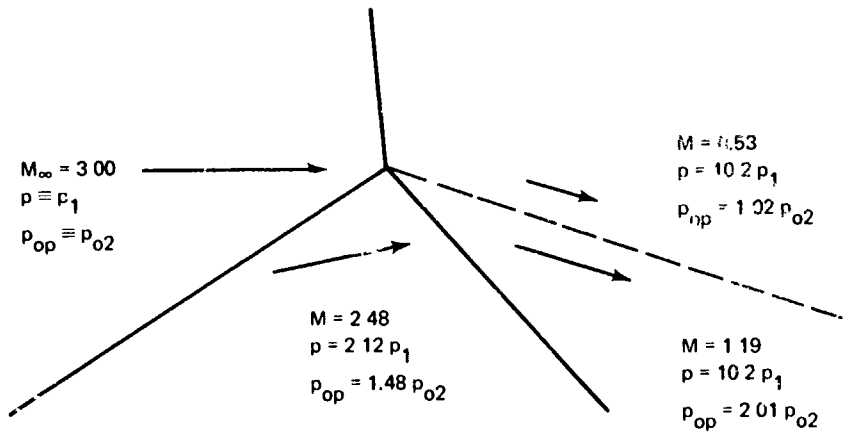

b) CALCULATED FOR 10 5° FLOW DEFLECTION

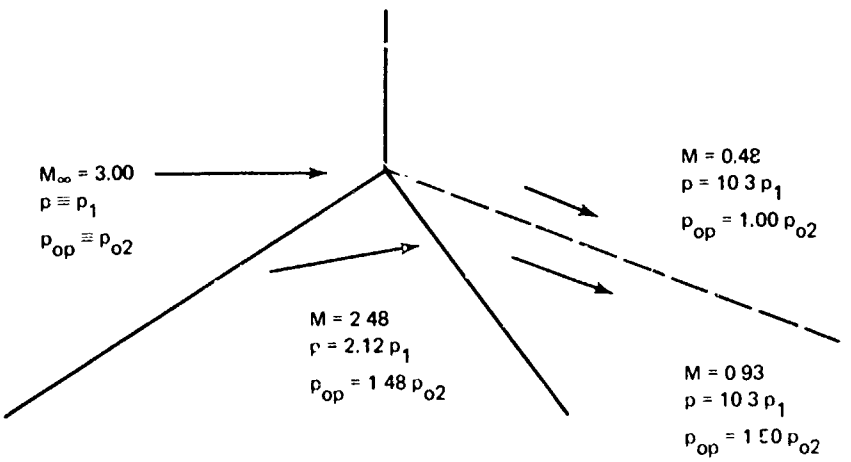

c) MEASURED

Fig. 34 Flow Field in the Vicinity of the Triple Point